POST COMBUSTION CO_2 CAPTURE THROUGH ADSORPTION PROCESS IN FIXED AND FLUIDIZED BEDS

A Thesis Submitted in Partial Fulfillment of the Requirements for the Degree of

DOCTOR OF PHILOSOPHY

H. LALHMINGSANGA

Registration No.10610317

DEPARTMENT OF MECHANICAL ENGINEERING

INDIAN INSTITUTE OF TECHNOLOGY GUWAHATI

May, 2015

CERTIFICATE

It is certified that the work contained in the thesis entitled **Post Combustion CO_2 Capture through Adsorption Process in Fixed and Fluidized Beds** by **H. Lalhmingsanga (Regn No. 10610317)**, a research scholar in the Department of Mechanical Engineering, Indian Institute of Technology Guwahati, India, for the award of the degree of the Doctor of Philosophy has been carried out under my supervision and this work has not been submitted elsewhere for a degree.

Dr. Pinakeswar Mahanta
Professor,
Dept. of Mechanical Engineering,
Indian Institute of Technology Guwahati.
May 2015.

ACKNOWLEDGEMENT

First of all I give thanks to Almighty God for all the guidance and blessing throughout my research work. I express my deepest gratitude to my supervisor, Prof. Pinakeswar Mahanta for his uncountable guidance and support. It was his constant inspiration and thoughtful suggestions which lead the research to present shape.

I would like to thank my doctoral committee members, Prof. Anoop K. Dass, Dr. Niranjan Sahoo and Dr. Anil Verma for their valuable suggestions and encouragement during my research work. I would like to acknowledge Indian Institute of Technology Guwahati (Dept. of Mechanical Engineering) for providing the funds and facilities for carrying out my research. I would also like to express my sincere gratitude to Prof. Juray De Wilde for his guidance and suggestion throughout my 8 months research work in UCL, Belgium. I would also like to thank the European Commission for their financial support throughout my stay in Belgium.

I would like to thank Prof. U. K. Saha, Dr. Lalsangzela Sailo, Dr. L. Patton for inspiring and encourage me to pursue my PhD and I would like to thank all my colleagues Mr. T. Moasunep Jamir, Dr. Pankaj Kalita, Mr. Lalthlamuana Ralte, Mr. PC Lalngilneia, Mr. Lalhriatzuala, Dr. Kim Jolly, Mrs. R. Laltleipuii, Ms. R. Lalbiaknungi, Mrs. Vanlalmuansangi Khenglawt, Dr. Laltanpuia for their inspiration and moral support throughout my research work. I extend my thanks to Mr. Mrinal Sarma and Mr. D. Chetri and other staff members of central workshop of IIT Guwahati for their help during the fabrication and assembly of experimental setup.

I would like to thank Ms. Jenie L. Pachuau for supporting me in good as well as difficult times throughout these years. I am very grateful to my beloved parents, my brother, my sisters and all other relatives for their immeasurable love, understanding, and unwavering support, which has made this feat possible.

H.Lalhmingsanga

NOMENCLATURES

A	Pre-exponential factor
A_s	Surface area of heater, m^2
A_r	Archimedes number, Dimensionless
Bi	Biot number, dimensionless
C_A	Gas-phase concentration of a component A, vol. %
C_s	Gas concentration at the surface, vol. %
D_e	Effective diffusion coefficient, $m^2\ s^{-1}$
D_K	Knudsen diffusivity, $m^2\ s^{-1}$
D_{AB}	Binary diffusivity of gas, $m^{2\ -1}s$
d_o	Mean particle pore diameter, m
d_p	Particle diameter, m
d_r	Reactor diameter, m
g	Acceleration due to gravity, $m\ s^{-2}$
h	Heat transfer coefficient, $W\ m^{-2}K^{-1}$
h_{avg}	Average heat transfer coefficient, $W\ m^{-2}K^{-1}$
Δh	Distance between pressure tappings, m
H	Height of the heater, m
k_f	External phase mass transfer coefficient, ms^{-1}
k_g	Mass transfer coefficient, $m\ s^{-1}$
K	Equilibrium constant, $m^3 mol^{-1} s^{-1}$
L_r	Reactor length, m
L_m	Distance between two consecutive pressure taps, m
M_A	Molecular mass of component A, $kg_{gas}\ kmol_{gas}^{-1}$
M_B	Molecular mass of component B, $kg_{gas}\ kmol_{gas}^{-1}$
M_{mix}	Molecular mass of gas mixture, $kg_{gas}\ kmol_{gas}^{-1}$
P	Absolute pressure, Pa
ΔP	Pressure drop, cm of H_2O
q_s	Concentration adsorb on the surface

q	Moles of adsorbate adsorbed per unit mass of adsorbent ($mol_{gas/}\ kg_{cat}$)
$\dot{Q}$	Heat supplied, W
r_A	Rate of adsorption, $mol_A\ kg^{-1}s^{-1}$
r	Particle radius, m
R	Gas constant, kJ $mol^{-1}K^{-1}$
Sc	Schmidt number, dimensionless
Sh	Sherwood number, dimensionless
t	Transient time from the introduction of the step/pulse input, s
T	Reactor temperature, K
T_s	Surface temperature, K
T_b	Bed temperature, K
U_s	Gas superficial velocity, m/s
U_{mf}	Minimum fluidization, m/s
v_A	Values of the atomic diffusion volumes
Z	Axial length of the reactor, m
τ	Tortuasity
ρ_{sus}	Suspension density, kg/m^3
ρ_s	Solid density, kg/m^3
ρ_g	Density of gas, kg/m^3
μ_g	Viscosity of gas, kg m^{-1} s^{-1}

CONTENTS

LIST OF FIGURES

LIST OF TABLES

ABSTRACT

Increasing CO_2 emissions in the environment leads to global warming which is an issue of great concern today. This awareness of increase in greenhouse gas emissions has resulted in the development of new technologies which would lower emissions of CO_2 from flue gas. At present, there are three major approaches for CO_2 capture: pre-combustion capture, oxy-fuel process and post-combustion capture. Post combustion capture offer some advantages as existing combustion technologies can still be used without radical changes on them. This makes post combustion capture easier to implement as a retrofit option compared to the other two approaches. Therefore, post combustion capture is the technology that will probably be deployed.

In the present work, CO_2 capture by post combustion technology using adsorption process in fixed as well as fluidized beds was studied. A comprehensive set of data and analysis for CO_2 adsorption equilibrium and kinetics is presented for zeolite 13X, zeolite 5A, zeolite 4A and activated carbon (coconut fibre based). Adsorption test had been carried out at a temperature ranging from 298 K to 333 K and CO_2 partial pressure of up to 0.4 MPa. The experimental data were correlated as a function of temperature and pressure to fit with different model equations such as (Langmuir, Freunlich, Toth and Sips).

The thermodynamics of CO_2 adsorption was also estimated for individual adsorbents using Van't Hoff's equation. The fixed bed adsorption process was simulated by considering a linear driving force (LDF) for the overall mass transfer and diffusivity factor. The LDF model acceptably reproduced all of the breakthrough curves and can be considered as adequate for designing an adsorption process to separate CO_2 from flue gas. The model sensitivity was analyzed by varying parameters such as bed height, flow rate, bed void fraction, and adsorbent pellet diameter to better understand the model.

A bubbling fluidized bed was also employed in order to investigate the effectiveness of CO_2 adsorption process in a fluidized bed. CO_2 adsorption was done onto the same adsorbents used in fixed bed process. In comparison to fixed bed, the employment of fluidized bed for CO_2 adsorption process presents an advantage of better gas-solid contact, which gives a better

coefficient of mass transfer. Fluidization also allows enhancement of maintaining relatively higher capture capacities at large values of the gas flow rate. In addition, the hydrodynamics of bubbling fluidized bed like suspension density, pressure drop, bed voidage profile and heat transfer characteristics were investigated.

CHAPTER 1
INTRODUCTION

1.1 BACKGROUND

The world's primary energy sources can be classified into three categories: i) fossil fuels such as petroleum oil, coal, and natural gas, etc. ii) renewable sources including biomass, geothermal energy, solar energy, hydro energy, tidal energy, and wind energy, etc. and iii) nuclear energy [Fridleifsson, 2003]. Fossil fuel shares the largest energy contribution, accounting for more than 80 per cent as shown in Figure 1.1.

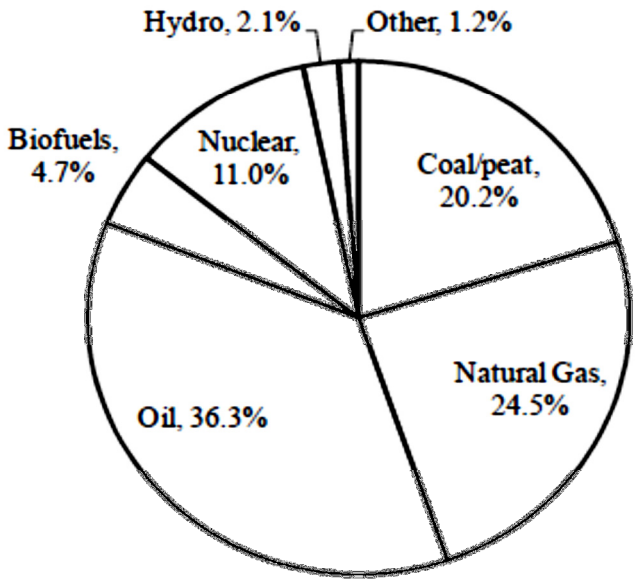

Fig 1.1 Primary sources of energy in the world in 2013 (IEA, 2013)

Burning fossil fuels for electricity and other forms of energy has been the most accepted and widespread practice in every industry for decades, and in some cases centuries. It is clear that fossil fuels are the dominant sources of the global primary energy demand and will likely remain so for the rest of the century. Recently, the use of fossil fuels has been recognized as a major threat to the environment regarding the associated excessive greenhouse gas emissions. The

combustion of fossil fuels leases a large amount of carbon dioxide (CO_2), one of the greenhouse gases contributing to global warming and climate change. Figure 1.2 shows the trends of atmospheric CO_2 at Mauna Loa Observatory till May 2015 [NOAA]. This unnatural addition to the greenhouse effect is known as global warming.

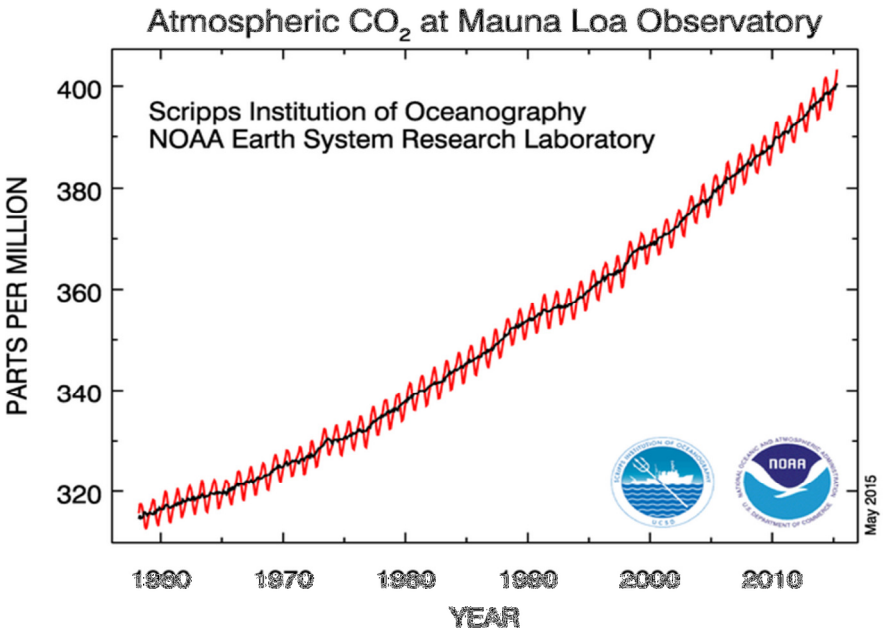

Fig 1.2 Atmospheric CO_2 at Mauna Loa Observatory [NOAA]

It is suspected that global warming may cause increase in storm activity, melting of ice caps on the poles, which will cause flooding of the inhabited continents, and other environmental problems. The increasing world energy demand could lead to a substantial increase in CO_2 emissions from 26.6 gigatonnes per year in year 2003 to 40.4 gigatonnes per year by 2030 [Quadrelli and Peterson, 2007]. While great efforts and investments were made by many nations to increase the share of renewable energy to the primary energy demand and to foster conservation and efficiency improvements of fossil fuel usage, addressing climate change concerns during the coming decades will likely require significant contributions from carbon capture and storage.

One strategy to reduce greenhouse gas emissions is to use so called “clean fuel” such as natural gas since it generates relatively low CO_2 emissions compared to other fossil fuels [Mokhatab et

al., 2006]. Natural gas is commonly produced from underground reservoirs. It is composed of methane (CH_4) as the primary constituent and heavier hydrocarbons such as ethane, propane, and butane, as well as non-hydrocarbons such as nitrogen, hydrogen sulfide, helium, and CO_2. It is to be noted that raw natural gas contains significant amounts of CO_2 that must be removed prior to the delivery to customers to reduce its impact on the environment.

Among the ways to control, reduce or mitigate the greenhouse effect, the capture of CO_2 from flue gases of industrial combustion processes and its storage in deep geological formations is now being considered as a serious option. Carbon capture and sequestration can be defined as the capture and secure storage of carbon that would otherwise be emitted to, or remain, in the atmosphere. Capture of CO_2 is the separation of that component from the gases where it is usually in relatively low concentration, into a separate highly concentrated stream, suitable for further specific processing (liquefaction, transportation and storage). Capture techniques are therefore inspired from classical gas purification techniques. For CO_2 capture from industries and power plants, three basic strategies are usually distinguished viz. pre combustion, oxy-fuel combustion and post combustion that will determine the nature and importance of the capture process by itself.

Pre combustion capture: Coal is gasified (rather than combusted) to produce a synthesis gas, or syngas, consisting mainly of carbon monoxide (CO) and hydrogen (H_2). A subsequent shift reaction converts the CO to CO_2, and then a physical solvent typically separates the CO_2 from H_2. For power generation, pre combustion carbon capture can be combined with an integrated gasification combined cycle (IGCC) power plant that burns the H_2 in a combustion turbine and uses the exhaust heat to power a steam turbine.

Oxy-fuel combustion: Oxy-fuel capture requires combustion of coal in pure oxygen (rather than air) so that the exhaust gas is CO_2-rich, which facilitates capture. The flue gas is a purge from this recycle stream, essentially composed of CO_2, thus not requiring a complex separation before compression. But, the energy penalty is displaced from CO_2 separation to the air separation process necessary to produce oxygen. The energy requirement is of the same order as that of final compression. If the oxygen is produced by cryogenic distillation, cold processes may be

conveniently integrated for these purifications. In any case, the processing is then limited to the CO_2 flow, and avoids treating large amounts of inert gases normally present in the flue gas. This is one of the major advantages of oxy-fuel combustion.

Post combustion capture: The gas is processed for CO_2 capture downstream of a conventional combustion. Post combustion capture typically uses chemical solvents to separate CO_2 out of the flue gas of a pulverized coal power plant. This may be applied to existing plants without major modifications. However, in most cases, large flow rates of dilute and low pressure, gas must be processed, implying very large equipment and a penalty on both investment and energy costs. Exceptions are for advanced power plants where combustion takes place under pressure. The largest potential applications are the numerous coal or oil-fired power plants. On the other hand, although they represent a lesser potential, high technology and high efficiency plants such as the natural gas combined cycle plants (NGCC) are probably best suited to host capture equipment.

Table 1.1 Typical CO_2 compositions in process streams [Car et al., 2008]

Process	**CO_2 concentration, vol. %**
Power plant flue gas	
Coal fired boiler	14
Natural gas fired boiler	8
Natural gas combined cycle	4
Coal-oxygen combustion	>80
Natural gas partial oxidation	40
Blast furnace	
Before combustion	20
After combustion	27
Cement kiln off-gas	14-33
Oil refineries and petrochemical plant fired heater	8

Existing power plants use air for combustion and generate a flue gas at atmospheric pressure and typically have a CO_2 concentration of less than 15 %. Thus the thermodynamic driving force for low CO_2 capture from flue gas is creating a technical challenge for the development of cost effective advanced capture processes [Figueroa et al., 2007]. The low concentration of CO_2 in power plant flue gas (13-15 % for coal fired power plant, 7-8 % gas fired power plant, etc.)

needs a large volume of gas to be handled, which results in large equipment sizes and high capital costs. Table 1.1 gives Typical CO_2 compositions in process streams.

1.2 TECHNOLOGY FOR CO_2 SEPARATION

Technology selection for CO_2 removal depends on the type and concentration of the impurities in the flue gas, temperature and pressure of the feed gas, required specifications of the gas product, volume of gas to be treated, cost (capital and operating) and environmental regulations. From the technical viewpoint, the removal of CO_2 can be achieved by a number of approaches, as shown in Figure 1.3.

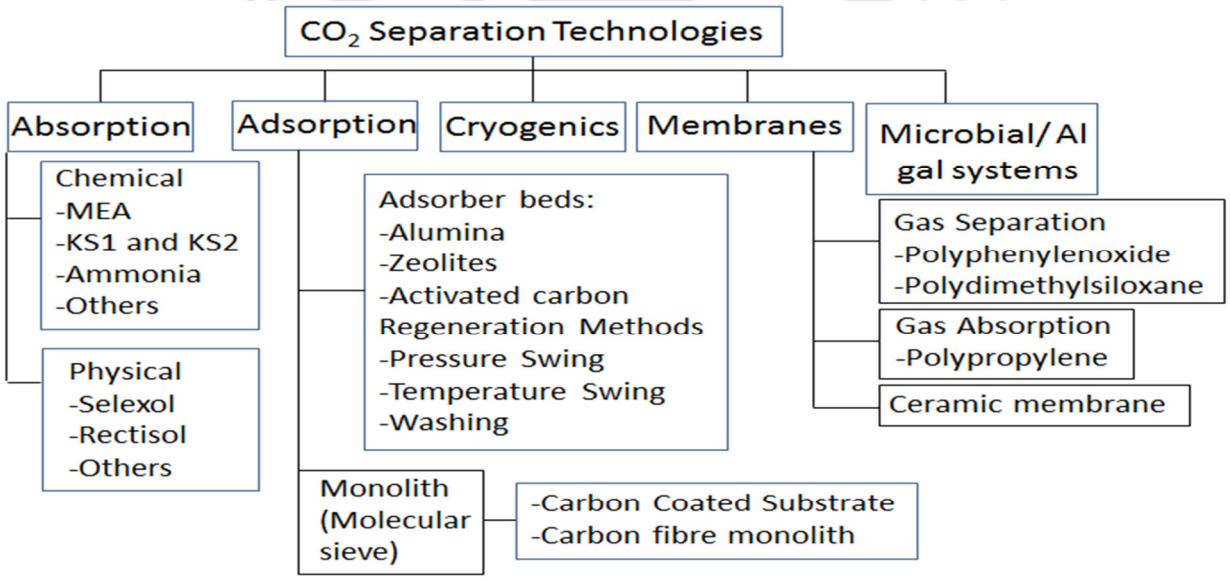

Fig 1.3 Process technologies for post combustion CO_2 capture [Rao and Rubin, 2002]

From Figure 1.3, it is clear that CO_2 capture techniques include absorption into a liquid solvent, adsorption onto a solid adsorbent, low temperature cryogenic distillation, permeation through a membrane, and chemical conversion [Rao and Rubin, 2002]. In general, gas absorption using a physical solvent and adsorption technologies are suitable for gas streams with high CO_2 partial pressure [Kidnay and Parrish, 2006]. Raw natural gas is usually available in the gas reservoirs with pressures up to 5000 psig or 340 atm, which provides considerably high partial pressure of CO_2 [Younger, 2004]. The absorption technology is commonly used for processing high volume gas streams while the adsorption onto solids is more suitable for smaller scale applications.

Adsorption technology provides low regeneration cost and non-corrosive behaviour, which makes this technology more applicable for the removal of CO_2 from flue gas [Rao and Rubin, 2002]. In this study, focus has been limited to the adsorption process for separating CO_2 from a flue gas.

1.3 ADSORPTION PROCESS

Separation of gases accounts for a major fraction of the production cost in chemical, petrochemical, and related industries. There has been a growing demand for economical and energy efficient gas separation processes. The new generation of more selective adsorbents developed in recent years has enabled adsorption based technologies to compete successfully with traditional gas separation techniques, such as cryogenic distillation and absorption. The last few decades have seen a considerable increase in the applications of adsorptive gas separation technologies, such as pressure swing adsorption (PSA), temperature swing adsorption (TSA) and electrical swing adsorption (ESA). PSA is a versatile technology for separation and purification of gas mixtures. While, initial applications of PSA included gas drying and purification of dilute mixtures, current industrial applications include solvent vapor recovery, air fractionation, production of hydrogen from steam-methane reformer (SMR) and petroleum refinery of gases, separation of hydrocarbons such as carbon monoxide-hydrogen, carbon dioxide-methane, and n-paraffins separation, and alcohol dehydration. Advent of commercial PSA operations started with the early patents on this subject granted to Skarstrom [Skarstrom, 1960], Guerin de Montgareuil and Domine [Guerin de Montgareuil and Domine, 1964]. PSA processes involve selectively adsorbing certain components of a gas mixture on a microporous and mesoporous solid adsorbent at a relatively high pressure, via gas-solid contact in a packed column, in order to produce a gas stream enriched in less strongly adsorbed components of the feed gas. The adsorbed components are then desorbed from the solid by lowering their gas-phase partial pressures inside the column to enable adsorbent re-usability. The PSA processes are normally associated to low energy consumption when compared to other technologies

Alternative procedure is TSA in which flue gas is passed over the bed and selective adsorption takes place on the adsorbent until it reach equilibrium. Desorption of gas can be done at elevated

temperature by supplying the additional heat. Additional requirement of heat in TSA makes it costlier than PSA. The other method is called electrical swing adsorption. In this method low voltage electric current is passed through the adsorbent. The ESA has the potential to reduce the cost of CO_2 capture compared with other conventional adsorption technologies as reported in literature. Therefore, ESA can be believed to be able to make the process of CO_2 capture more cost-effective than TSA and PSA. Figure 1.4 shows a general flow diagram for CO_2 capture via adsorption.

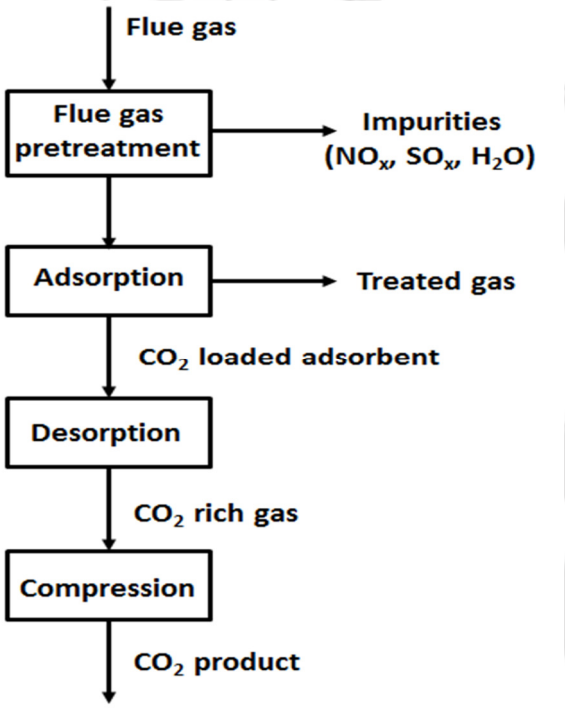

Fig 1.4 Basic flow diagram for the capture of CO_2 via adsorption [Spigarelli et al., 2013]

In CO_2 adsorption processes the flue gas stream must go through a pretreatment stage to reduce the concentration of impurities such as NO_x, SO_x, and H_2O in the gas stream. These impurities compete with CO_2 molecules for adsorption sites, drastically reducing the CO_2 adsorption capacity of the adsorbent. It is particularly important that the flue gas be dried prior to adsorption. Water has been shown to not only compete for adsorption sites, but to degrade the crystal structure of some adsorbents. After pretreatment, the gas should be cooled to around room temperature before the adsorption stage. Most adsorbents exhibit a drastic decrease in adsorption capacity at elevated temperatures (100 ˚C). Depending upon the adsorbent, CO_2 will be adsorbed either by weak physical interactions (physisorption) or strong chemical interactions

(chemisorption). Physisorption is usually accompanied by a lower heat of reaction than chemisorption, making the desorption stage less energy intensive. After adsorption, the solid adsorbents go through a desorption stage.

During desorption, gaseous are driven off the adsorbent and the adsorbent is consequently regenerated in the process. The two most common approaches to desorption are pressure swing and temperature swing processes. In pressure swing systems the adsorption stage is carried out at an elevated pressure so when the pressure within the system is reduced, the CO_2 is desorbed from the solid. In a temperature swing system, the temperature of the system is increased to drive CO_2 from the adsorbent. The advantage to a temperature swing system is that the adsorbent can be regenerated while maintaining a high CO_2 partial pressure. This avoids the heavy energy penalty associated with having to recompress the CO_2, as is the case in pressure swing systems. However, regeneration with pressure swing systems can be accomplished in matter of seconds, as opposed to hours with temperature swing systems [Pires et al., 2006].

1.4 RESEARCH MOTIVATION

Greenhouse gases have a direct influence on the environment, causing extreme weather changes, a global temperature increase, the loss of ecosystems and potentially hazardous health effects for people. CO_2 is on of the major greenhouse gas that can negatively influence the quality of air and increase the global warming. The global increase in atmospheric CO_2 comes mainly from combustion of fossil fuels. In 1992, global emissions of CO_2 added to the atmosphere as a result of human activities amounted to 26.4 billion metric tons per year, of which 84 % was from industrial activities [World Resources, 1996–97]. On average, about half of the CO_2 emissions caused by fossil fuels have remained in the atmosphere, the rest have been absorbed by the ocean and by land ecosystems [Bousquet et al., 2000]. According to IPCC's Special Report on Emissions Scenarios (SRES), global CO_2 emissions due to industrial energy consumption are projected to increase from 6.0 GtC yr^{-1} in 1990 to 9.0–12.1 GtC yr^{-1} by 2020 depending on the underlying scenario (IPCC, 2000a). Therefore, concerns over the gradual increase in the atmospheric CO_2 concentration and its impact on climate change have prompted a global research effort to capture CO_2 from point source emissions and stabilize its concentration in the

atmosphere. To achieve mid to long term CO_2 reduction targets, cost effective CO_2 capture from fossil fuel power plant and subsequent sequestration options need to be evaluated keeping in view of world's growing demand of energy.

The current techniques for removing CO_2 from flue gases emitted by thermal power stations are mainly based on absorption method, according to which gases undergo washing in packed column with the use of various solutions which are called wet technologies. Along with these technologies, dry methods for separating CO_2 from other components of gas flow (membrane, adsorption, etc.) are also being developed. The use of PSA and TSA process has become considerably increasing in the applications of adsorptive gas separation because of its versatile technology. PSA processes operate at ambient temperatures and do not require any solvent for product recovery or adsorbent regeneration. Hence, PSA processes are cost effective compared to traditional technologies, and are especially desirable when lower production rates or lower product purities are required. Also, pressure manipulation serves as an extra degree of thermodynamic freedom, thus introducing significant flexibility in process design as compared with conventional technologies such as distillation, extraction or absorption.

Both adsorption rate and adsorption capacity are vital for evaluating the performance and practicality of the CO_2 adsorption process, the behaviour of CO_2 adsorption kinetics and equilibrium must therefore be characterized systematically for the selected adsorbents. Although commercial applications of PSA and TSA processes in a fixed bed have grown rapidly, existing as well as emerging new applications present research challenges in terms of developing a systematic formulation for obtaining optimal operation strategy with detailed PSA bed models, and obtaining exhaustive experimental data for the kinetic and equilibrium behavior for novel adsorbents to accurately model multicomponent adsorption isotherm and mass transfer phenomena.

A number of research projects associated with the adsorption properties of CO_2 gas on different adsorbents were reported based on a fixed bed experiment. Most of these projects focused on adsorption equilibrium (or adsorption isotherms) at different temperatures and pressures onto zeolite based and activated carbon based materials. Recent development shows an improvement

in commercial adsorbent materials with higher adsorption capacity and selectivity like Activated carbon honeycomb monolith – Zeolite13X hybrid system, zeolites NaKA and nano-NaKA, FAU zeolites and zeolite 13X prepared from bentonite. As it can be seen that a number of sorbents like zeolite, activated alumina, activated carbons, etc. have been utilized and cost of the sorbents play a vital role for the process to be economical. Therefore, in order to decrease the cost of the adsorbents, low cost and abundantly available materials like coconut fiber based activated carbon presents a promising potential. Coconut fiber, olive stones, nut shells and many other biomass materials have been converted to activated carbon for used as adsorbents because of their high surface area [Yang and Lua, 2003]. Coconut is abundantly available in tropical regions and the unwanted shells are just wasted as garbage. Hence, the wasted coconut shell can be converted to activated carbon and used as adsorbents material. Thus, coconut fiber based activated carbon, which is cheap and abundantly available locally, is a potential adsorption material for the proposed study.

Fluidized bed technology is one of the promising technologies for CO_2 adsorption apart from the conventional fixed bed technology. Fluidized bed technology is a versatile technology and has been used for several purposes; such as fluidized bed reactors, fluid catalytic cracking, combustion, heat or mass transfer or interface modification, such as applying a coating onto solid items. In fluidized beds, the contact of the solid particles with the fluidization medium is greatly enhanced when compared to fixed beds. This behavior in fluidized combustion beds enables good thermal transport inside the system and good heat transfer between the bed and its container which can also be applied for adsorption process. Yi et al., 2007 have reported the used of fluidized bed for continuous operation of potassium based dry sorbent for CO_2 capture and Winaya et al., 2001 have studied the effect of pressure and CO_2 concentration on heat transfer at high temperature in a pressurized circulating fluidized bed combustor. But, detail report has not been reported about the adsorption capacity and the enhancement of adsorption capacity by using fluidized bed technology. A fluidized bed is known as a proper process to control high volumes of flue gases, and dry sorbents can be used to cut down the cost for control, so the use of dry sorbents in a fluidized bed is considered as a proper process to remove carbon dioxide economically [Lee et al., 2004]. Therefore, a thorough study in this area is needed to improve CO_2 adsorption process in a fluidized bed.

1.5 SCOPE AND OBJECTIVES FOR PRESENT WORK

The objective of the present work is to capture CO_2 from flue gas (dry basis) by using adsorption process in fixed bed as well as fluidized beds. The following research tasks are set in order to achieve the objectives of the present study:

1. Adsorption of CO_2 on coconut fibre based activated carbon and compared with different adsorbent materials such as zeolite 13X, zeolite 5A and zeolite 4A in a fixed bed.
2. Regeneration study of the adsorbents (zeolite 13X, zeolite 5A, zeolite 4A and activated carbon) in a fixed bed.
3. Study of adsorption equilibriums and kinetics of CO_2 adsorption on the adsorbents at different temperatures and pressures in a fixed bed.
4. Simulations of CO_2 adsorption process in a fixed bed with all adsorbents considered in this study.
5. Performance evaluation of a bubbling fluidized bed in terms of CO_2 adsorption, bed hydrodynamics and heat transfer characteristics with zeolite 13X, zeolite 5A, zeolite 4A and activated carbon and its comparison with fixed bed system.

1.6 THESIS OUTLINE

This report consists of eight chapters in total. Chapter 2 contains the literature reviews based on the present objectives. Characterization detail of adsorbent material used in the present study has been presented in Chapter 3. Chapter 4 presents breakthrough curve and isotherm models used for CO_2 adsorption in the fixed bed. Details of the experimental setup, experimental procedures, and experimental conditions for CO_2 adsorption experiments are described in Chapter 5. Chapter 6 reports the experimental, simulation results and discussion in the fixed bed system with validation of the results. Chapter 7 gives the experimental results and discussion in a fluidized bed and its comparison with fixed bed. Conclusions and scope for future works are presented in Chapter 8.

CHAPTER 2

LITERATURE REVIEW

2.1 INTRODUCTION

In the present chapter, literature survey and scopes for present investigations are discussed based on the three types of CO_2 capture strategies viz. Pre combustion, Oxy-fuel combustion and Post combustions. Review on experimental studies of CO_2 adsorption in a fixed bed based on the capture technology like absorption, adsorption, membrane separation and cryogenic distillation has been described. Literatures for modeling and simulation of CO_2 adsorption are also reported based on the system heat transfer effect which includes isothermal and non-isothermal process. Lastly, review on CO_2 adsorption in a fluidized bed is reported. Section 2.5 summaries the chapter and also explains the scope for present investigations.

2.2 PRE COMBUSTION CO_2 CAPTURE

Pre combustion process is related to the treatment of synthesis gas (syngas) composed principally of CO and hydrogen. Mori et al., 1993, have examines a concept based largely on existing technologies that could significantly reduce CO_2 emissions from large-scale stationary combustors. Unlike other measures proposed previously that call for the removal of CO_2 from post flame gases, here carbon is separated from the fuel as CO_2 before combustion, through oxidation with superheated steam on a catalyst followed by preferential absorption into a recyclable liquid solvent or by staged phase transformations of the CO_2. The resulting gas stream, comprising primarily hydrogen, is burned in place of the original fuel. Containment of the extracted CO_2 is accomplished by liquefaction and discharge into the deep ocean. A thermo-economic analysis of a 500 MW methane-fired, steam power plant fitted with the pre-combustion CO_2 removal system indicates moderate cost and energy expenditures.

Pre combustion rate is premised on the production of syngas, removal of CO_2 and combustion of H_2 [Steeneveldt et al., 2006]. In some ways it is oxymoron because CO_2 is obviously not normally available for capture prior to combustion, as CO_2 is a product of coal combustion, not a natural precursor. All types of fossil fuels can be gasified (partially combusted, or reformed) with sub stoichiometric amount of oxygen at elevated pressures typically in the range of 30-70 atm to produce a syngas predominantly, CO and H_2. Thereafter, steam is added to syngas and passed through the bed packed with catalysts, onto which water gas shift reaction takes place that convert CO into CO_2. In water gas shift reaction, the addition of steam and reduction of temperature actually promote the conversion of CO into CO_2 and increase the yield of H_2 [Gibbins et al., 2008]. From CO_2 and H_2 bearing stream, CO_2 is separated and sent to the compression unit and pure H_2 is further used as input to a combined cycle to produce electricity as shown in Figure 2.1 [Feron and Hendriks, 2005].

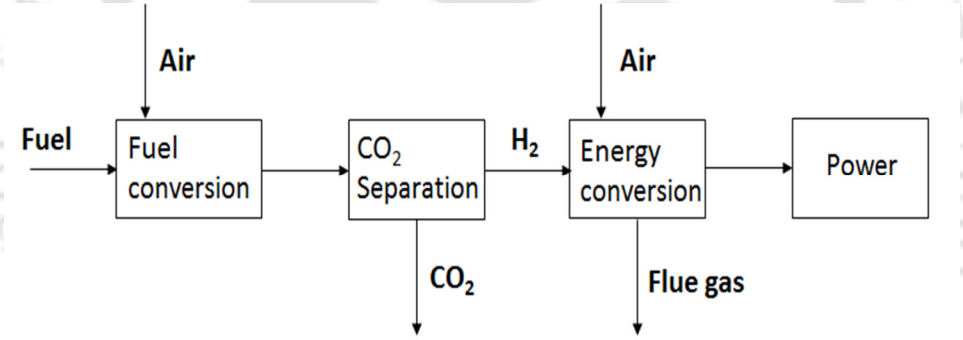

Fig 2.1 Schematic of pre combustion CO_2 capture process [Feron and Hendriks, 2005]

The separation process typically uses a physical solvent such as rectisol and selexol available at low cost, Hydrotalcite-based materials to improve conversions in the water-gas shift (WGS) and steam-reforming (SMR) reaction [Cobden et al., 2007]. Nord et al., 2009 have analyzed a cycle designed for capturing the greenhouse gas CO_2 in a natural gas combined cycle power plant. Included in the thermodynamic analysis are design calculations, as well as steady-state off-design calculations.

Seo and Kang, 2010 have studied enhancing CO_2 separation for pre-combustion capture with hydrate formation in silica gel pore structure. They reported the enrichment of hydrate phase with CO_2 in gas hydrates, formed from a CO_2 and H_2 gas mixture when using silica gels to form

the hydrate. While, Scholes et al., 2010 have reviewed CO_2 capture from pre combustion process strategies for membrane gas separation. Romano et al., 2010 focuses on pre-combustion techniques applied to natural gas combined cycles. The predicted LHV efficiency for the base configuration is about 50%.

CO_2 is dissolved at higher pressure and then released as the pressure is reduced. No heat is required to regenerate the solvent and CO_2 can be released at above atmospheric pressure. The energy requirement for CO_2 separation and compression in pre combustion capture can be in the order of half of that required for post combustion capture [Gibbins et al., 2008]. This process has a good advantage i.e. utilization of physical solvent which are available at low cost and require low energy for regeneration [Figueroa et al., 2008]. The main disadvantage of pre-combustion capture is that it requires a chemical plant in front of the turbine. Complicated chemical processes normally cause extra shut-downs of the plant, which can result to a lower power output [Soodabeh et al., 2012]. Other disadvantages are non-gaseous feed stocks, requirement of the cleaned gas stream and possible expensive scrubbing for high NO_x emission control [Babu et al., 2014]. Presence of CO_2 at much higher concentrations in syngas makes CO_2 capture less expensive for pre-combustion capture, in comparison with post-combustion capture. Currently, there are few gasification plants in full-scale operation and capital costs are higher than pulverized coal-fired power plants [Blomen et al., 2009]. Summary of significant developments of distinct nature during past decade for pre combustion CO_2 capture are presented in Table 2.1.

Table 2.1 Summary of significant developments in the area of pre combustion CO_2 capture

References	Objective	Methodology	Result
Lyngfelt et al., 2001	Chemical Looping Combustion (CLC)	Metal oxide oxygen carrier is used to supply oxygen required for combustion, and separating combustion products CO_2 and H_2O. The reduced metal oxide is subsequently oxidized with air.	Very less amount of energy is required for CO_2 separation. The process is faster and yields higher concentration CO_2 for easy capture and sequestration.
Willis et al., 2006	Metal organic frameworks (MOF)	Metal organic frameworks (MOFs) are a new class of hybrid material built from metal ions and organic bridging ligands are used for adsorb CO_2.	High storage capacity is possible, and the heat required for recovery of the adsorbed CO_2 is low. MOF-177 has shown one of the highest surface areas and adsorption capacity for CO_2 at elevated pressure.
Linga et al., 2007	Hydrate formation coupled with membrane separation	Hydrates are used along with membranes	Hydrate crystal formation from CO_2 /N_2 mixtures showed that CO_2 prefers the hydrate phase. CO_2 recovery was found to be 36.7–42.1% in one stage at 11.0 and 10.0MPa.
Drage et al., 2009	Development of Activated Carbon based adsorbents	Effect of porosity of phenolic resin (Novolak) beads on CO_2 capture	Maximum CO_2 adsorption capacity of 58 wt.% (13 mmol g-1) at 3 MPa
Heldebran et al., 2009	CO_2 Binding Organic liquid (CO_2 BOL)	CO_2 BOLs are used for CO_2 absorption and the energy requirement for recovery of CO_2 is studied	Free energy requirement for binding is CO_2 is small and independent of alcohol. Since the specific heats of CO_2 BOLs are about 50% lower than water based amines, lesser energy is required for recovery of CO_2.

Soodabeh et al., 2012	Separation of CO_2 by Multiwall Carbon Nanotubes (MWCNT)	Adsorption of CO_2 by MWCNT was investigated at 218-318 ˚C and 40 bars.	Temp has no significant effect on H_2 when compared to CO_2. Higher pressure and lower temperature increases the CO_2 adsorption. This differential adsorption is a promising tool in future.
Alvis et al., 2012	Improving adsorption characteristics of MDEA	Piperazine is used as promoter for CO_2 adsorption which increases the reaction speed. Effect of solvent strength, MEDA-piperazine composition and temperature are studied	CO_2 adsorption is very sensitive to piperazine content (Amine strength worsens the absorption due to higher viscosity. Adsorption of CO_2 increases with temperature till 50 ˚C and suddenly decreases beyond.
Casas et al., 2013	MOF and UiO 67/MCM-41 adsorbents for pre combustion CO_2 Capture by PSA	Adsorbent material is packed into a column and exposed to three different CO_2/H_2 mixtures at a given temp (25 ˚C) and in a broad range of pressures (1–25 bar). Complete PSA simulations are conducted for CO_2 purity and recovery as objectives	USO-2-Ni MOF increases both the separation performance and the productivity of the PSA process with respect to activated carbon. UiO67/ MCM-41 hybrid exhibits a slightly worse separation performance, but a better specific adsorbent productivity than activated carbon
Babu et al., 2014	Enhanced kinetics of hydrate formation for the clathrate process in the presence of two liquid promoters namely THF and TBAB in a fixed bed reactor	Silica sand was used as a medium to capture CO_2 from CO_2 /H_2 gas mixture by hydrate crystallization	Higher driving force resulted in higher gas consumption and significantly reduced induction time. This study indicated better hydrate formation kinetics with the use of THF in an FBR configuration for CO_2 capture from a fuel gas mixture.

2.3 OXY-FUEL COMBUSTION FOR CO_2 CAPTURE

Oxy-fuel combustion is a promising technology for capturing of CO_2 from flue gas or to modify the combustion process so that the flue gas has a high concentration of CO_2 for easy separation [Kiga et al., 1997]. In this process fuel is burned in combustion chamber in the environment of pure O_2 (>95%) mixed with recycled flue gas (RFG) as shown in Figure 2.2. In the most frequently proposed version of this concept, a cryogenic air separation unit is used to supply high purity oxygen. This high purity oxygen is mixed with RFG prior to combustion or in the boiler to maintain combustion conditions similar to an air fired configuration [Va'rheyi et al., 1999. This is necessary because currently available materials of construction cannot withstand at high temperatures resulting from coal combustion in pure oxygen. Flue gas stream from this system contains mainly CO_2 and water vapor. The water is easily removed by condensation, and the remaining CO_2 can be purified relatively at low cost. The CO_2 content of the dry flue gas varies in the range of 70-95% depending upon the fuel, the process used, the air in leakage, the O_2 purity and the excess O_2 [Shaddix et al. 2003, 2010].

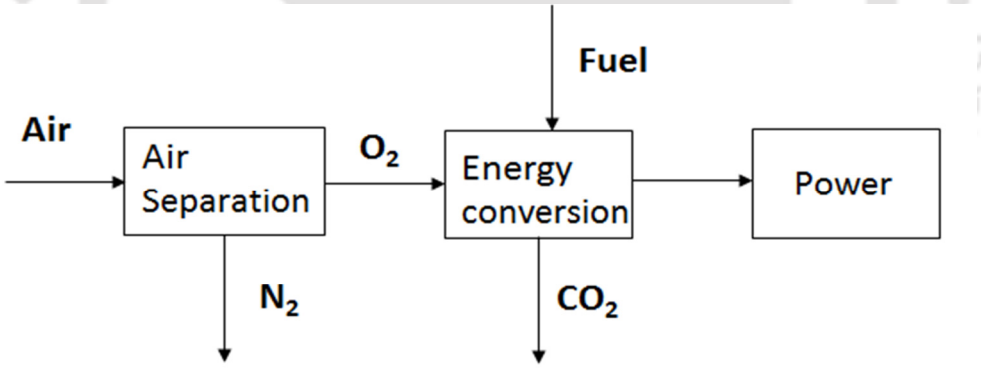

Fig 2.2 Schematic of oxy-fuel CO_2 capture process [Feron and Hendriks, 2005]

Krishnamoorthy et al., 2003 have studied CO/CO_2 ratio inside char particles. A detailed char particle combustion model was used to calculate the CO/CO_2 in char particle and to simulate influence of the variation of CO_2 and O_2 in the bulk gas. As a result of decreased flue gas volume and increased concentration of CO_2, the cost of carbon capture in oxy-fuel combustion is less than other conventional methods but the cost of air separation and flue gas recirculation significantly reduces the economic benefit. It uses oxygen instead of air for combustion of fuel and thus no NO_x will form. By utilizing this technology 60-70% NO_x emission is reduced

compared to air-fired combustion [Blomen et al., 2009; Hjärtstam et al., 2009]. Czakiert et al., 2010 have studied Oxy-fuel circulating fluidized bed combustion in a small pilot-scale test rig. Coal combustion under the elevated partial pressure of oxygen in a circulating fluidized bed environment was investigated. The fuel used was bituminous coal. The concentration of oxygen in the air was increased to 35% per volume. Excess oxygen ranged from 1.1 to 1.3 and the temperature ranged from 1073 K to 1273 K. A CFB combustor of 0.1 MW was adapted for oxy-combustion. Taniguchi et al., 2010 have done prediction of lean flammability limit and flame propagation velocity for oxy-fuel fired pulverized coal combustion.

Many researchers have reported that the volatile release is higher during pyrolysis in a CO_2-rich environment than in a N_2-rich environment. Al-Makhadmeh et al., 2009 reported that the CO_2 environment enhances the mass release during coal pyrolysis above 850 ˚C by approximately 10% for a medium volatile bituminous coal and 11–14% for lignite due to Boudouard reaction. The investigations were performed in a drop tube furnace in N_2 and CO_2 environments for both coals at temperatures ranging from 700 to 1100 ˚C. Rathnam et al., 2006 and Rathnam et al., 2007 measured the volatile yields of four Australian pulverised coals under simulated air (O_2/N_2) and oxy-fuel (O_2/CO_2) combustion environments using a drop tube furnace (DTF) maintained at 1400 ˚C. It was found that the volatile yields were higher in CO_2 for all of the four coals studied. Also, the high temperature volatile yields of all coals were higher than their respective volatile yields obtained by the proximate analysis. Zeng et al., 2008 studied devolatilisation of pulverised samples of a lignite coal, a sub-bituminous coal, and an eastern high-volatile bituminous coal at different temperatures inN_2-entrained and CO_2-entrained flows in an entrained-flow reactor. They reported that for the Illinois-6 coal, the mass release in the CO_2 environment was higher than that released in a N_2 environment for temperatures below 1400 ˚C. Moreover, Wall et al., 2009 have studied char characteristics and found that the effect of CO_2 environment was rank dependent.

Molina et al., 2009 studied ignition of groups of particles of a U.S. high-volatile bituminous coal under oxygen concentrations ranging from 12 vol.% to 48 vol.%, with N_2 or CO_2 as balance gas, at two gas temperatures (857 ˚C and 1377 ˚C). Molina and Shaddix, 2007 showed via single particle experiments that the presence of CO_2 and a lower O_2 concentration increase the ignition

delay time but have no measurable effect on the time required to complete volatile combustion, once initiated. In addition, it was found that particle ignition and devolatilisation properties in a mixture of 30 vol. % O_2 in CO_2 were very similar to those in air. At 857 ˚C, the experiments showed that as oxygen concentration increased, ignition delay decreased. This difference was more evident with N_2 as balance gas than with CO_2. The specific influence of the gasification reactions has recently been investigated by Shaddix et al., 2010 and Hecht et al., 2010. They conclude that in contrast to the previous results for CO_2 gasification, the presence of the steam gasification reaction increases the overall char conversion rate (slightly) for combustion at all investigated O_2 concentrations and for wet or dry recycle conditions. Andersson et al., 2008a have compared the radiative heat transfer in flames of oxy cases to corresponding conditions in an air case during combustion of lignite in the Chalmers 100 kW oxy-fuel test facility. Andersson et al., 2008b in another study investigated the changes in the soot-related radiation intensity between different propane flames, two oxy cases and an air case, in the same 100 kW oxy-fuel test unit. The oxy cases with 21 and 27 vol. % O_2 in the recycled flue gas were run with different amounts of dry RFG, which in principle only consisted of CO_2 from combustion and some excess O_2. Detail summary about the bench and pilot scale experimental studies on gas temperature and heat transfer in atmospheric oxy-coal combustion are given in Table 2.2

Gopan et al., 2014 had presented performance of a novel Staged Pressurized Oxy-Combustion (SPOC) process, which has the potential of increasing plant efficiency even further via reduction of auxiliary loads associated with flue gas recycle and flue gas cleanup. They suggests that the SPOC process has a potential to increase the average efficiency of coal based power generation even with carbon capture, in contrast to the conventional carbon capture processes in the US. Roy et al., 2014 have done an experimental investigation on oxy-fuel fluidized bed combustion using Victorian brown coal. They observed around 92% CO_2 in dry flue gas using 12% steam delivered in to the combustion chamber. Besong et al., 2014 have studied about design parameters affecting the performance of CO_2 purification units in oxy-fuel combustion. They assessed the effect of design parameters on performance including CO_2 product purity, recovery rate and specific power consumption. They found a good performance when treating flue gas of high CO_2 concentration, with purity of over 98%, recovery rate over 93%, and power consumption of 165 kWh/t CO_2 captured.

Table 2.2 Bench and pilot scale experimental studies on gas temperature and heat transfer in atmospheric oxy-coal combustion

References	Fuel	Facility	Recycle mode	Results
Abele et al., 1988	Wage coal from Colorado	117 kWth, bench scale furnace, i.d. 0.6 m	Wet/Dry FGR	Flue gas recycle ratios [$(CO_2+H_2O)/O_2$ in the oxidant] of 3.25 and 2.6, in wet and dry recycle respectively, matches the overall heat transfer of the air-fired furnace
Woycenko et al., 1995	Coal	2.5 MW, 2×2 m internal square cross-section	CO_2/O_2 mixture	58-61% of the flue gas is recycled for stable combustion and matched convective heat transfer coefficient and radiative heat flux
Nozaki et al., 1997	Bituminous coals from UK and international sources	Down-fired 20 kWth combustor	Wet FGR	Oxy-Propane combustion: With an O_2 mole fraction of 25%, the temp profiles in the furnace can be matched with that of air-propane combustion. Soot formation also plays an important role in the radiation intensity in air and oxy-combustion of propane. Calculated gas radiation is higher in oxy-combustion than in air combustion, but contributes only 30%e50% of the total radiation intensity. Oxy-Lignite coal combustion: With an O_2 mole fraction of 25%, the temp distribution can be matched with that of air-fuel combustion; the flue gas temp at the furnace outlet are lower in all the oxy-fuel cases than in air-fuel case.
Liu et al., 2005	Propane and lignite coal	100 kWth	CO_2/O_2 mixture	Gas temperatures of the oxy-fuel flame with a wet recycle ratio of 53% (39.3% O_2 in the burner gas) are lower before the level 3 measurement port, and higher at all following levels.
Tan et al., 2006	Low- and medium-volatile bituminous Coal	1.2 MWth horizontal combustion test facility	Dry FGR	When using an average oxygen mole fraction of 27% in the burner streams, the maximum flame temperature in oxy-fuel combustion is 100-150 ˚C lower than the air-fuel flame temp. The gas temp downstream of the burner are almost matched with that of air-fuel combustion.

Wall et al., 2009	Russian and South African coals	0.5 MWth, RWEn combustion test facility	Wet/Dry FGR	When using a secondary gas stream with an oxygen mole fraction of 30%, and dry recycled flue gas as the primary gas, the gas temp near the burner is lower in oxy-fuel combustion; the gas temp is greatly increased with direct oxygen injection; drying the primary gas increases the gas temp by 150 ˚C near the burner.
Hjartstam et al., 2009	Three Australian coals	1.2 MWth pilot scale vertical test facility	Simulated Dry FGR	Peak radiative heat flux values are inversely related to the recycle ratio. Conversely, the convective heat transfer values increase with increasing recycle ratio. A matched radiative heat transfer is established at recycle ratio between 68% and 72% for Russian coal, and between 72% and 75% for South African coal, respectively. The experimental data show that matched heat transfer characteristics can be established with about 74% dry recycle ratio for Russian coal.
Rehfeldt et al., 2009	Tselentis coal	1 MWth, horizontal firing	Wet FGR	When air is used as the primary stream, an O_2 concentration of 30% in the secondary stream produces matching gas temp profiles. When an oxygen concentration of 30% is used in both primary and secondary stream, the resulting gas temperature is higher than air-coal combustion.
Rehfeldt et al., 2009	Lausitz lignite coal from Germany	500 kWth, down-shot firing	Wet FGR	Gas temperatures of the oxy-fuel flame with a dry recycle ratio of 76% (21.3% O_2 in the burner gas) are lower than the temp in air-fired flame.
Smart et al., 2010	Bituminous, sub-bituminous, and lignite coals	0.3 MWth, (VCRF), cylinder down-flow, 0.6 m inner diameter	CO_2 /O_2 mixture, or Partial FGR with make-up CO_2	With an O_2 mole fraction of 28%-35%, the gas temperatures and heat fluxes can be matched with those of the air-coal combustion.

Luo et al., 2012	membrane 40 $Mn_{1.5}Co_{1.5}O_{4-d}$ – 60$Ce_{0.9}$ $Pr_{0.1}$ O_{2-d}	High-temp oxygen permeation cell, alumina tube of Ø=16 mm at 950 ˚C in air for 5 h with a gold paste and quartz tube (Ø=24 mm)	Air/CO_2	An oxygen permeation flux of 0.48 mL cm^{-2} min^{-1} was obtained at 1000 ˚C under an air/CO_2 oxygen partial pressure gradient through a membrane with a thickness of 0.3 mm. The 40MCO–60CPO dual phase membrane can be operated for at least 60 h when pure CO_2 was used as sweep gas, suggesting that the 40MCO–60CPO dual phase membrane is CO_2 stable.
Soundararajan et al., 2013	Bituminous Douglas premium coal	Oxygen rich environment with gross electric power output of 774 MW for the baseline case and 792 MW	CO_2 /O_2 mixture	Recovery of latent heat from the flue gases is increased due to the elevated dew point in the pressurized case. This results in a net LHV and HHV efficiency improvement of 1.7 percentage points each over the baseline case. In both the cases, over 90% of the produced CO_2 is captured and compressed to 110 bar after removal of volatiles and other pollutants such as SO_x and NO_x
Roy et al., 2014	Victorian brown coal	fluidized bed quartz reactor (of around 550 mm high and an inner diameter of 40 mm),	CO_2 /O_2 / N_2 mixture	The CO_2 concentration in flue gas decreases with the increase in oxygen concentration in oxidant, as expected. At the same oxygen concentration in the combustion environment, the flue gas CO_2 concentration increases only slightly with the bed temperature. Oxy-fuel combustion atmosphere with steam results in higher CO_2 concentration in flue gas. Around 92% CO_2 in dry flue gas was observed using 12% steam delivered in to the combustion chamber.

2.4 POST COMBUSTION CO_2 CAPTURE

Post combustion capture involves removal of CO_2 from flue gas, which comes from the thermal power plant combustion chamber as shown in Figure 2.3 [Feron and Hendriks, 2005]. Existing power plants used air for combustion and generate a flue gas at atmospheric pressure and typically have a CO_2 concentration of less than 15%. Thus, the thermodynamic driving force for low CO_2 capture from flue gas is creating a technical challenge for the development of cost effective advanced capture processes.

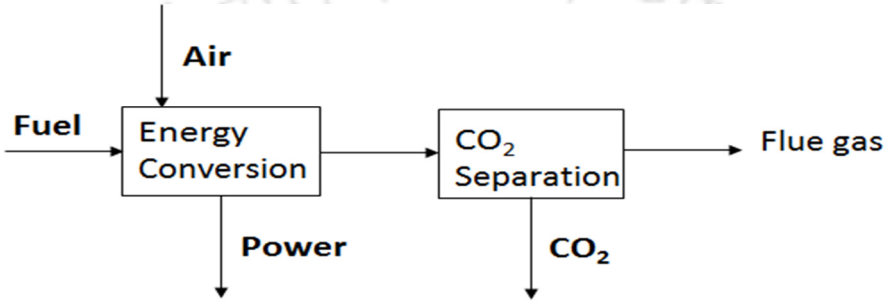

Fig 2.3 Schematic of post combustion CO_2 capture process [Figueroa et al., 2008]

Post combustion capture technology has a higher thermal efficiency for conversion to electricity than pre combustion Integrated Gasifier Combined Cycle (IGCC). It appears likely to give lower total electricity costs than pre combustion capture for natural gas plants [Yang et al., 2008]. Separation of CO_2 from flue gas stream of post combustion system is challenging for several reasons. The relatively high temperature of the flue gases offers a design challenge. Another challenge is that powerful chemical solvents have to be used for low concentration of CO_2 capture and regeneration of the solvents to release CO_2 which will require a large amount of energy [Gibbins et al., 2008]. Current post combustion technologies employ methods such as chemical absorption, adsorption, gas separation membranes, and cryogenic distillation which are discussed in detail in the following sections.

2.4.1 CHEMICAL ABSORPTION

Chemical absorption is the preferred method for capturing CO_2 from post combustion flue gas streams containing low to moderate partial pressures of CO_2 (3–20%) [3]. The term absorption

refers to the separation process in which a gaseous component is separated from a gas stream by the use of a liquid. The gaseous component comes into contact with the liquid and is absorbed from the gas phase into the liquid phase [Yang et al., 2008]. The liquid used for absorption is often referred to as the solvent or absorbent. Factors which need to be considered when choosing an absorbent are the solubility of the gaseous component in the absorbent and reactive properties of the gaseous component and the absorbent. For example, CO_2 is considered an acid gas. This means that when absorbed by water based absorbent, an acidic solution will form. Thus, for acid gas absorption it is desirable if the absorbent is alkaline. Alkaline solutions are basic in pH which enables the neutralization of any acid formed upon absorption of the gas, thereby increasing the amount of gas which can be absorbed for a given volume of liquid. A well-known acid gas absorption process is the removal of SO_2 from combustion gas streams, called flue gas desulphurization (FGD). In FGD SO_2 is removed from flue gas streams by countercurrent contact with lime slurry in a packed bed absorption column [Babcock and Wilcox, 1992]. The lime slurry neutralizes any acid formed when the SO_2 is absorbed into solution.

In CO_2 absorption processes it is common for the flue gas stream to first go through a pretreatment step to remove impurities such as particulate matter, SO_X, and NO_X. The degree to which the flue gas needs to be treated will vary depending upon the fuel being combusted, the absorption process/equipment design, and the interactions between the absorbent and impurities. Several chemical absorption processes do exist, differing in the absorbent used to capture CO_2. The four major processes are: amine absorption, aqua ammonia absorption, dual-alkali absorption and sodium carbonate (Na_2CO_3) slurry absorption [Olajire et al., 2010; Pires et al., 2011].

2.4.1.1 AMINE ABSORPTION

Amine absorption has been used by the natural gas industry for over 60 years to remove CO_2 from natural gas to produce food and beverage grade CO_2 [Yang et al., 2008]. Amines are derivatives of ammonia (NH3), with one or more of the hydrogen groups being substituted with a functional group (e.g. ethanol), common amines include monoethanol amine (MEA), diethanolamine (DEA), and methyl diethanolamine (MDEA); with the most common being

MEA due to its low cost. Basic MEA absorption will be used as an example going forward. The CO_2 is absorbed by, and chemically reacts with, the MEA solution to form a MEA carbamate and bicarbonate solution. The reaction can be seen in Equation 2.1 [Herzog, 2004]. The weight % MEA in solution can vary from 15–35% depending upon the process.

$$C_2H_4OHNH_2 + H_2O + CO_2 \longleftrightarrow C_2H_4OHNH_3^+ + HCO_3^- \quad (2.1)$$
$$\Delta H_{rx} = -20 kcal/mol$$

2.4.1.2 AQUA AMMONIA ABSORPTION

The aqua ammonia (NH_3) process has gained interest because of speculation that it could simultaneously remove NO_x and SO_x along with CO_2 from flue gases [Resnik et al., 2004]. For absorption with ammonia, the flue gas is cooled to 15–27 ˚C (due to the volatility of ammonia) then contacted with the ammonia solution in a packed bed absorption column to capture CO_2, and possibly NO_2 and SO_3. The reaction mechanisms for CO_2 capture in an ammonia solution are seen in Equation 2.2 and 2.3 [Yun et al., 2003; Figueroa et al., 2008; Liu et al., 2009; Olajire et al., 2010].

$$2NH_{3(aq)} + CO_{2(g)} + H_2O_{(l)} \rightarrow (NH_4)_2CO_{3(S)} \quad (2.2)$$

$$NH_{3(aq)} + CO_{2(g)} + H_2O_{(l)} \rightarrow NH_4HCO_{3(s)} \quad (2.3)$$

Possible products formed during CO_2 capture using aqueous ammonia include solid ammonium carbonate and bicarbonate. Bai and Yeh reported the formation of solid NH_4HCO_3 upon sparging CO_2 through an ammonia solution [Bai et al., 1997]. Yeh and Bai also found that a 35 wt.% ammonia solution has a carrying capacity of 1.20 kg CO_2/kg NH_3 in a clean gas stream (CO_2/N_2) [Yeh et al., 1999]. If the impurities NO_x and SO_x are present in the flue gas it may be advantageous to simultaneously capture them along with CO_2 using the ammonia solution. For simultaneous capture of NO_x and SO_x, pretreatment entails an oxidation stage in which the NO_x and SO_x are oxidized to NO_2 and SO_3. Ammonia solutions can only absorb the NO_2 and SO_3 forms of NO_x and SO_x gases.

2.4.1.3 DUAL ALKALI ABSORPTION

The dual alkali absorption approach is a modification of the Solvay process. To understand what the dual alkali approach is proposing, it is necessary to first have an understanding of the Solvay process. The Solvay process is a two-step process which converts CO_2 into Na_2CO_3 for commercial use. In the first step of the Solvay CO_2 is reacted with sodium chloride (NaCl), ammonia, and water to produce sodium bicarbonate ($NaHCO_3$) and ammonium chloride (NH_4Cl), as seen in Equation 2.4 [Yang et al., 2008; Olajire et al., 2010].

$$CO_{2(g)} + NaCl_{(aq)} + NH_{3(aq)} + H_2O_{(l)} \rightarrow NaHCO_{3(s)} + NH_4Cl_{aq} \quad (2.4)$$

Ammonia represents the primary alkali and is used to catalyze the absorption of CO_2. The NaCl is added to increase the concentration of Na in solution. This helps increase the precipitation of $NaHCO_3$. In the second step of the Solvay process the solid $NaHCO_3$ is filtered out of solution and heated to produce commercial grade Na_2CO_3. The leftover NH_4Cl solution is reacted with the secondary alkali, calcium hydroxide ($Ca(OH)_2$), to regenerate the NH_3 as seen in Equation 2.5 [Huang et al., 2001].

$$NH_4Cl_{(aq)} + Ca(OH)_{2(aq)} \rightarrow 2NH_{3(aq)} + CaCl_{2(aq)} + 2H_2O_{(l)} \quad (2.5)$$

The main reason the Solvay process is not applicable to post combustion capture of CO_2 is that $Ca(OH)_2$ is used for regeneration. Calcium hydroxide is produced from lime which is formed by calcination of $CaCO_3$. The high energy demand of the calciner and CO_2 production from calcination make this process undesirable for large scale CO_2 capture.

2.4.1.4 ABSORPTION WITH SODIUM CARBONATE SLURRY

Using Na_2CO_3 solutions CO_2 was captured in the early 1900s for the production of dry ice [Howe et al., 1928; Comstock et al., 1937]. Knuutila and coworkers have conducted a computer simulation to examine using a Na_2CO_3 slurry to capture CO_2. The simulations varied the Na_2CO_3 wt.% (10–30%), the inlet liquid temperature (45–70 ˚C), inlet flue gas temperature (45–70 ˚C), liquid to gas (L/G) ratio (2.1–5.5), and the stripper pressure (1–2 bar) to determine the optimal CO_2 capture efficiency and amount of energy required to operate the stripper. Optimal conditions determined by the simulation were: 30 wt.% Na_2CO_3 slurry, inlet liquid temperature of 60 ˚C, inlet flue gas temperature of 70 ˚C, L/G ratio of 2.3, and a stripper pressure of 2 bar. At these

conditions, the simulation predicted 90 % CO_2 capture efficiency and an energy requirement of 3.2 MJ/kg CO_2 in the stripper. A sulphur free flue gas was assumed for the simulations. The simulated gas stream consisted of $CO_2/N_2/H_2O$ vapor [Knuutila et al., 2009].

As previously mentioned, for the capture of CO_2 the simulations found that a 30 wt.% Na_2CO_3 slurry and an inlet flue gas temperature of 70 ˚C was optimal. This creates an environment in which $NaHCO_3$ precipitates out of solution allowing for more Na_2CO_3 to dissolve in solution; thereby increasing the CO_2 capacity of the solution. The capture of CO_2 and precipitation of $NaHCO_3$ via the carbonate slurry can be seen in Equation 2.6 and 2.7 [Knuutila et al., 2010].

$$CO_3^{2-}{}_{(aq)} + H_2O_{(l)} + CO_{2(g)} \rightarrow 2HCO_3^- \quad (2.6)$$

$$Na^+{}_{(aq)} + HCO_3^{-1}{}_{(aq)} \longleftrightarrow NaHCO_{3(s)} \quad (2.7)$$

There was no mention made to the CO_2 carrying capacity of the slurry in the study performed by Knuutila and coworkers. However, a quick calculation based on Equation 2.6 gives a theoretical carrying capacity of 0.73 kg CO_2/kg CO_3^{2-}, higher than that of MEA (0.40 kg CO_2/kg MEA). If impurities are present it is likely that this carrying capacity will decrease. For example, if SO_2 is present in the flue gas it may be absorbed by the solution, most likely creating sodium sulfite (Na_2SO_3) and sodium bisulfate ($NaHSO_3$) in solution [Wappela et al., 2009]. This would lower the carrying capacity of the Na_2 CO_3 slurry but provide a multi pollutant control system. Pretreatment of the flue gas would be optional when using Na_2CO_3 slurry.

2.4.2 MEMBRANE SEPARATION

Membrane separation processes are currently used commercially for CO_2 removal from natural gas; in these streams, the overall pressure and CO_2 concentration are high and the stream consists mainly of CO_2 and CH_4 [Metz et al., 2005]. This stream is far different from the stream which would be encountered in post combustion flue gas streams which contain impurities such as NO_x and SO_x at atmospheric pressure. A simplified flow diagram of post combustion membrane based CO_2 capture can be seen in Figure 2.4 [Olajire et al., 2010; Khoo et al., 2006]. The membrane acts as a filter to remove one or more gas components from a mixture and generate a component rich permeate. The driving force behind the performance of membranes is the

pressure differential between the feed side and the permeate side of the membrane, as seen by Fick's Law in Equation 2.8 [Scholes et al., 2008].

$$j_i = \frac{P_i^*}{\delta} A_m \Delta p \tag{2.8}$$

where j_i is the flux of component i across the membrane (cm^3/s), P_i* is the permeability of the membrane in terms of component i (10^{-10} cm^3(STP) cm/s cm^2 cmHg), δ is the membrane thickness (cm), A_m is the membrane area (cm^2), and Δp is the pressure difference (cmHg) across the membrane. Fick's Law shows the importance of the pressure differential and permeability in membrane separation; as the pressure differential and permeability increase the flux of a specific component across the membrane will also increase. There are two characteristics that describe the performance of a membrane, permeability (commonly expressed in units of barrer) and selectivity. Permeability is defined as the volume of a gas species passing through the membrane per unit time and area. Selectivity is determined by the difference in permeability of the gas species: selectivity quantifies a membranes preference to pass one gas species over another [Treybal et al., 1955]. A brief discussion follows about organic and inorganic membranes with regards to CO_2 removal from CO_2/N_2 gas streams. Also discussed are mixed matrix membrane systems and hybrid membrane/absorption systems.

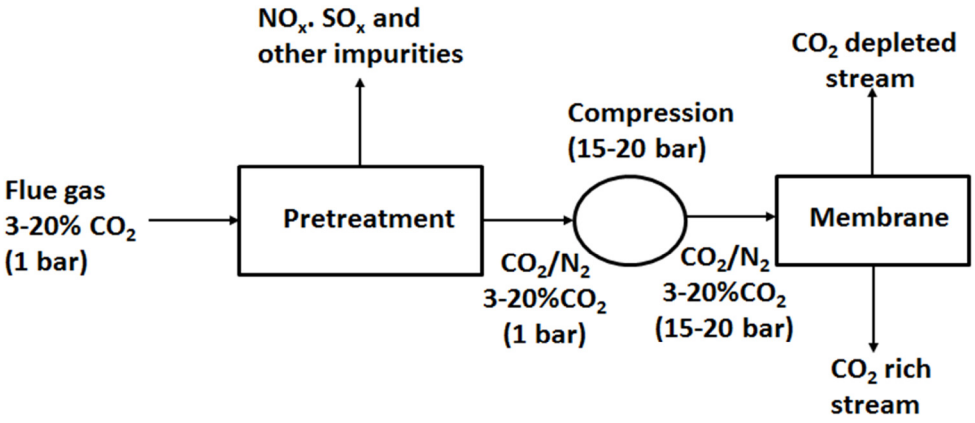

Fig 2.4 Process flow diagram for membrane based CO_2 capture [Pires et al., 2011]

A large variety of polymeric membranes provide good permeability and selectivity towards CO_2 in CO_2/N_2 gas streams [Pwell, 2006]. These include polyimides, polycarbonates, polyethylene oxides (PEO), polyacetylenes, polyaniline, poly (arylene ether)s, polyarylates, polyphenylene ethers and polysulfones [Stern et al., 1989; Lin et al., 1994; Illing et al., 2001]. While, Inorganic

membranes can be divided into two categories: porous and non-porous. In general, the non-porous membranes are used for highly selective separation of small molecule gases. The porous membrane systems consists of a porous thin top membrane layer which is cast on a porous support, usually metallic or ceramic, to provide mechanical strength. The support must offer minimal mass transfer resistance with respect to the component being removed [Xu et al., 2002; Pixton et al., 1995; Aguiler-Vega et al., 1993]. Porous inorganic membranes are cheaper than the non-porous membranes, but are less selective with respect to CO_2. Inorganic membranes also suffer from the disadvantage of difficult scale up to large surface areas. Common porous inorganic materials include alumina, silica, and zeolites. Mixed matrix membranes are designed to enhance the properties of polymeric membranes. They consist of micro or nano sized inorganic particles incorporated into a polymeric matrix. The addition of inorganic particles enhances the physical, thermal, and mechanical properties of a polymeric membrane thus better suiting them for CO_2 removal from flue gases. Challenges associated with mixed matrix membranes include their high cost, brittleness, and difficult commercial scale manufacture [Yang et al., 2008].

Membrane contactor systems combined a membrane with an absorption liquid, such as an amine, into one unit. The absorption liquid could be any liquid used for absorbing CO_2. The target of these systems is to reduce the size of the absorption unit associated with traditional CO_2 absorption systems [Favre et al., 2012]. With membrane contactors the gas phase is isolated from the liquid phase via a porous, water repellent polymeric membrane. It is crucial that the gas and liquid phase do not mix, thus the membrane should be hydrophobic. The flue gas stream is fed along one edge of the membrane while the absorption liquid is fed along the other edge. The CO_2 will diffuse through the membrane where it contacts, and is absorbed by, the absorption liquid. The remainder of the flue gas is vented to the atmosphere [Xu et al., 2002].

2.4.3 CRYOGENIC DISTILLATION

Cryogenic distillation has been utilized for years to separate atmospheric air into its primary components, but it is a relatively novel idea for post combustion capture of CO_2. In a cryogenic separation system, CO_2 is physically separated from other gas stream constituents on the basis of

dew and sublimation points [Khoo et al., 2006; Tuiniera et al., 2010]. The main advantage to cryogenic separation is that no chemical reagents are needed. Two cryogenic separation technologies for post combustion capture of CO_2 have been proposed: (1) Clodic and Younes have proposed a process in which gaseous CO_2 is de-sublimated onto the surface of heat exchanger fins and then recovered as liquid CO_2 at elevated pressures [Clodic et al., 2002]; (2) Tuinier and coworkers have proposed a process using packed beds where the CO_2 is de-sublimated onto the packing material then released to produced gaseous CO_2 [Tuiniera et al., 2010]. Each process will be discussed in more detail to better understand the differences between the two. The process proposed by Clodic and Younes has been studied on pretreated gas streams of $CO_2/H_2O/N_2$ and has 93% CO_2 removal efficiency from a 15% CO_2 containing gas stream. A simplified process flow diagram can be seen in Figure 2.5.

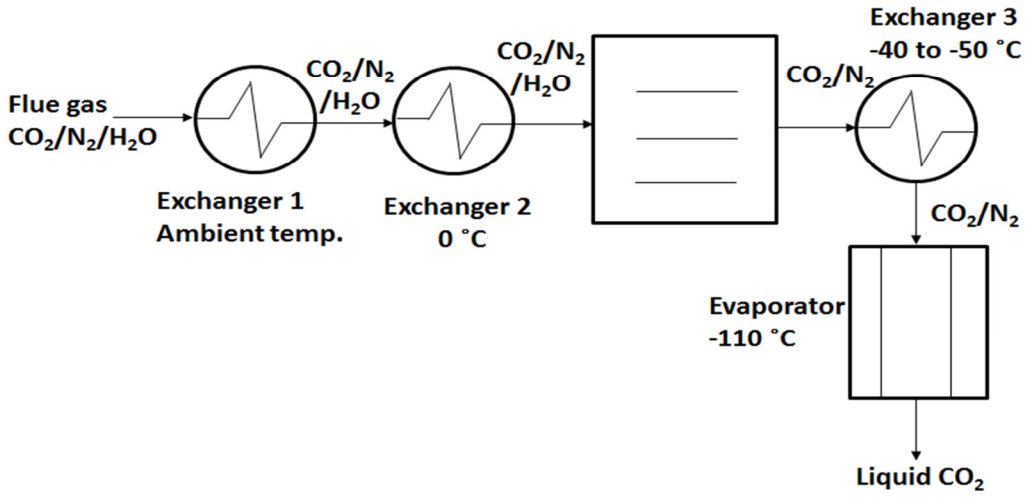

Fig 2.5 Process flow diagram for cryogenic distillation of CO_2 [Clodic et al., 2002]

First, the entering flue gas stream (60–100 ˚C) is cooled to near ambient conditions using ambient air and water. The water helps to remove any residual particulates in the gas stream. The flue gas then enters a second heat exchanger where the temperature is reduced to just above 8 ˚C to remove water vapor. The flue gas is then passed through a dehydrator to remove any trace elements of water. (Since the operating temperature of the system is well below the freezing point of water, it is critical that all traces of water be removed from the system to prevent unwanted pluggin and system efficiency degradation from ice formation. The water levels in the dry flue gas must be reduced to 1.1×10^{-4} g H_2O/g dry flue gas.) After the remaining water is

removed from the flue gas, third exchanger is used to bring the flue gas temperature down to -40 to -50 ˚C. This stage is primarily used to condense trace gases or any unburned hydro carbons still present. The flue gas stream, now composed of CO_2/N_2, is sent to an evaporator operated at an average temperature of -110 ˚C. The CO_2 de-sublimates onto the cold surface in the evaporator while the N_2 exits unaffected. The solid CO_2 is then recovered as a liquid by 'heating' the system to -56 ˚C under 520 kPa (roughly 5 atm) of pressure [Pires et al., 2011; Tuiniera et al., 2010].

The process proposed by Tuinier and coworkers looks to circumvent the drawbacks associated with Clodic's process, such as the need for complete H_2O removal and costly high pressure vessels. Tuinier's technology utilizes three packed beds to continuously capture CO_2. Each bed operates a different cycle: capture, recovery, and cooling. During the capture cycle CO_2 is separated from the $CO_2/H_2O/N_2$ gas stream in a packed bed at -150 ˚C. In the capture stage the H_2O first condenses out of the gas stream onto the packing material. As the H_2O in the gas stream becomes depleted the CO_2 will then start to de-sublimate onto the cold packing material. As the fresh flue gas is fed to the bed it heats up the packing material causing the de-sublimated CO_2 to transition to the gas phase producing a gaseous CO_2 stream. The CO_2 stream is then fed to the recovery bed at roughly -70 ˚C. Due to the increased partial pressure of CO_2 in this stream some CO_2 will, again, de-sublimate onto the cold packing material. As the fresh CO_2 stream continues to be fed to the recovery bed the packing material is heated up. This causes the desublimated CO_2 to transition to the gas phase again, creating a concentrated CO_2 stream which is compressed for various uses. During the cooling cycle the H_2O remaining in the beds is removed and vented to the atmosphere [Tuiniera et al., 2010; Clodic et al., 2005].

For cryogenic distillation processes, the flue gas still needs to go through a pretreatment step to remove impurities such as NO_x and SO_x to increase the concentration of CO_2 in the gas stream. As the concentration of CO_2 in the gas stream increases, the temperature that the gas stream must be cooled to for CO_2 de-sublimation becomes less negative. For example, at 2% CO_2 in the gas stream the temperature required for de-sublimation is -116 ˚C, while at 15% CO_2 the temperature required is -99 ˚C. For operation it is recommended the flue gas stream contain greater than 10%

CO_2, as lower concentrations of CO_2 will lead to higher cooling requirements per mass of CO_2 captured [Clodic et al., 2005].

2.4.4 ADSORPTION PROCESS

CO_2 capture using solid adsorbents is considered one of the most promising technologies for CCS [Figuera et al., 2008]. Gas adsorption is a separation process in which a gaseous component is separated from a gas stream by the use of a solid material. The adsorption processes are based on significant intermolecular forces between gases (including CO_2) and the surfaces of certain solid materials (such as molecular sieves and activated carbon). Depending on the temperature, partial pressure, surface force and adsorbent pore sizes, single or multiple layers of gases can be adsorbed [Axel et al., 1997]. In CO_2 capture by adsorption technology, a packed column is mainly filled by spherical adsorbent and CO_2 bearing stream is passed through the column. CO_2 is attracted towards the adsorbent and adheres on the surface of adsorbent. After achieving the equilibrium, desorption takes place to get CO_2 in pure form and regenerated adsorbent can be utilized for further cycle. This process can be carried out in different manners as discussed in the preceding section.

A number of adsorption processes are used commercially for adsorbent process, including pressure swing adsorption (PSA), vacuum pressure swing adsorption (VPSA), electrical swing adsorption (ESA) and thermal or temperature swing adsorption (TSA). A number of research works have been done using the processes mentioned above on different types of adsorbent materials. Recent developments have demonstrated that PSA is a promising option for separating CO_2 due to its ease of applicability over a relatively wide range of temperature and pressure conditions, its low energy requirements, and its low capital investment cost [Agarwal et al., 2010b]. Many studies concerning CO_2 removal from various flue gas mixtures by means of PSA processes have been addressed in the literature. Prior to the design of an adsorption process, selecting an appropriate adsorbent with high selectivity and working capacity, as well as a strong desorption capability, is key to separating CO_2. As a result, a wide variety of adsorbents like activated carbon, zeolites, silica gel, activated alumina, urea–formaldehyde and melamine–formaldehyde resins, poly-ethylenimine and hollow fibre carbon membranes based adsorbents,

etc. have been investigated for this purpose [Chue et al., 1995; Sircar et al., 1998; Xu et al., 2005; Drage et al., 2007; He et al., 2009].

2.4.4.1 CO_2 ADSORPTION ONTO ZEOLITE 13X

Most research studies on CO_2 adsorption by zeolite 13X have been aimed at determining the adsorption isotherm at low pressure ranges close to atmospheric pressure (up to 1.2 atm). Costa et al., 1991 measured the CO_2 adsorption isotherm at different temperatures and up to 1 atm. Calleja et al., 1994 also measured the isotherm at the low pressure range (up to 0.9 atm) and fitted the obtained data with different isotherm models. Chue et al., 1995 measured the CO_2 adsorption isotherm so as to evaluate the performance of zeolite 13X in a pressure swing adsorption process. The measurement was made up to 1.05 atm. Lee et al., 2002 investigated the CO_2 adsorption equilibrium on zeolite 13X at low pressure (1 atm). The isosteric heat of adsorption was also analyzed from the obtained equilibrium data. Li et al., 2008 and Zhang et al., 2009 reported the use of zeolite 13X for removing CO_2 from flue gas containing humidity and other impurities. They also provided the adsorption isotherm at 1.2 atm and breakthrough analysis of CO_2 removal. Wang and Levan, 2009 measured the adsorption isotherm at different temperatures and up to 1 atm. The obtained data were fitted with the Toth model.

There are only a few studies focusing on CO_2 adsorption by zeolite 13X at medium pressure ranges. Harlick and Tezel, 2004 investigated the adsorption capacity and the heat of adsorption for a number of adsorbents including zeolite 13X at pressures up to 2.5 atm. Merel et al., 2008 compared the adsorption performance between zeolites 13X and 5A at pressures up to 4.9 atm and reported the adsorption isotherm, as well as breakthrough curves of CO_2 adsorption. For studies at high pressure ranges, Cavenati et al., 2004 measured the CO_2 adsorption isotherm and analyzed the isosteric heat of adsorption at pressures up to 49.4 atm. Zhang et al., 2010 investigated the adsorption equilibrium and kinetics at different temperatures and up to 29.6 atm.

2.4.4.2 CO_2 ADSORPTION ONTO ZEOLITE 5A

The adsorption of CO_2 by zeolite 5A has been studied since 1970`s. In 1980, Yucel and Ruthven investigated the adsorption isotherm and kinetics at pressure as low as 0.4 atm. The adsorption

kinetics, activation energy, and heat of adsorption were reported by Triebe and Tezel, 1995 for the removal of CO_2 from air. Pakseresht et al., 2002 investigated adsorption equilibrium at different temperatures at intermediate pressure (up to 9.9 atm). Tlili et al., 2009 reported the adsorption equilibrium and breakthrough curve at 1 atm. Saha et al., 2010 studied the adsorption equilibrium and kinetics of CO_2 adsorption from air and methane at 1.05 atm. Finally, Liu et al., 2011 investigated the equilibrium isotherm at different temperatures and the pressure up to 1 atm. For the high pressure range, Chen et al., 1990 reported the adsorption isotherm at pressures up to 54.5 atm. Kim et al., 1995 studied the isotherm, heat of adsorption, and breakthrough curves for removal of CO_2 from H_2 gas at 27.5 atm.

2.4.4.3 CO_2 ADSORPTION ONTO ZEOLITE 4A

Eagan and Anderson, 1975 investigated the CO_2 adsorption isotherm for zeolite 4A at pressures up to 1.02 atm. Yucel and Ruthven, 1980 measured the CO_2 adsorption kinetics at different temperatures at 0.4 atm. Siriwardane et al., 2001 reported the use of zeolite 4A for the separation of CO_2 from a high pressure flue gas stream at 20.4 atm. Ahn et al., 2004 investigated the equilibrium isotherm and kinetics at 0.8 atm.

2.4.4.4 CO_2 ADSORPTION ONTO ACTIVATED CARBON

Most research studies on CO_2 adsorption by activated carbon have been carried out at high pressure ranges. Amoros et al., 1996 studied the CO_2 adsorption characteristics of activated carbon at pressures up to 39.5 atm. Dreisbach et al., 1999 measured and modeled the adsorption isotherm at 59.2 atm. The use of activated carbon for removing CO_2 from the flue gas was investigated by Siriwardane et al., 2001 at 20.4 atm and by Millward and Yaghi, 2005 at 44.4 atm. They also reported the corresponding CO_2 adsorption equilibrium. Sudibandriyo et al., 2003 investigated CO_2 adsorption on activated carbon at a very high pressure of 133.3 atm. Drage et al., 2009 reported the equilibrium capacity and kinetics of CO_2 adsorption from synthetic gas at 39.5 atm. For low pressure applications, Chue et al., 1995 investigated the CO_2 adsorption isotherm at 1.05 atm. Guo et al., 2006 measured and modeled the isotherm and isosteric heat of

adsorption at 3.9 atm. Vaart et al., 2000 reported the CO_2 adsorption isotherm at a pressure of 7.9 atm.

2.4.4.5 OTHER TYPE OF ADSORBENTS

Recent development shows an improvement in adsorbent materials with higher adsorption capacity and selectivity like Activated carbon honeycomb monolith – Zeolite13X hybrid system, zeolites NaKA and nano-NaKA, FAU zeolites and zeolite 13X prepared from bentonite [Ribeiro et al., 2013; Cheung et al., 2013; Thang et al., 2014; Chen et al. 2014]. The PSA process is based on preferential adsorption of the desired gas on a porous adsorbent at high pressure, and recovery of the gas at low pressure. Thus, the porous sorbent can be reused for subsequent adsorption. PSA technology has gained interest because of the low energy requirements and low capital investment costs. Development of regenerable sorbents that have high selectivity, high adsorption capacity, and high adsorption/desorption rates for CO_2 capture is critical for the success of the PSA process. Cost of the sorbent is also a major factor that needs to be considered for the process to be economical [Tlili et al., 2009; Guerrin and Domine, 1964].

Literature survey indicates that there have been many attempts to obtain low cost activated carbon for adsorbents material for air pollution control as well as waste water treatment. The agricultural waste includes raw materials such as wheat, corn [Lanzetta and Di Blasi, 1998], olive stones, bagasse birch, miscanthus [Minkova et al., 2000; Minkova et al., 2001], sunflower shell, pinecone, rapeseed, cotton residue, olive residues [Haykiri-Acma et al., 2005; Predel and Kaminsky, 1998]. Other promising raw materials for activated carbon from cheap materials include grape seeds, cherry stones, nut shells [Savova et al., 2001], cotton stalk [Putun et al, 2005], Peanut hull [Girgis et al., 2002], hazelnut shells [Aygun et al., 2003], bamboo waste [Mahanim et al., 2011] and rice straw [Ahmedna et al., 2000]. The use of agricultural by-products for activated carbon production as well as the influence of ash content, pyrolysis and activation conditions on the activated carbon quality is investigated by many authors. The high ash content of rice straw makes it difficult to achieve a sufficiently high surface area [Ahmedna et al., 2000]. While, highly microporous carbons with high surface areas are produced by chemical activation of hazelnut, walnut and almond shells and of apricot stones (Aygün, et al.,

2003). But, due to the unavailability of these materials, other materials like Coconut fiber will be considered because of its low cost and availability in abundant.

2.4.5 MODELING OF CO_2 ADSORPTION IN A FIXED BED

In most adsorption process, the adsorbent is in contact with a fluid in a packed bed. An understanding of the dynamic behavior of such systems is therefore required for rational process design and optimization [Rutherford and Do, 2000a]. The dynamic behavior of an adsorption column system can be classified based on the nature of the gas- solid equilibrium relationship of fluid constituents and the complexity of the mathematical model required for describing the mechanism by which the mass transfer from the fluid to the solid phase occurs [Ruthven, 1984]. Table 2.6 provides a comprehensive classification scheme of the summary of the fixed bed column mathematical models for CO_2 adsorption developed over the last three decades. All of the models assume that the gas phase the ideal gas law. The flow pattern is described by the plug flow or axially dispersed plug flow model. It is further assumed that the radial gradients of concentration and, where applicable, temperature and pressure are negligible. The assumption that the radial gradient is negligible has been widely accepted in many other studies [Jee et al., 2002; Kim et al., 2004, 2006].

2.4.5.1 DEVELOPMENT AND ANALYSIS OF MATHEMATICAL MODEL

The fixed-bed column mathematical models are used to predict the transient behavior of the concentration and temperature profiles for any defined changes in the initial parameters such as feed concentration, temperature, and flow rate. A complete mathematical model capable of describing the dynamic behavior of a fixed-bed adsorption system is established based on a set of fairly complex partial differential and algebraic equations (PDAEs) constructed from conservation of mass, energy, and momentum and augmented by appropriate transport rate equations and equilibrium isotherms [Hwang et al., 1995]. The models used to represent a PSA process differ mainly in the form of the mass transfer rate, the form of the equilibrium isotherm, thermal effects, and the pressure drop along the bed. General descriptions of the above-mentioned items are presented in the following subsections. Many mathematical models for gas–

solid adsorption in an adsorption column have been published over the past few decades, and there is still interest in developing a description of the dynamic evolution of such systems [Afzal et al., 2010; Leinekugel-le-Cocq et al., 2007].

2.4.5.2 FLUID PHASE MATERIAL BALANCE

The transient gas phase component mass balance, which includes the axial dispersion term, convection flow term, accumulation in the fluid phase, and source term caused by the adsorption process on the adsorbent particles, can be represented by the following equation for a differential control volume of the adsorption column [Ruthven, 1984; Yang, 1987]:

$$-D_{zi}\frac{\partial^2 c_i}{\partial z^2}+\frac{\partial}{\partial z}(uc_i)+\frac{\partial c_i}{\partial t}+\left(\frac{1-\varepsilon_b}{\varepsilon_b}\right)\rho_p\frac{\partial \bar{q}_i}{\partial t}=0 \tag{2.9}$$

where c_i represents the adsorbate concentration in the fluid phase; z is the distance along the bed length; u is the fluid velocity; t denotes time; ε_b is the bed void fraction; ρ_p is the particle density; q_i denotes average concentration of component i in adsorbent particle, which forms a link between the fluid and solid-phase mass balance equations; and the effects of all mechanisms that contribute to axial mixing are lumped into a single effective axial dispersion coefficient, D_{zi}, which can be estimated using the following correlation [Da Silva et al., 1999;Ruthven, 1984; Wakao and Funazkri, 1978; Welty et al., 2000;Yang, 1987]:

$$\frac{\varepsilon_b D_{zi}}{D_{mi}}=20+0.5Sc\,\mathrm{Re} \tag{2.10}$$

where D_{mi} is the molecular diffusivity of component i and Sc and Re are the Schmidt and Reynolds numbers, respectively. The above equation, Equation 2.9, is used to find the distribution of gas composition along the bed. Assuming no radial dependence of concentration and solid loading, c_i and q_i, represent cross-sectional average values (these variables are functions of t and z). The well-known Danckwert's boundary conditions for a dispersed plug flow system can be assumed as follows [Khalighi et al., 2012; Wehner and Wilhelm, 1956]:

$$D_{zi}\frac{\partial c_i}{\partial z}\Big|_{z=0}=-u\Big|_{z=0}\left(c_i\Big|_{z=0}-c_i\Big|_{z=0}\right) \tag{2.11}$$

$$\frac{\partial c_i}{\partial z}\Big|_{z=L}=0 \tag{2.12}$$

where $c_i\big|_{z=0}$ represents the feed composition for component i and L is the bed length. In the above model, Equation 2.9, if the flow pattern is represented as plug flow, axial dispersion can be neglected, and therefore the term $-D_{z_i}\left(\frac{\partial^2 c_i}{\partial z^2}\right)$ can be dropped, reducing Equation 2.9 to a first order hyperbolic equation. This is a reasonable approximation, particularly for large industrial units, for which the term representing the axial dispersion is very small density and hence gas velocity vary along the bed. The following equation expressing the overall material balance for the bulk phase in the adsorption column is used to find the velocity distribution through the bed [Ko et al., 2005]:

$$-D_{zi}\frac{\partial^2 C}{\partial z^2}+\frac{\partial (uC)}{\partial z}+\frac{\partial C}{\partial t}+\left(\frac{1-\varepsilon_b}{\varepsilon_b}\right)\rho_p\sum_{i=1}^{n}\frac{\partial \bar{q}_i}{\partial t}=0 \tag{2.13}$$

where C is the total concentration in the bulk phase and n is the number of components.

2.4.5.3 COMPLEXITY OF KINETIC MODELS

The term $\frac{\partial \bar{q}_i}{\partial t}$ in Equation 2.9 represents the overall rate of mass transfer for component i (at time t and distance z) averaged over a particle. The mass balance for an adsorbent particle yields the adsorption rate expression, which may be written as:

$$\frac{\partial \bar{q}_i}{\partial t}=f(q_i, c_i) \tag{2.14}$$

For an isothermal system, the expressions for the concentration profiles in both phases, c_i (z, t), q_i (z, t), is given by the simultaneous solution of Equation 2.9 and 2.14, subject to the initial and boundary conditions imposed on the column. For non-isothermal systems, an energy balance must also be taken into account. In this case, all equations are coupled because, in general, both the equilibrium concentration and the rate coefficients are temperature dependent. Although the mass transfer rate expression, Equation 2.14, was written here as a single equation, it commonly consists of a set of equations comprising one or more diffusion equations with their associated boundary conditions. It is worth noting that a kinetic model is basically a mass balance that involves different variables describing mass transfer mechanisms within the adsorbent particle

[Chahbani and Tondeur, 2000]. A variety of mass transfer kinetic models with different degrees of complexity can be found in the literature. Mass transfer kinetic models can be classified into two main categories based on the assumption of local equilibrium or the existence of mass transfer resistance between the adsorbent particle and the fluid phase.

Hassan and Ruthven, 1986 developed dynamic model for a PSA air separation process based on linearized mass transfer rate expressions and binary Langmuir equilibrium. Constant pressure was assumed during adsorption and desorption steps but the variation in flow rate through the column due to adsorption was accounted for. While Farooq and Ruthven, 1990 developed a micropore diffusion model for a binary bulk pressure swing adsorption gas separation based on Langmuir equilibrium and allowing the concentration dependence of the diffusivity in accordance with the chemical potential gradient as the driving force. The model parameters have been determined from single-component and binary breakthrough curve measurements.

Baron, 1993 had done modeling of PSA process with 5A molecular sieve as an adsorbent. He deals with equilibrium-driven separations and examples of equations for equilibrium, transport phenomena and flow in packed beds were discussed. A general overview of the different proposed or tested models associated numerical methods and available software was given. Serna-Guerrero and Sayari, 2010 investigated the adsorption kinetics of CO_2 on amine-functionalized mesoporous silica at low concentrations. Experimental data of CO_2 uptake as a function of time at temperatures between 25 and 70 ˚C were fit to a series of kinetic models, namely Lagergen's pseudo-first and pseudo-second order and Avrami's kinetic models. The best fit was obtained using Avrami's model, as it provided a fractional reaction order, which has been associated with the occurrence of multiple adsorption pathways. In addition, simulations of CO_2 adsorption in a column packed with amine-grafted mesoporous silica using computational fluid dynamics were carried out to predict breakthrough curves.

A basic study of fixed-bed column mathematical simulations is essential for understanding the performance of the adsorption processes under various conditions to improve PSA operations and to develop new, more efficient PSA cycles. From the literature survey, it was evident that the design and modeling of a fixed bed adsorption system require the simultaneous solution of a set

of coupled PDEs representing mass, energy, and momentum conservation together with transport rate and equilibrium equations. The simultaneous solution of such a rather complex system of PDEs requires complicated numerical solutions, and the computation time is often inconveniently long. Therefore, the use of reduced models with satisfactory prediction capabilities is recommended to decrease the computational time and facilitate optimization. One option to simplify fixed-bed adsorption calculations is to simplify the representation of mass transfer phenomena within the adsorbent particles.

This section provides a fairly comprehensive review of the mathematical modeling of fixed bed adsorption of CO_2 conducted by various researchers over the last three decades. Various models for gas–solid adsorption equilibrium as well as different mass transfer mechanisms were reviewed. The majority of the models reviewed here include the effects of a finite mass transfer rate, resulting in a theoretical representation that more closely approximates a real process. Some of these models consider the effects of heat generation and heat transfer in the adsorbent bed, which may affect the adsorption rates. Terms corresponding to the pressure drop and velocity changes across the bed, which influence heat and mass transfer dynamically during the adsorption process, were also included in a few models. Summary of reviews on the dynamics model of CO_2 adsorption in a fixed bed is presented in Table 2.4.

Table 2.3 Reviews on the dynamics model of CO_2 adsorption in a fixed bed

Author	Model assumptions					Application	solution
	Equilibrium relationship	Flow pattern	Mass transfer rate	Heat effects	others		
Shendalman and Mitchell, 1972	Linear equilibrium isotherm	Plug flow	Local equilibrium model	Isothermal	No radial variation in cont. Negligible pressure drop Trace system	PSA separation of carbon dioxide from a He–CO_2 mixture using silica gel	Analytical results from a linear mathematical model obtained by the method of charactstics
Cen and Yang, 1985	A hybrid Langmuir–Freundlich isotherm	Plug flow	Local equilibrium/ linear driving force (LDF) approximation model	Non-isothermal	No radial variations in cont. and temp. Thermal equilm between the fluid and particles	Separation of coal gasification products containing H_2 , CO, CH_4, H_2S, and CO_2 by PSA using activated carbon	The model was solved using an implicit finite difference method which was stable and convergent
Raghavan et al., 1985	Linear equilibrium isotherm	Axial dispersed plug flow	LDF approximation with non-constant coefficient	isothermal	Negligible radial gradient of concentration Negligible pressure drop Trace system	PSA separation of carbon dioxide from a He–CO_2 mixture using silica gel	Sol. to the model eq. was obtained by orthogonal collection and using finite diff. methods with consistent results
Kaguei et al., 1989, 1985	Linear equilibrium isotherm	Axial dispersed plug flow	Pore diffusion model	Non-isothermal	Negligible radial cont. gradient Radial temp. and pre. profile in the column/uniform temp. in column	Theoretical and experimental studies on the CO_2 capture in a column packed with activated carbon particles	Analytical solution was performed in the Laplace domain under the condition of a semi-infinite column

Ahn and Brandani, 2005	Langmuir isotherm	Axial dispersed plug flow	LDF approximation model	isothermal	No radial variations in concentration	Prediction of the dynamics of CO_2 breakthrough in a carbon monolith column	The system of partial differential-algebraic eq (PDAEs) was coded in gPROMS software to obtain a numerical model
Grande and Rodrigues, 2008	Multisite Langmuir isotherm	Axial dispersed plug flow	A rigorous descriptn for macrpore diff. model as well as an LDF approx for micropre diff	Non-isothermal	No radial variations in temp, pr, and conc The pr. drop was described by Darcy's law	Low- concentration CO_2 removal from flue gas streams by electric swing adsorption using monolith	The mathematical model was solved using gPROMS 3.01 (PSE Enterprise, United Kingdom)
Shen et al., 2010	Virial isotherm model/Multisite Langmuir isotherm	Axial dispersed plug flow	Rigorous description of macropore and micropore diffusion models	Isothermal	Negligible radial conc. gradient, Constant vel. within the column	Adsorption of CO_2 on pitch-based activated carbon	Simulations of the presented mathematical model were performed in gproms using the orthogonal collocation on finite elements
Agarwal et al., 2012 a,b	Dual-site Langmuir isotherm	Plug flow	LDF approx. model with lumped mass transfer coefficient	Non-isothermal	No radial variations in temp, pr. and conc. The pr drop along the bed was calculated by the Ergun equation	CO_2 capture from an 85% to 15% N_2–CO_2 feed mixture using PSA cycles/ CO_2 capture from a synthesis gas feed mixture (55% H_2 and 45% CO_2) using PSA cycles	Finite volume method was applied in both spatial and time domains, and the resulting large scale non-linear progr problem (NLP) was solved using an interior point NLP solver

Mulgund math et al., 2012	Langmuir isotherm	Axial dispersed plug flow	LDF approximation model for external fluid film mass transfer.	Non-isothermal	Negligible Radial temp and conc gradients Negligible pressure drop	Fixed-bed adsorption of CO_2 from a CO_2–N_2 gas mixture (10% CO_2 in 90% N_2) using zeolite 13X	-

2.4.6 REVIEWS OF CO_2 ADSORPTION IN FLUIDIZED BED

The fluidized bed pressure-temperature swing adsorber is a new application of the CFB technology and expected to be very energy efficient for the CO_2 capture and recovery. A fluidized bed is known as a proper process to control high volumes of flue gases, and dry sorbents can be used to cut down the cost for control. So, the use of dry sorbents in a fluidized bed is considered as a proper process to remove CO_2 economically [Hoffman and Pennline, 2001]. Fluidization allows enhancement of maintaining relatively higher capture capacities at large values of the gas flow rate [Valverde et al., 2012]. Only a few researchers have worked in this area and some of the literatures are reviewed below;

Pugsley et al., 1994 have simulated a novel energy efficient CO_2 separation known as the Circulating Fluidized Bed Pressure-Temperature Swing Adsorber (CFB-PTSA). A hydrodynamic model for the gas and solid flow structure in the riser of circulating fluidized bed was combined with a competitive adsorption model for CO_2, NO_2, and oxygen mixture on a type X-Zeolites, as described by the adsorb ideal solution theory, to predict the reaction performance. Simulation performed at various operating condition and flue gas CO_2 concentration indicated that CO_2 recovery decreases with increasing concentration at a fixed solid circulation flux, but the purity of the recovered product increases. Recoveries in the range of 65-88.5% and product purities of 75-90% CO_2 were predicted.

Reichhold and Hofbauer, 1995 developed an internally circulating fluidized bed for continuous adsorption and desorption. This system can be used more generally for many other reaction/regeneration operations. It helps to separate and to recover gaseous pollutants and reusable compounds (e.g. CO_2, SOS, organic solvent vapors, along with other gases). Two fluidized beds were arranged next to each other. The partition wall in the upper and lower part of the fluidized beds had horizontal openings to let solid matter pass through. As the two beds were fluidized at different rates, the bed material starts to circulate between the two beds. The bed material doubles as an adsorbent. In the adsorption zone, polluted gas was used for fluidization; in the desorption zone, heated air or steam was used. The main differences from conventional fixed-bed adsorbers were that plants can be built in a more compact manner, higher flow rates

could be achieved and separate optimization of the two zones (adsorption zone, desorption zone) was possible.

Lee et al., 2004 have studied CO_2 adsorption with attrition of dry sorbents in a fluidized bed to provide basic data for process development. Therefore, in their study, activated carbon, activated alumina, molecular sieve 5A, and molecular sieve 13X, which have been used in fixed bed process, were used as dry sorbents to control CO_2 in a fluidized bed. In addition, the characteristics of CO_2 adsorption and attrition of the dry sorbents were investigated.

Cho et al., 2006 have investigated characteristics of attrition and adsorption to remove CO_2 in fluidized bed using activated carbon, activated alumina, molecular sieve 5A and molecular sieve 13X. For every dry sorbent, attrition mainly still occurs in the early stage of fluidization and attrition index (AI) of molecular sieve 5A and molecular sieve 13X were higher than those of activated carbon and activated alumina. Percentage loss of adsorption capacity of molecular sieve 5A and molecular 13X were 14.5% and 13.5%, but that of activated carbon and activated alumina were 8.3% and 8.1%, respectively. Overall attrition rate constant (Ka) of activated alumina and activated carbon were lower than other sorbents.

Veneman et al., 2012 prepared supported amine sorbents by physical impregnation of silica and polymethyl-methacrylate (PMMA) with tetra-ethylenepentamine (TEPA) and studied for post combustion CO_2 capture purposes in a lab scale circulating fluidized bed (CFB) reactor. Sorbent amine loading and support pore size effects were investigated by thermal gravimetric analysis (TGA). The sorbent CO_2 capacity was found to be a strong function of amine loading and pore volume. Significant improvement of the sorbent CO_2 adsorption capacity (3.5 mol kg^{-1}) was achieved by tuning these variables. CO_2 was captured from dry simulated flue gas applying a temperature difference of only 70 ˚C between the adsorber column (40 ˚C) and the desorber column (110 ˚C). A high (90%) purity CO_2 product gas was produced at the regenerator outlet in continuous mode using these supported amine sorbents.

Valverde et al., 2012 analyzed the CO_2 adsorption performance in a fluidized bed of a modified adsorbent, which was obtained by dry mixing a $Ca(OH)_2$ fine cohesive powder (Geldart C) with

a fluidizable silica nano powder. The silica nanoparticle agglomerates serve as carriers of the adsorbent $Ca(OH)_2$ fine particles, which were thus provided with a vehicle for improved fluidization. As the gas flow rate was increased, gas channeling in the fluidized bed of the original adsorbent causes a rapid decrease of the time for CO_2 breakthrough in the effluent gas (BT) and the capture capacity at CO_2 breakthrough (XBT). In contrast, because of the improvement of gas–solid contact efficiency, BT and XBT were appreciably increased for the modified adsorbent. Thus, even though the silica nanoparticle agglomerates do not contribute directly to CO_2 adsorption, fluidization enhancement allows for maintaining relatively higher capture capacities at large values of the gas flow rate.

2.5 SUMMARY OF LITERATURE REVIEWS AND SCOPE FOR PRESENT STUDY

As it is seen from the above literature reviews there are various works which have been done on carbon capture technology. Summary and findings of previous investigation on different types of carbon capture technology such as Pre-Combustion, Oxy-Fuel Combustion and Post Combustions are discussed as follows.

Post combustion capture technologies possess the greatest potential for near term implementation at fossil fuel fired power plants because they can be retrofit to existing facilities with the least difficulty. Of the current post combustion capture technologies, chemical absorption with amines is the most mature technology. However, every post combustion capture approach still suffers from the same design challenge: how to design a system to handle the enormous volume of flue gas produced from fossil fuel combustion. The advantage of Oxy-fuel combustion is that NO_x formation is suppressed and CO_2 can easily be separated by cooling the flue gas stream to condense out the H_2O. However, the equipment needed to obtain the large volume of oxygen needed is costly to operate and retrofitting to existing facilities is difficult. Current facilities are not designed to handle the elevated temperatures seen with combustion in oxygen rich atmospheres. Also, retrofit of an existing plant to incorporate pre combustion technology is very difficult and costly. Thus, pre combustion capture applies only to IGCC plants, which in themselves have high investment and operational costs. At the current state of development pre

combustion technology should only be applied if a new IGCC facility is being constructed. Cryogenic distillation capture is behind in development compared to the other technologies. Until Cryogenic distillation capture is demonstrated on a larger scale it will remain an unviable option for CO_2 emission reductions.

Absorption is matured technology for post combustion capture but solvent losses, corrosion and high cost of separation are the main issues for this process. A wide range of adsorbents have been used for CO_2 adsorption process. Low selectivity and low capacity of the available adsorbents make adsorption process ineffective for large scale industrial applications. Hence, research focus has to be pointed on low cost and easily available adsorbents like waste biomass. Thermally assisted pressure swing regeneration illustrates the potential of steam stripping for the regeneration of the adsorbents. High pressure adsorbents for pre combustion capture demonstrate high adsorption capacities, dependent upon the micro-pore surface area. Regeneration has been demonstrated by both thermal and pressure swing techniques. Thermal swing regeneration has excellent potential in that over two thirds of the adsorption capacity can be regenerated whilst retaining pressure, therefore saving on the high energy penalties associated with re-compression of the gas. Both techniques offer good adsorption, and potential advantages over the current solvent absorption systems.

It was evident from the literature that the design and modeling of a fixed bed adsorption system require the simultaneous solution of a set of coupled PDEs representing mass, energy, and momentum conservation together with transport rate and equilibrium equations. The simultaneous solution of such a rather complex system of PDEs requires complicated numerical solutions, and the computation time is often inconveniently long. Therefore, the use of reduced models with satisfactory prediction capabilities has been used in the present work to decrease the computational time and facilitate optimization. Also, it has been reported that the employment of fluidized bed for adsorption process gives a better gas-solid contact, which results in a better coefficient of mass transfer. Fluidization allows enhancement of maintaining relatively higher capture capacities at large values of the gas flow rate. Hence, a thorough investigation is necessary on the fluidized bed system to fully understand that there is an improvement in the adsorption capacity of particular adsorbents by using a fluidized bed. Out of the present literature

reviews an objective for the thesis work has been extracted. The detail objectives for the present work are presented in chapter 1.

2.6 SUMMARY

In this chapter, review of literature and scope for present investigations were discussed. Literature reviews based on the type of capture strategies were presented. Reviews on experimental studies of CO_2 adsorption in a fixed bed as well as fluidized bed were presented. Reviews of CO_2 adsorption based on the type of adsorbents used like zeolite 13X, zeolite 5A, zeolite 4A and activated carbon were discussed thoroughly. Also, review on modeling and simulation of CO_2 adsorption were reported based on the system heat transfer effect which include isothermal and non-isothermal process. Finally summary of the literature reviews were discussed. In the following Chapter (Chapter 3) characterization of the adsorbents used in this study are presented.

CHAPTER 3

CHARACTERIZATION OF ADSORBENTS

3.1 INTRODUCTION

In adsorption process, adsorbent material is a component, which plays the crucial role. It is the solid material on which adsorption occurs. Commercially useful adsorbents can be classified by the nature of their structure (amorphous or crystalline), by the sizes of their pores (micropores, mesopores, and macropores), by the nature of their surfaces (polar, nonpolar or intermediate), or by their chemical composition. All of these characteristics are important in the selection of the best adsorbent for any particular application. Therefore, this chapter presents the adsorbent material characterization of zeolite 13X, zeolite 5A, zeolite 4A and activated carbon.

3.2 METHOD

In this study, three different adsorbents such as zeolite 13X, zeolite 5A and zeolite 4A were used for CO_2 adsorption experiments and compared with the locally available coconut fiber based adsorbent. Characterization of the adsorbent materials has been done using proximate analysis. Surface area and pores of the adsorbent materials were determined by N_2 adsorption using a surface area analyzer at CIF, IIT Guwahati.

3.2.1 PROXIMATE ANALYSIS

Proximate analysis indicates the percentage by weight of the Fixed Carbon, Volatiles, Ash, and Moisture Content in coal. The amounts of fixed carbon and volatile combustible matter directly contribute to the heating value of coal. Fixed carbon acts as a main heat generator during burning. High volatile matter content indicates easy ignition of fuel. The ash content is important in the design of the furnace grate, combustion volume, pollution control equipment and ash

handling systems of a furnace. In the proximate analysis, moisture (M), Ash (A) and volatile matter (VM) are determined. Fixed carbon (FC) is obtained from the following equations:

$$FC= 100 - (\%M + \%A + \%VM) \quad (3.1)$$

There are standard tests to determine proximate analysis. Moisture is determined by drying 1 g of sample at 105 ˚C for 1 hr. Weight loss is expressed in % of initial weight of sample;

$$\% M= (\text{Weight loss/ Weight of sample}) \times 100 \quad (3.2)$$

Ash is weight of residue obtained after complete combustion of 1 g of sample at 700-750 ˚C.

$$\% A= (\text{Weight of residue/ Weight of sample}) \times 100 \quad (3.3)$$

Volatile matter is the weight loss obtained on heating 1 g sample at 950 ˚C for 7 minutes in the absence of air.

Total weight loss of moist sample = Weight loss due to volatile matter + Moisture;

Weight loss due to VM= Total weight loss – moisture;

$$\% VM= (\text{Weight loss to VM/ Weight of sample}) \times 100 \quad (3.4)$$

3.2.2 DETERMINATION OF COMPOSITIONS

Surface analyses, chemical analysis and imaging on a variety of materials were performed using a Scanning Electron Microscope (SEM) at CIF, IIT Guwahati (Appendix I). The Scanning Electron Microscope is equipped with an Energy Dispersive Spectrometer (EDS). SEM/EDS provide chemical analysis of the field of view or spot analyses of minute particles.

3.2.3 SURFACE AREA AND PORES DETERMINATION

The gas adsorption method is a method for measuring the amount of gas adsorbed on the surface of a powder sample as a function of the pressure of the adsorbate gas, and is used to determine the surface area of a powder sample. Measurements are usually performed at the boiling point of liquid nitrogen (-196 ˚C). When the gas is physically adsorbed by the powder sample, the following relationship holds when P/P_0 is in the range of 0.05 to 0.30 for pressure P of the adsorbate gas in equilibrium for the volume of gas adsorbed, V_a,

$$\frac{1}{V_a\left(\frac{P_0}{P}-1\right)} = \frac{(C-1)}{V_m C} \times \frac{P}{P_0} + \frac{1}{V_m C} \quad (3.5)$$

P: Partial vapour pressure of adsorbate gas in equilibrium (kPa)

P_0: saturated pressure of the adsorbate gas at -196 ˚C (kPa)

V_a: Volume of gas adsorbed at equilibrium (mL)

V_m: Volume of gas adsorbed in a monolayer (mL)

C: Dimensionless constant related to the enthalpy of adsorption and condensation of the adsorbate gas.

The specific surface area, S, is determined from V_m, the volume of gas adsorbed in a monolayer on the sample.

$$S = \frac{V_m \times N \times a}{m \times 22400} \quad (3.6)$$

S: Specific surface area (m^2/g)

N: Avogadro constant

A: Effective cross-sectional area of one adsorbate molecule (m^2)

m: mass of the test powder (g)

For the present study, Surface area and pores were determined by using a Quantachrome surface analyzer (Appendix I). The samples were first vacuumed at 573 K for more than 5 h before the adsorption isotherms were generated by dosing nitrogen on the adsorbents.

3.3 QUALITY OF ADSORBENT MATERIALS

In an adsorption process the gaseous component comes into contact with the solid and is adsorbed from the gas phase onto the solid surface. The solid material used for adsorption is often referred to as the adsorbent and the gas species being adsorbed, the adsorbate (in this study the adsorbate is CO_2). When considering adsorption for CO_2 capture, it is important that the adsorbent possess certain qualities, such as [Yang et al., 2012]:

1. High CO_2 adsorption capacity: as a rule of thumb, an adsorbent should possess an adsorption capacity of 0.088–0.176 g CO_2/ g adsorbent.
2. High surface area: a high surface area suggests more surface sites for CO_2 adsorption, possibly leading to a high adsorption capacity.
3. Fast kinetics: the faster the kinetics, the faster CO_2 will adsorb.
4. High CO_2 selectivity: CO_2 should preferentially adsorb to the adsorbent. Selectivity also determines the purity of the CO_2 produced during desorption.
5. Mild regeneration conditions: the milder the regeneration conditions (i.e. temperature and pressure) the less costly the regeneration stage will be.
6. Stability during the adsorption/desorption cycle: the lifetime of the adsorbent has a significant impact on the operating cost of the system.
7. Tolerance to impurities: the adsorbent must be tolerant to common flue gas impurities such as NO_x, SO_x, and water vapor. Impurities can significantly reduce the adsorption capacity with respect to CO_2 and even degrade the adsorbent crystal structure.
8. A wide range of tunable properties: allows the absorbent to be tailored to various operating environments.
9. Low cost: adsorbents degrade over time, the cost to replace them should them should be minimal.

For the present studies, low cost and abundantly available locally, coconut fibre based activated carbon was employed as the adsorbent material and compared with commercial zeolites like zeolite 13X, zeolite 5A, zeolite 4A. The general nature and compositions of activated carbon and zeolites are discussed in the following sub section.

3.3.1 ACTIVATED CARBON BASED ADSORENTS

The specific characteristics, physical and chemical properties of activated carbons, depend on both organic precursor and activation processes. Activated carbons are advantageous as adsorbents and catalyst supports because they offer high surface area, developed pore volume, unique surface properties and the opportunities for surface chemistry modification. Activated carbon materials have random cross-linked networks, which provide highly developed and

accessible internal pore structures pertinent to the adsorption of contaminants. The activation of organic precursor consists of two steps: carbonization and activation. During carbonization, volatile organic components are eliminated and the carbon structure rearranges into graphite sheets laid out random order. After carbonization, the carbonaceous skeleton obtained has a significant internal porosity. During activation, an oxidizing agent attacks the carbons located at the edges of the graphitic sheets, resulting in the pores being opened and widened to create the desired micro and mesopore structure [Meljac et al., 2005].

There are two main methods, physical and chemical, by which the organic precursors are activated. Chemical activation employs an oxidizing agent which is normally alkali and alkaline earth metals or acids such as KOH, K_2CO_3, NaOH, Na_2CO_3, $AlCl_3$, $ZnCl_2$, $MgCl_2$ and H_3PO_4, [Bansal et al., 1988]. The oxidizing agent is mixed with the precursor material and heated at high temperature (600-1000°C), resulting in simultaneous carbonization and activation [Meljac et al., 2005]. Although, washing treatments are carried out after activation/ carbonization, the oxidizing agent still lingers on the carbon surface and changes its surface chemistry. In physical activation, the carbon material is carbonized at high temperature before undergoing reactions in the gaseous phase with CO_2, or steam [Tsai et al., 2002]. Physical activation is more expensive, but the final product is clear of chemical additives.

3.3.2 ZEOLITE BASED ADSORBENTS

Zeolites form a family of minerals, which have been known since the 18^{th} century, but they remained a curiosity for scientists and collectors until 60 years ago, when their unique physicochemical properties attracted the attention of many researchers. Zeolites are porous crystalline aluminosilicates. The zeolite framework consists of an assemblage of SiO_4 and AlO_4 tetrahedra, joined together in various regular arrangements through shared oxygen atoms to form an open crystal lattice containing pores of molecular dimensions into which molecules can penetrate. There are more than 50 different available types of aluminosilicate zeolites with pore openings ranging from less than 5 Å to larger than 10 Å [Webster et al., 1999]. These porous, crystalline, hydrated aluminosilicates of alkali and alkaline earth cations possess a three dimensional structure. The negative charge created by the substitution of an AlO_4 tetrahedron for

a SiO_4 tetrahedron is balanced by exchangeable cations (e.g., Na^+, K^+, Ca^{2+}, Mg^{2+}), which are located in large structural channels and cavities throughout the structure. These cations play a very important role in determining the adsorption and gas-separation properties of zeolites.

These properties depend heavily on the size, charge density, and distribution of cations in the porous structure. These natural minerals are found with a Si/Al ratio ranging between 3 and 5 [Zhao et al., 1998]. Synthetic zeolites are manufactured on a large scale for industrial use, but natural zeolites have not yet found extensive application as commercial molecular sieves, even though a few, particularly clinoptilolite are abundant in volcanogenic sedimentary rocks. Of more than the 40 natural zeolites species known today, clinoptilolite is the most abundant in soils and sediments [Armenta et al., 2001].

3.3.2.1 STRUCTURE

Like most silicates the zeolites are based on TO_4 tetrahedra, where T is an aluminium or silicon atom. The vast 3-dimensional networks are a result of all four corners for the tetrahedra being shared, producing low density microporous materials. Zeolite structures can be thought to exist of finite or infinite (chains, layers etc.) component units. The finite units which have been found to occur are shown in Figure 3.1.

(a) ZEOLITE A

The simplest synthetic zeolite is the zeolite A with a molecular ratio of one silica to one alumina to one sodium cation. The zeolite A synthesis produces precisely duplicated sodalite units which have 47% open space, ion exchangeable sodium, water of hydration and electronically charged pores. These properties lead to the various uses of natural and synthetic zeolites. The aluminosilicate framework of zeolite A can be described in terms of two types of polyhedra; one is a simple cubic arrangement of eight tetrahedra and the other is the truncated octahedron of 24 tetrahedra or β-cage. The aluminosilicate framework of zeolite A is generated by placing the cubic D4R units ($Al_4Si_4O_{16}$) in the centers of the edges of a cube of edge 12.3A. This arrangement produces truncated octahedral units centered at the corners of the cube. Each corner

of the cube is occupied by a truncated octahedron (β-cage) enclosing a cavity with a free diameter of 6.6 A. The center of the unit cell is a large cavity, referred to as the α-cage, occupy the apices of a truncated cuboctahedron. The unit cell of zeolite A contains 24 tetrahedra, 12 AlO_4 and 12 SiO_4. When fully hydrated, there are 27 water molecules. The electrostatic valance rule requires an alternation of the AlO_4 and SiO_4 tetrahedra, because the Si/Al ratio is 1:1. Normally, zeolite A is synthesized in the Na form. Other cationic forms are easily prepared by ion exchange in aqueous solution [Breck, 1973]. The schematic structure of zeolite A is given in Figure 3.2.

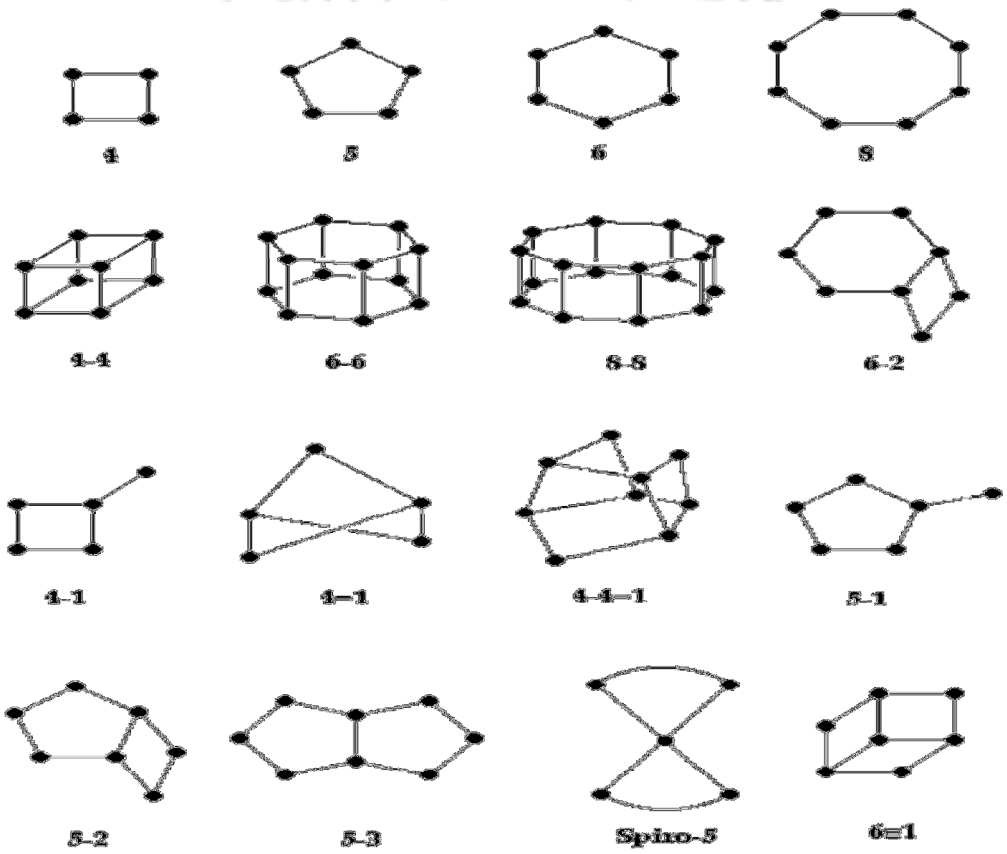

Fig 3.1 Secondary Building Units (SBU's) in zeolites. The corner of the polyhedra represents tetrahedral atoms.

(b) ZEOLITE X AND Y

The faujasite-type zeolites all have the same framework structure as indicated in Figure 3.3. The general composition of the unit cell of faujasite is $(Na_2, Ca, Mg)_{29}$ $[Al_{58}Si_{134}O_{384}].240H_2O$. The SBU's are double six rings and the FD is 12.7 nm^{-3}. The unit cell contains eight cavities, each of

diameter ≈13 A. The three dimensional channels which run parallel to [110], have 12 ring windows with free apertures of about 7.4 A. The difference between zeolites X and Y is in their Si/Al ratios which are 1-1.5 and 1.5-3, respectively [Breck, 1973].

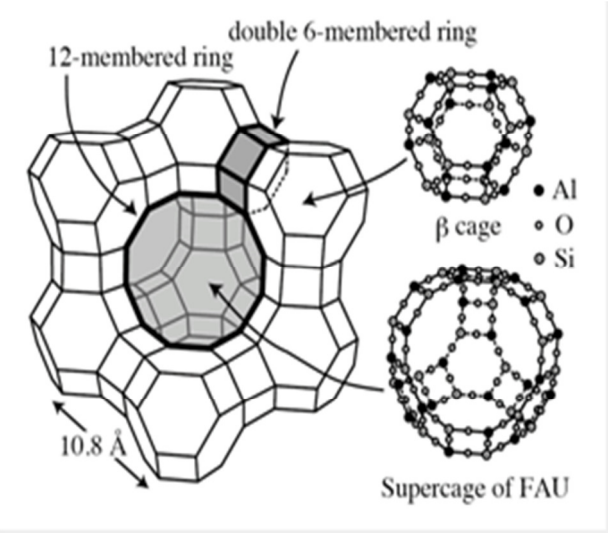

Fig 3.2 Structure of Zeolite A

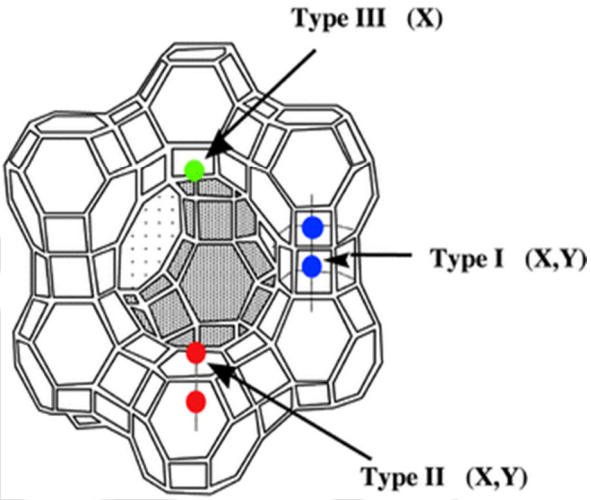

Fig 3.3 Structure of X and Y synthetic zeolites

3.4 RESULTS AND DISCUSSION

3.4.1 COMMERCIAL ZEOLITES

Three types of commercial zeolites were used in the present work for CO_2 capture using adsorption process. The properties of commercial zeolite 4A, zeolite 5A and zeolite 13X which were purchased from local chemist are given in Table 3.1 and they were of a pellet type. The photo and SEM images of zeolite 4A, zeolite 5A and zeolite 13X are shown in Figure 3.4 through Figure 3.9 respectively. The SEM result clearly showed that there are impurities present on the three zeolites. When the SEM micrographs of 4A and 13X are compared, on a 10μm scale, the crystal size of 4A zeolites which are about 3.5 μm are greater than that of 13X zeolites which are approximately 2 μm.

Table 3.1 Properties of zeolites

Properties	**4 A**	**5A**	**13 X**
Surface area (m^2/g)	434	650	720
Pore diameter (Å)	4.0	5	10
Bulk density (kg/m^3)	700	680	639
Particle diameter, d_p (mm)	1.5	2	2
Composition (wt %)			
Sodium	10.8	3.8	11.9
Aluminum	13.6	14.8	14.3
Silicon	16.1	16.7	17.8
Calcium	0.8	7.8	0.6
Potassium	0.9	0.8	0.2
Magnesium	1.2	1.0	1.3

Fig 3.4 Photograph of zeolite 4A

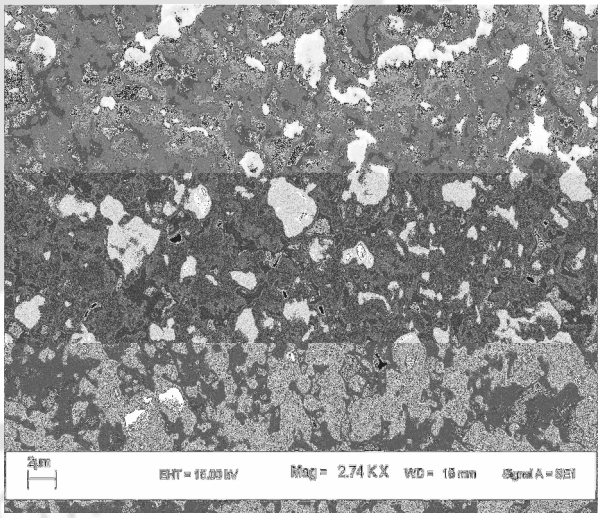

Fig 3.5 SEM image of zeolite 4A

Fig 3.6 Photograph of zeolite 5A

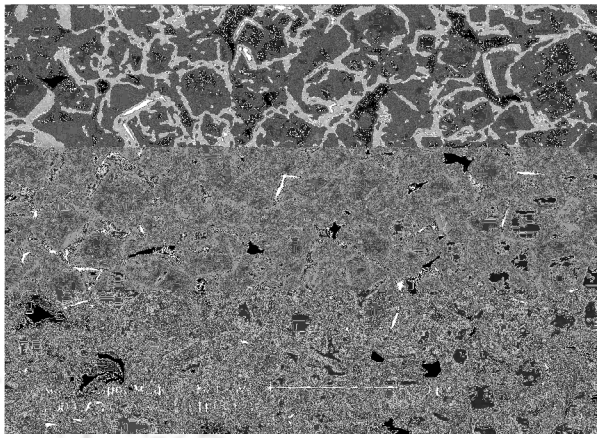

Fig 3.7 SEM image of zeolite 5A

Fig 3.8 Photograph of zeolite 13X

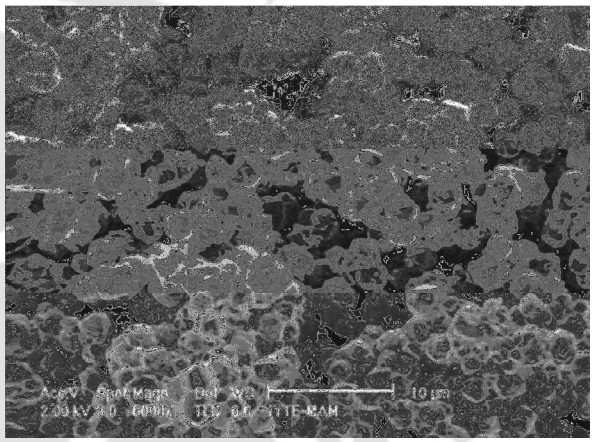

Fig 3.9 SEM image of zeolite 13X

3.4.2 ACTIVATED CARBON FROM COCONUT FIBRE

The activated carbon (coconut fibre based) used was obtained from a local area. It was pilled and the fibrous part was collected and was broken into small pieces. The coconut fibre was washed with water, dried in the sun for 10 hrs and transfer to the furnace. The coconut pieces were burnt distinctively in the furnace for an hour at a temperature of 350 °C. The charcoal produced was withdrawn from the furnace and sieved to obtain a mean particle diameter of 0.92 mm as shown in Figure 3.10. SEM image shows the development of a number of pores and a large surface area for trapping the incoming gas molecules at a magnitude of 2.00 KX as shown in Figure 3.11.

Fig 3.10 Photograph of activated carbon

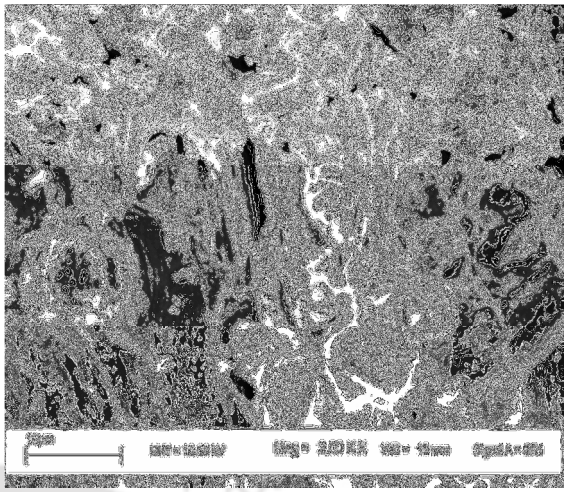

Fig 3.11 SEM image of activated carbon

The material characterization was done for proximate and ultimate analysis and details of the physical and chemical properties are given in Table 3.2.

Table 3.2 Properties of activated carbon

BET surface area (m^2/g)			354
Pore volume (cc/g)			0.0683
Bulk density (kg/m^3)			350
Particles diameter (mm)			0.92
Chemical compositions (wt %)			
C	*O*	*Cl*	*K*
41.28	36.00	6.01	33.71
Proximate Analysis (wt %)			
Ash	*Moisture*	*Fixed Carbon*	*Volatile*
4.8	10.63	14.49	70.08

Both the size and distribution of micro-pores, meso-pores and macro-pores determine the adsorptive properties of adsorbents. Small pore sizes will not trap large adsorbate molecules and large pores may not be able to retain small adsorbates, whether they are charged polar molecules or uncharged non-polar compounds [Ahmedna et al., 2004]. It can be seen that the surface area of activated carbon from coconut fiber is very low as compared to commercial zeolite 13X and

zeolite 5A while very closed to zeolite 4A due to their structural nature. For good adsorbents, the surface area is very important parameters like other physiochemical characteristics.

3.5 SUMMARY

In this chapter characterization of the adsorbent materials like zeolite 13X, zeolite 5A, zeolite 4A and activated carbon. Method of the characterization and the general nature of the adsorbent used in this study were also described. The next chapter (chapter 4) presents the breakthrough curve and Isotherm model for CO_2 adsorption in the fixed bed with the adsorbents considered in this study.

CHAPTER 4

BREAKTHROUGH AND ISOTHERM MODELS FOR CO_2 ADSORPTION

4.1 INTRODUCTION

In most adsorption processes, the adsorbent is in contact with a fluid in a packed bed. An understanding of the dynamic behavior of such systems is therefore required for rational process design and optimization [Do, 1998]. The dynamic behavior of an adsorption column system can be classified based on the nature of the gas–solid equilibrium relationship of fluid constituents and the complexity of the mathematical model required for describing the mechanism by which the mass transfer from the fluid to the solid phase occur [Ruthven, 1984]. The gas–solid adsorption equilibrium indicates the limiting capacity for solute separation from the gas phase into the solid phase. It is the most important process that controls the dynamic behavior of a packed column so that the general nature of a mass transfer zone is determined entirely by the equilibrium isotherm. Therefore, due to variations in the composition/temperature with respect to time and location within the adsorption column and the consequent effects on the adsorption equilibrium relation, a comprehensive gas–solid equilibrium model is needed.

Several authors have reported experimental evidence of these effects in a column packed with microporous adsorbents [Carta, 2003]. The complexity of the mathematical model in turn depends on the concentration level, the choice of rate equation and the choice of flow model [Ruthven, 1984]. In addition, temperature changes may also affect the concentration profiles, particularly for high concentration feeds in which the heat of adsorption generates thermal waves in both axial and radial directions. Therefore, apart from the mass transfer effects on adsorption rate, the effects of heat generation and heat transfer in the adsorbent bed must also be considered [Rezaei and Grahn, 2012]. Moreover, the axial pressure along the bed may not be constant. As a consequence, a momentum balance also has to be included in the model.

For the present study temperature had been considered constant for the mathematical modeling purpose as discuss below.

4.2 MATHEMATICAL MODELING

The fixed bed mathematical models are used for predicting the transient behavior of concentration and temperature profiles for any defined changes in the initial parameters such as feed concentration, temperature, and flow rate. A complete mathematical model capable of describing the dynamic behavior of a fixed bed adsorption system is established based on a set of fairly complex partial differential and algebraic equations constructed from conservation of mass appropriate transport rate equations and equilibrium isotherms. The models used to represent a PSA process differ mainly in the form of the mass transfer rate, the form of the equilibrium isotherm, thermal and the pressure drop along the bed. The mathematical model of the isothermal, dynamic adsorption breakthrough process in a fixed bed is based on transient material balance, gas phase and intra-pellet mass transfer, the adsorption equilibrium relationship, boundary conditions, and initial conditions. Liner driving force model (LDF) seems to be suitable choice for simulating adsorption breakthrough curve and the schematic diagram of the reactor is shown in Figure 4.1. The assumptions made are:

- the pressure drop is very low, the velocity and density of the fluid are constant;
- the system is isothermal during whole process based on experimental observation of 6 K maximum temperature swing;
- effect of radial and axial dispersion are neglected;
- bed porosity is uniform;
- vapor is considered as an ideal gas; and plug flow is assumed.

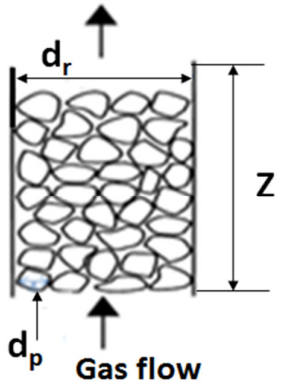

Fig 4.1 Schematic diagram of the fixed bed reactor

The mass balance on a portion of the bed is given by Equation 4.1;

$$\varepsilon_b \frac{\partial C_A}{\partial t} + \rho_b \frac{\partial q}{\partial t} + u_s \frac{\partial C_A}{\partial z} = 0 \tag{4.1}$$

The lumped-parameter LDF model was used to describe the intrapellet mass transfer as follows in Equation 4.2:

$$\frac{\partial q}{\partial t} = k_g (q_s - q) \tag{4.2}$$

Concentration of the compound at the column inlet is the initial concentration, C_0:

$$C_A = C_0 \text{ for } z = 0 \text{ and } t > 0$$

Initial conditions:

$$q = 0 \text{ for } z \geq 0 \text{ and } t = 0$$

$$C_A = C_0 \text{ for } z = 0 \text{ and } t = 0$$

$$C_A = 0 \text{ for } z > 0 \text{ and } t = 0$$

The numerical method was calculated by Finite Difference Method. Forward finite difference explicit scheme was used in this study. The mass transfer coefficient, k_g, parameter can be considered as an adjustable parameter. Thus, fitting simulation results and experimental data allows this parameter to be determined.

To be able to use a pseudo-homogeneous plug-flow model and focus on the kinetics, it is necessary to verify different criteria, i.e. for plug flow. The experimental conditions employed in the present work are given in Table 5.3. Conventional criteria for ideal plug flow are [De Wilde et al., 2000]:

$$\mathbf{d_r/d_p > 10, \quad L/d_p > 20} \text{ ;}$$

$$\mathrm{Re} = \rho_{mix} u_s d_p \Big/ \mu_{mix} \tag{4.3}$$

The Reynold`s number can be calculated from Equation 4.3. For the given conditions and for the zeolite 4A sorbent, $d_r/d_p = 20 > 10$ and $L/d_p = 133.33 > 20$. For zeolite 5A and zeolite 13X, $d_r/d_p = 15 > 10$ and $L/d_p = 100 > 20$. For activated carbon, $d_r/d_p = 54.34 > 10$ and $L/d_p = 217.39 > 20$. The particle Reynold's number given in Equation 3 for zeolite 4A is found as Re = 13.26 > 10, for zeolite 5A and zeolite 13X, Re = 17.68 and for activated carbon Re = 14.54 at

an influent flow rate of 15 LPM. Hence, the conventional criteria have been satisfied and plug flow can be assumed.

For transient experiments, Dekker [Dekker et al., 1995] proposed a set of conditions to verify the influence of internal and external diffusion on the adsorption or reaction rate. For spherical particles, the Biot number can be calculated from Equation 4.4:

for negligible external resistance, $\mathbf{Bi_m > 20}$,

$$\text{with,} \quad Bi_m = {k_g r}/{D_K} \tag{4.4}$$

for negligible internal resistance, $\mathbf{Bi_m > 20}$ and

$$\zeta_{in} = [(D_e/\varepsilon_p r^2)t] \geq 0.25 \tag{4.5}$$

The latter criterion relates the rate of adsorption or reaction with the time scale of the transient experiment as shown in Equation 4.5. Hence, intra-particles mass transfer resistance can also be neglected. For packed beds, the gas-solid mass transfer coefficient was modeled in terms of the Schmidt (Sc) and Reynolds number (Re). The Sherwood number (Sh) is calculated from a correlation as given in Equation 4.6 to Equation 4.8 [Chihara et al., 1978]:

$$Sh = 2 + (1.1)(Sc)^{1/3}(\mathrm{Re})^{0.6} \tag{4.6}$$

with :

$$Sc = \frac{\mu_{mix}}{\rho_{mix} D_{AB}} \tag{4.7}$$

$$Sh = \frac{k_g d_p}{D_{AB}} \tag{4.8}$$

Diffusion of CO_2 in air is considered. The binary diffusivity for diffusion of a component B can be calculated by using the Fuller Schlettler-Gridding method as given in Equation 4.9 [Yang, 1997]:

$$D_{AB} = \frac{0.00143\, T^{1.75} \sqrt{\frac{1}{M_A} + \frac{1}{M_B}}}{P\left[\left(\sum v_A^{1/3}\right) + \left(\sum v_B^{1/3}\right)\right]^2} \tag{4.9}$$

The Knudsen diffusivity can be calculated from Equation 4.10 [Yang, 1997]:

$$D_K = \frac{d_o \sqrt{\frac{8RT}{\pi M_{mix}}}}{3} \tag{4.10}$$

The effective diffusivity (De) is related to molecular, Knudsen, and surface diffusivities, which can simply be calculated by means of Bosanquet equation given in Equation 4.11 [Stephan et al., 2001]:

$$\frac{1}{D_e} = \tau\left(\frac{1}{D_{AB}} + \frac{1}{D_k}\right) \tag{4.11}$$

Table 4.1 Summary of mass transfer and diffusivity parameters

Parameters	Zeolite 13X	Zeolite 5A	Zeolite 4A	Activated carbon
D_e	0.417×10^{-5}	0.357×10^{-5}	0.357×10^{-5}	0.324×10^{-5}
D_k	3.16×10^{-9}	2.66×10^{-9}	2.66×10^{-9}	1.5×10^{-8}
Sc	0.649	0.549	0.549	0.486
Sh	6.547	6.246	6.246	6.32
K_g	0.137	0.115	0.115	0.102
Bi_m	3.98×10^{4}	3.8×10^{4}	3.7×10^{4}	4.2×10^{3}

4.3 ISOTHERM MODELS

Four types of isotherm models like Langmuir, Freundlich, Sip`s and Toth isotherm model were used to fit the experimental data as discuss in the following sub section.

4.3.1 PURE GAS ADSORPTION ISOTHERMS

Adsorption isotherm is the relationship between the amount of gas adsorbed and pressure or relative pressure at constant temperature. A useful indication of the mechanisms of surface coverage and/or pore filling can be obtained by visual inspection of an isotherm. The overall shape of an isotherm is governed by the nature of the gas-solid system, the pore structure of the adsorbent and the operational temperature.

The majority of physisorption isotherms may be grouped into six types according to IUPAC classification as shown in Figure 4.2. In most cases at sufficiently low surface coverage the isotherm reduces to a linear form, which is often referred to as Henry's Law Region. The main feature of a Type I isotherm is the long plateau, which is indicative of a relatively small amount of multilayer adsorption on the open surface. Micropore filling may take place either

in pores of molecular dimensions at very low p/p° or in wider micropores over a range of higher p/p°. A type II isotherm is normally associated with monolayer-multilayer adsorption on an open and stable external surface of a powder, which may be non-porous, macroporous or even to a limited extent microporous.

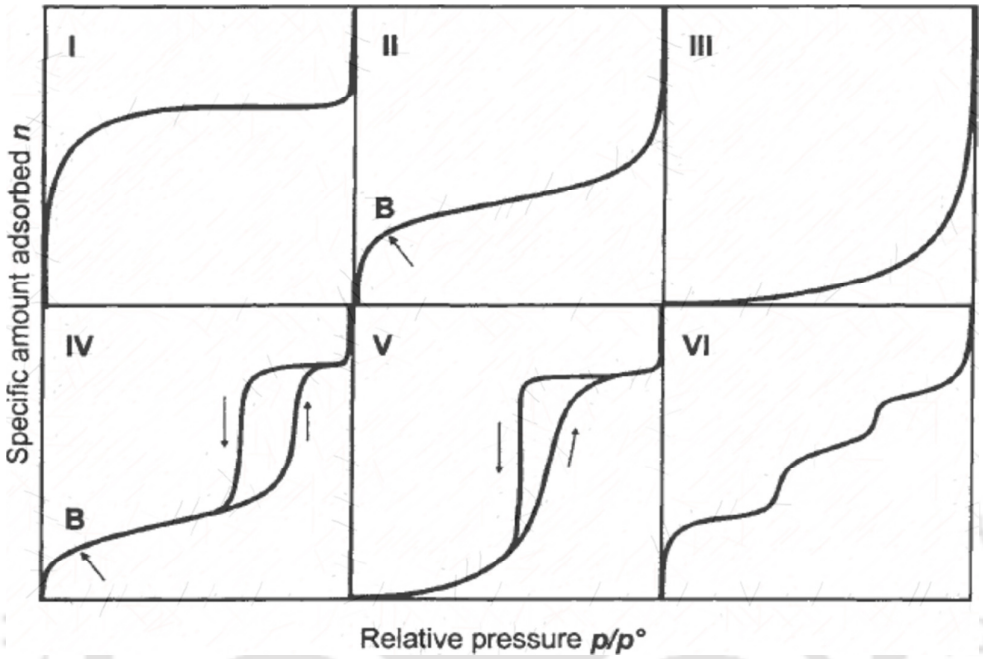

Fig 4.2 The six main types of gas physisorption isotherms

Type III isotherms are confined to a few systems in which the overall adsorbent-adsorbate interactions are weak in comparison with relatively strong adsorbate-adsorbate interactions. Isotherms of this kind are not common. Characteristic features of the type IV isotherm are its hysteresis loop, which is associated with capillary condensation taking place in mesopores, and the limiting uptake over a range of high p/p°. The type V isotherm is uncommon; it is related to the type III isotherm in that the adsorbent-adsorbate interaction is weak but is obtained with certain porous adsorbent.

The type VI isotherm, in which the sharpness of the steps depends on the system and the temperature, represents stepwise multi-layer adsorption on a uniform non-porous surface. Among the best examples of type VI isotherms are those obtained with argon or krypton on graphitized carbon blacks at liquid nitrogen temperature. There are some models which help characterizing the adsorbent to see if the adsorbent has the desired properties for a certain

application. The interaction parameters of these models indicate the extent of heterogeneity of the adsorbent being investigated.

4.3.2 LANGMUIR MODEL

The simplest theoretical model for monolayer adsorption is due to the Langmuir model. The basic assumptions on which the model is based on are as follows; 1) Molecules are adsorbed at a fixed number of well-defined localized sites, 2) Each site can hold one adsorbate molecule, 3) All sites are energetically equal and 4) There is no interaction between molecules adsorbed on neighbouring sites.

The Langmuir adsorption method is still the most widely used procedure for the determination of the surface area of porous materials. The Langmuir equation is given in Equation 4.12 and 4.13 [Langmuir, 1918; Morse et al., 2010].

$$q = \frac{q_m KP}{1 + KP} \tag{4.12}$$

$$K = A\exp\left(\frac{Q}{RT}\right) \tag{4.13}$$

where q is the amount of CO_2 adsorbed at the the equilibrium pressure P, T is the adsorption temperature, A is the affinity constant at infinite temperature, Q is the heat of adsorption, and R is the gas constant and q_m is the amount of CO_2 adsorbed with monolayer coverage. p/q vs P graph gives Langmuir plot. From slope and intercept, K and q_m values are calculated respectively. Parameter K is the Langmuir constant and it is a measure of how strong an adsorbate molecule is attracted onto a surface. When the affinity constant A is larger, the surface is covered more with adsorbate molecule as a result of the stronger affinity of adsorbate molecule towards the surface. Besides, increase in temperature decreases the amount adsorbed at a given pressure. This is due to the greater energy acquired by the adsorbed molecule to evaporate.

4.3.3 FREUNDLICH MODEL

This is the first known empirical equation that can fit the adsorption isotherm data deviating from the ideal situation due to the complexity of the adsorbent surface. The mathematical

form of the Freundlich model is given in Equation 4.14 [Siriwardane et al., 2005; Freundlich, 1907]:

$$q = KP^{1/n} \tag{4.14}$$

where K and n are constants (n > 1). According to Freundlich equation the plot of ln q against ln P should be linear. The Freundlich isotherm can be applied to adsorption systems with heterogeneous adsorbent. This model does not follow Henry's law behaviour at low pressure and presents no finite limit at the higher pressure.

4.3.4 TOTH MODEL

This model is a semi-empirical isotherm with three parameters. It can be used to describe an adsorption system with sub-monolayer coverage, and it can also predict the adsorption behaviour of gases at both low and high pressure. The mathematical form of this model is given in Equation 4.15 [Toth, 1971; Cavenati et al., 2004]:

$$\frac{q}{q_m} = \frac{P}{\left(b + P^n\right)^{1/n}} \tag{4.15}$$

which also contains three adjustable parameters (q_m , b and n) but has the advantage that it appears to gives a more extensive range of fit when applied to type I isotherms.

4.3.5 SIP'S MODEL

This model is the combined form of the Langmuir and Freundlich isotherms. In the Freundlich model, the amount of gas adsorbed is increased indefinitely with pressure. A combined model is proposed by Sip`s (1948) to avoid this limitation. The mathematical form of this model is shown in Equation 4.16 [Siriwardane et al., 2005]:

$$\frac{q}{q_m} = \frac{(bP)^{1/n}}{1 + (bP)^{1/n}} \tag{4.16}$$

The difference between this equation and the Langmuir equation is the additional parameter 'n'. If this parameter is unity, Sips equation is reduced to Langmuir equation which can be applied for ideal surfaces. Hence the parameter 'n' could be regarded as the parameter characterizing the system heterogeneity. The system heterogeneity could be result of the solid or the adsorbate or a combination of both. The parameter 'n' is usually greater than unity, and therefore the larger is this parameter the more heterogeneous is the system.

4.3.6 ERROR ANALYSIS

To allow the use of the obtained adsorption isotherms for different purposes, the equilibrium data were correlated into different isotherm models. These models are the Langmuir, Freunlich, Toth and Sips equations presented above. Nonlinear regression analysis was performed to determine the model parameters for individual adsorbents. The average percent deviation quantity, Δq, or the adsorbed amounts were calculated using the following formula given in Equation 4.17 [Morse et al., 2010]:

$$\Delta q\% = \frac{100}{h}\sum_{j=1}^{h}\left|\frac{N^{\exp} - N^{cal}}{N^{\exp}}\right| \tag{4.17}$$

where h is the number of experimental data and N^{exp} and N^{cal} are the experimental and calculated number of moles that are adsorbed by the adsorbent pellet.

4.5 ACKNOWLEDGEMENT

The CO_2 breakthrough modeling was done in UCL, Belgium under Marie-Curie (IRSES) project FP7-PEOPLE-2012-IRSES, project no. 312261, project name: iComFluid: International Collaboration on Computational Modelling of Fluidized Bed Systems for Clean Energy Technologies. Therefore, I would like to give a special thanks to Juray De Wilde, Professor, UCL, Belgium for his guidance throughout my reseach work in Belgium (Feb – Oct, 2013). Also, I would like to thanks all the staffs and research Scholar in the Department of Materials and Process Engineering, UCL, Belgium for their help and support.

4.6 SUMMARY

Mathematical model and the isotherm models for CO_2 adsorption in a fixed bed using LDF adsorption model are presented in this chapter. Detail results and discussion from the present chapter are presented in Chapter 6. The next chapter (Chapter 5) presents the experimental set up, experimental procedures and experimental conditions for the fixed and fluidized beds.

CHAPTER 5

EXPERIMENTAL SETUP AND PROCEDURE

5.1 INTRODUCTION

Adsorption occurs whenever a solid surface is exposed to a gas or liquid and it is defined as the enrichment of material or increase in the density of the fluid in the vicinity of the interface. The term adsorption may also be used to denote the process in which adsorptive molecules are transferred to, and accumulate in the interfacial layer. Its counterpart desorption, denotes the converse process in which the amount adsorbed decreases. Based on the nature of the bonding between the adsorbate molecule and the solid surface, adsorption can be categorized as either physical adsorption, which does not involve chemical bonding or chemisorption which involves chemical bonding. CO_2 adsorption experiments were carried out in this study to measure the adsorption equilibrium or isotherm and the kinetics or uptake rate of CO_2 on the selected adsorbents under different temperatures and pressures. Details of the experimental equipment and experimental procedures are provided in this chapter.

5.2 EXPERIMENTAL SETUP FOR FIXED BED STUDY

The adsorption isotherm and uptake rate (kinetics) for all adsorbents were measured using gravimetric gas adsorption apparatus designed and fabricated in the Centre for Energy Laboratory, IIT Guwahati. The experimental set-up for the adsorption test consists of a CO_2 cylinder and Gas Compressor interconnected through a pipe to the system as shown in Figure 5.1. The Gas Compressor could provide sufficient pressure up to 10 kg/cm^2 with a discharge capacity of 84 Liter per minute (LPM). The gas mixing chamber was made up of a Galvanized Iron (GI) pipe of 20 mm diameter and 80 mm in length to sufficiently mixed the incoming CO_2 (13.8 vol%) and air from the gas compressor at a constant rate. Ceramic wool was wrapped around the reactor above the heater coil which was attached to the outer surface of the reactor.

Fifteen different thermocouples (K-type) were inserted in the bed at different positions to measure the bed temperatures with thermocouple accuracy of ±0.5%. The thermocouples were connected to data acquisition system and the measured results were transfer to the computer.

A Glass Tube Rotameter of the range 0-35 LPM was used to control the mass flow rate and measure the mass flow rate of the incoming gas. The reactor was made up of GI pipe with 30 mm diameter with 1.5 mm wall thickness and 200 mm in height. The adsorption reactor was a packed column filled with the adsorbent of interest. A pressure monitoring system capable of measuring up to 0.5 MPa was attached to know the incoming pressure with an accuracy of ±0.5%. Experiments were carried at varying pressure to see the effect of pressure in the adsorption process at a constant temperature. A number of needle valves were attached in the system to control the system operation at the require rate. Flue Gas Analyzer (KM9106) was used to measure the inlet sample gas and the outlet gas properties (Appendix I). The apparatus was tested for leak absence and for accuracy through calibrations with an empty tank. An electric oven was used for treating the adsorbents prior to the adsorption experiments. An auto-calibrated microbalance was used for weighing the adsorbent samples.

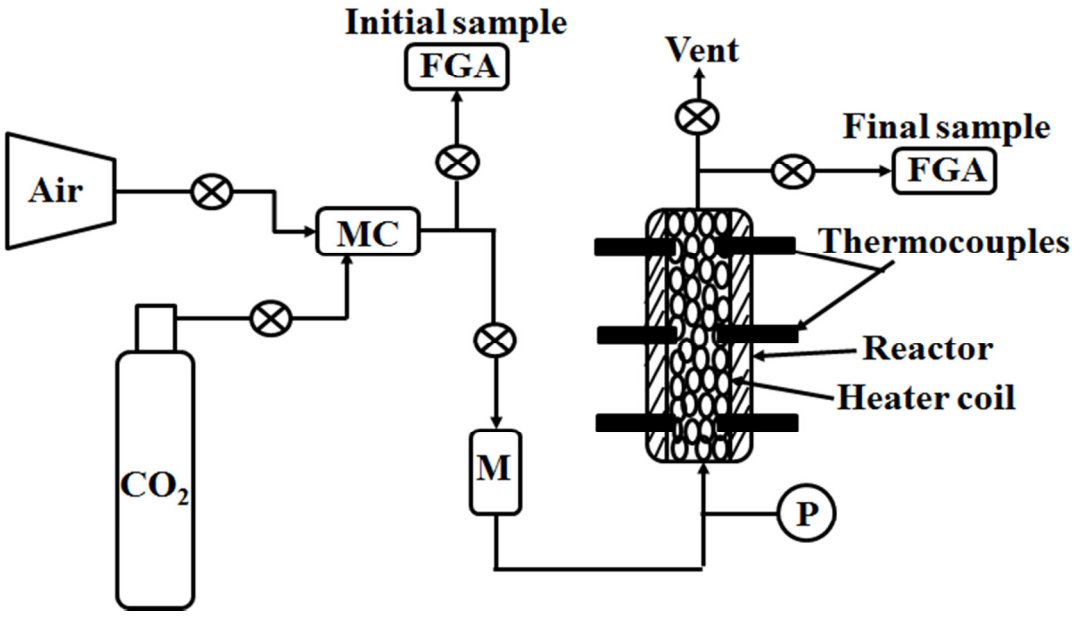

Fig 5.1 Schematic of the experimental setup for fixed bed. MC: Mixing chamber; M: Mass flow meter; P: Pressure gauge; FGA: Flue Gas Analyzer

5.3 EXPERIMENTAL SETUP FOR FLUIDIZED BED STUDY

The experimental investigation of hydrodynamics and adsorption characteristics of zeolites 4A, zeolite 5A, zeolite 13X and acivated carbon were conducted in a bubbling fluidized bed as shown in Figure 5.2. The bed was connected to a Centrifugal type of blower coupled with a 20 HP electric motor to supply air and CO_2 cylinder. The column consist of a pipe 50 mm diameter and consist of two section along the height; one mild steel pipe of 300 mm in height at the bottom where the heating section was arranged and one plexi-glass pipe of 1000 mm in height. At the bottom porous metal wire mesh of 20 μm was placed as a gas distributor and metal scrap was placed below for the distributor to reduce the pressure drop. At the top of column, a wind filter was installed to prevent fine particles flying out. Figure 5.3 shows the photo of experimental set-up of the fluidized bed for CO_2 adsorption.

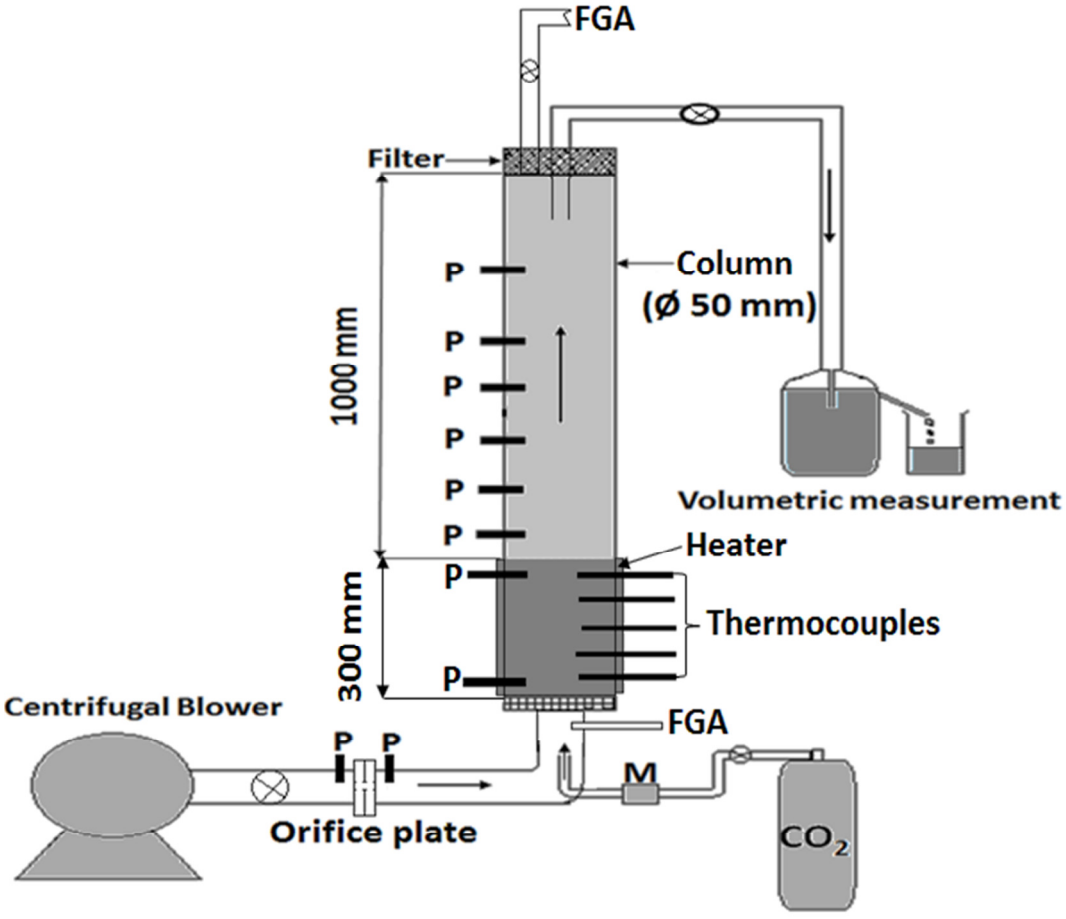

Fig 5.2 Schematic diagram of experimental setup for CO_2 adsorption in fluidized bed

Fig 5.3 Photograph of experimental setup for CO_2 adsorption in fluidized bed

A Glass Tube Rotameter of the range 0-35 LPM was used to control the mass flow rate and measure the mass flow rate of the incoming gas. A manometer was also placed before the column in order to measure the superficial velocity of the incoming air by using the relation; $U_0 = 2.026\sqrt{\Delta P}$ m/s. The pressure drop was measured at different location in the column by using a manometer. The pressure tapping are provided along the bed height at 100 mm intervals to observe the pressure fluctuations, to determine the minimum fluidization, to determine the suspension density and to determine the axial voidage of the bed. Flue Gas Analyzer (KM9106) was used to measure the inlet sample gas and the outlet gas properties. Work had been done to develop a process in which CO_2 was adsorbed onto zeolite 13X, zeolite 5A, zeolite 4A and AC from a gas stream containing approximately 13.8 vol. % of CO_2 in order to imitate properties of flue gas from power plant. The apparatus was tested for leak absence and for accuracy through calibrations with an empty bed.

5.3.1 DESCRIPTION OF HEAT TRANSFER PROBE

Detail of the heat transfer probe is shown in Figure 5.4. Heat transfer probe has a dimension of ID 50 mm and 300 mm height. Adequate insulation with mica sheet and ceramics wool was provided around the probe. Electrical energy input to the heater is controlled by variac and measured with wattmeter. Thermocouples (K-type) were inserted in the heating section to measure the bed temperatures with accuracy of ±0.5% (Appendix III). The thermocouples wires were connected to channels of the temperature module of the Data Acquisition system and temperatures are recorded by system directly.

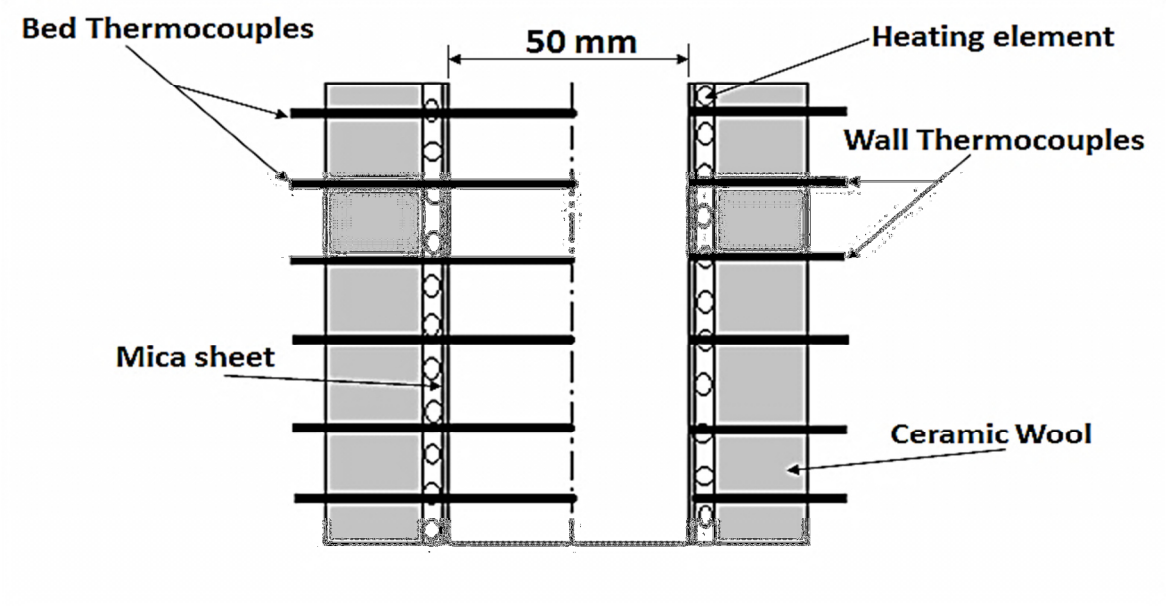

Fig 5.4 Schematic diagram of heating section in fluidized bed

5.4 EXPERIMENTAL PROCEDURES FOR FIXED BED STUDY

Prior to the adsorption experiment, the selected adsorbent was heated in an oven so as to remove any moisture and unwanted gases. After being heated 3 hrs, the adsorbent was cooled down at room temperature. The adsorbent was then weighed and loaded into the adsorption column. The process employed a single-bed pressure swing adsorption unit. For the adsorption process, first the air was allowed to flow through the reactor and then followed by carbon dioxide. To maintain equal flow rate and pressure of both the flows, the gas mixture was allowed to pass

through the mixing chamber. The flow of air was then stopped and allowed only the pure CO_2 to flow through the reactor for measurement of the mass of CO_2 adsorbed per the mass of the adsorbent. To know the effective adsorbed mass on the adsorbent materials $Q_{eff,}$ two quantities were defined: Q_t that is the mass containing the reactor including the adsorbents and Q_d which is the mass of the empty reactor or dead volume. The Q_{eff} was then calculated with the equation as follows: $Q_{eff}=Q_t-Q_d$.

The specific adsorption capacity for a certain component is defined as the total amount of the component adsorbed per mass unit of the sorbent and was compared with the experimental data [De wilde et al., 2000]:

$$\text{Specific Capacity} = \frac{S}{W} u_s \int_{t=0}^{t=end} (C_0 - C) dt \tag{5.1}$$

The adsorbent material like zeolite 4A, zeolite 5A, zeolite 13X and activated carbon are packed in the adsorption columns where the gas stream is introduced at a regular time period until the adsorbent reaches its saturation point. Experimental conditions for the measurement of adsorption isotherm and kinetics the fixed bed are given in Table 5.1.

Table 5.1 Experimental conditions for fixed bed study

Bed weight	*20 g*
Reactor length	*200 mm*
Reactor diameter	*30 mm*
Influent CO_2 concentration	*13.8 vol%*
Inlet flow rate	*15 LPM*
Bed porosity	*0.5*
Superficial velocity	*0.13 m/s*
Adsorption temperature	*298 K- 333 K*
Adsorption pressure	*0.4 MPa*

The saturated column then undergoes the desorption operation during which the adsorbed CO_2 is released under controlled pressure and temperature, and the adsorbent capacity is restored for

more adsorption. The performance of CO_2 adsorption depends on two primary characteristics like adsorption equilibrium and adsorption kinetics.

5.5 EXPERIMENTAL PROCEDURES FOR FLUIDIZED BED STUDY

Experiments were conducted with four different inventory viz. zeolite 4A, zeolite 5A, zeolite 13X and activated carbon. Table 5.2 gives details of the operating parameters for the fluidized bed study. The weights of the inventory were changed from 200 g to 300 g to find out its effect on the behavior of the fluidizations. The experiments were divided into three parts:

Table 5.2 Experimental condition for fluidized bed study

Bed weight , W	*200 g, 250 g, 300 g*
Reactor length, L	*1300 mm*
Reactor diameter, d_r	*50 mm*
Inlet CO_2 concentration, C_0	*13.8 vol.%*
Adsorption temperature, T	*298 K –333K*
Superficial velocity, U_s	*0.8 m/s -2.1 m/s*
Adsorption pressure, P	*0.4 MPa*
Density of feed (air + CO_2), ρ_g	*1.22 kg/m^3*
Viscosity of feed (air + CO_2), μ_g,	*17.96×10^{-6} kg/m sec*

1. **Hydrodynamic study:** Prior to the start of actual experiments, some trial runs were taken to have an idea about the control and measurement of operating parameters. A known quantity of the inventory was loaded into the main column through the top of the column. The blower was then started and only air was allowed to flow through the bed with the help of air control valve. As the air flow was slowly increased the bed started to expand. When the air velocity was further increased and exceeded the terminal velocity of particles, entrainment of solid begun. The desired air flow rate was maintained by adjusting the flow through the orifice meter. In this study, the pressure drop and velocity were recorded to measure the voidage profile and suspension density.

2. **Heat transfer study:** The require quantity of inventory (zeolite 4A, zeolite 5A, zeolite 13X and activated carbon) was loaded into the main column through the top of the column. The switch of heater was then put on. A predetermined heat flux was set by controlling the variac after adjusting the power from wattmeter. The blower was then started and air was allowed to flow through the bed with the help of air control valve. The air flow rate was slowly increased and then the desired air flow rate was maintained. Heat flux to the tune of 230.63 W/m^2 was applied to the heat transfer probe. The gas particle emulsion while passing over the heat transfer probe gets heated till the steady state condition was reached. In order to measure the effect of CO_2 on the heat transfer, the CO_2 cylinder was opened and allowed to flow in the column to mix with the air.

3. **Adsorption study**: In order to measure the adsorption capacity, first, the air was allowed to flow through the bed and then followed by CO_2. The flow of air was then stopped and allowed only the pure CO_2 (99.99) to flow through the bed for measurement of the volume of CO_2 adsorbed per mass of the adsorbent. The volumetric measurement consists of a brine solution and connected to a conical flask. When the pure CO_2 passed through the bed, it was then allowed to displace the brine solution; the amount of displaced water collected in the conical flask was considered the outlet volume. To know the effective adsorbed amount on the adsorbent materials V_{eff}, two quantities were defined: V_i, that is the initial volume of CO_2 before entering the bed and V_o, which is the outlet volume of CO_2 collected in conical flask. The V_{eff} was then calculated with the equation as follows: $Q_{eff}=V_i-V_o$. The temperature of the bubbling fluidized bed was maintained at a temperature ranging from 298 K to 333 K by using variac.

5.6 SUMMARY

In this chapter, development of CO_2 adsorption unit for a fixed as well as fluidized beds study and their experimental procedure have been discussed. The results of the experimental work carried out as per the experimental procedure are presented in following Chapter 6 and Chapter 7. The experimental data and the specifications of the equipment used in the experiments are presented in the appendix.

CHAPTER 6

CO_2 ADSORPTION IN THE FIXED BED – RESULTS AND DISCUSSION

6.1 INTRODUCTION

This chapter presents the experimental results of CO_2 adsorption on the selected adsorbent materials: zeolite 13X, zeolite 5A, zeolite 4A and activated carbons in a fixed bed. The experimental breakthrough curves were compared with the simulated results. The CO_2 adsorption experiments were conducted under test conditions provided earlier in Chapter 5 (Table 5.1). The results reported here can be categorized into six main aspects: i) CO_2 adsorption equilibrium indicating the maximum capacity of each adsorbent material ii) CO_2 adsorption kinetics indicating the rate of adsorption activity iii) CO_2 breakthrough curve presenting the transient behaviour and its comparison with the simulated results and iv) Thermodynamics of adsorption v) Adsorbents regeneration studies vi) validation of the results with the available literatures. The effects of process parameters (temperature and pressure) on the adsorption behaviour are also discussed in this chapter. The equilibrium data were analyzed further for heat of adsorption.

6.2 ADSORPTION ISOTHERM

In this study, the CO_2 adsorption for each adsorbent was measured under a series of isothermal conditions (i.e., 298 K, 308 K, 318 K and 333 K). For a given temperature, the amount of adsorption was obtained as a series of data pairs that shows the maximum amount CO_2 adsorbed at the corresponding partial pressure of CO_2 gas. Figure 6.1 shows the relationships between the adsorbed amount of CO_2 and the adsorption pressure for zeolite 13X. The amount of CO_2 adsorbed by using zeolite 13X is 4.97 $gmol_{CO_2} kg^{-1}_{sorbent}$ at a temperature 298 K and 0.4 MPa. It

also reveals the typical behaviour showing the effect of temperature on the CO_2 adsorption capacity. That is, an increase in adsorption temperature from 298 K to 308 K leads to a reduction in the amount of adsorbed CO_2. Rising temperature simply provides more internal energy to CO_2 molecules in the gas phase. It should be noted that the increasing internal energy allows gaseous molecules to diffuse at a greater rate, but, at the same time, it reduces the chance for the CO_2 to be restrained or trapped by fixed energy adsorption sites on the adsorbent surface.

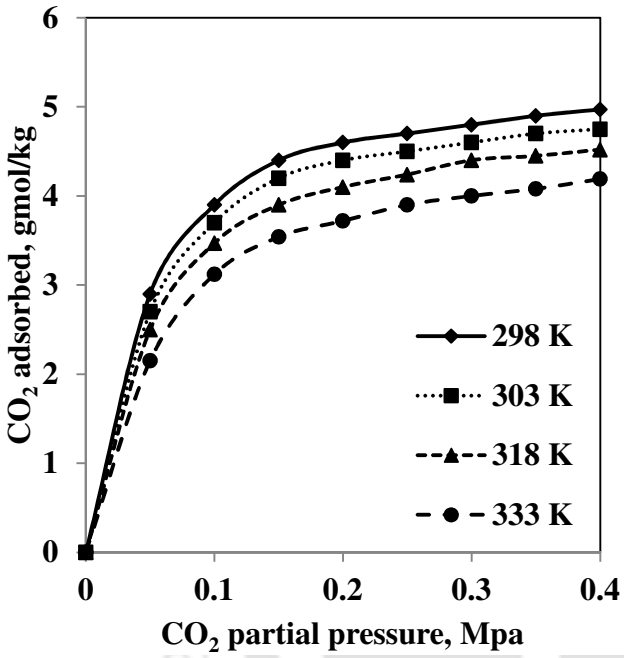

Fig 6.1 CO_2 adsorption isotherm on zeolite 13X

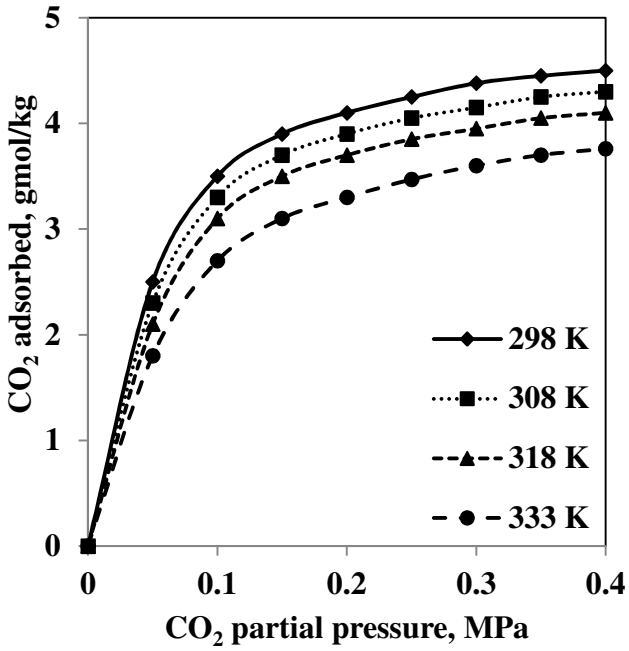

Fig 6.2 CO_2 adsorption isotherm on zeolite 5A

Figures 6.2 – 6.4 shows a similar pattern of adsorption isotherm for zeolite 5A, zeolite 4A and activated carbon respectively. The amount of CO_2 adsorbed by using zeolite 5A is 4.52 $gmol_{CO_2} kg^{-1}_{sorbent}$ while zeolite 4A gives the lowest adsorption capacity among the zeolite based adsorbent with an amount of 4.22 $gmol_{CO_2} kg^{-1}_{sorbent}$ at 0.4 MPa and a temperature of 298 K. Activated carbon gives the lowest adsorption capacity with an amount of 4.14 $gmol_{CO_2} kg^{-1}_{sorbent}$ among all the adsorbents considered in this study. At higher temperature, CO_2 adsorption capacity for all adsorbents is decrease by 20 to 30 percent. In addition, the slope of adsorption isotherm curves reveals the strength of interaction between CO_2 molecules and adsorption sites for individual adsorbents. It appears that zeolite based adsorbents exhibit strong adsorption.

Note that the isotherm curves reported here were obtained from the experiments using pure CO_2 gas. These pure component isotherms can be used together with the real adsorption solution theory (RAST) model for the design of a multi-component adsorption system. It can be seen that all isotherm curves exhibit common behavior regardless of temperature and adsorbent type which mean the amount of CO_2 adsorbed on the adsorbent increases very rapidly with the increase in pressure over the low pressure range, and it tends to stabilize as the pressure continues to increase. This isotherm behaviour follows the type-I isotherm category according to IUPAC adsorption isotherm classification [Keller et al., 2005], which indicates a monolayer adsorption mechanism, commonly applied to microporous adsorbents as shown in Figure 4.1 in Chapter 4.

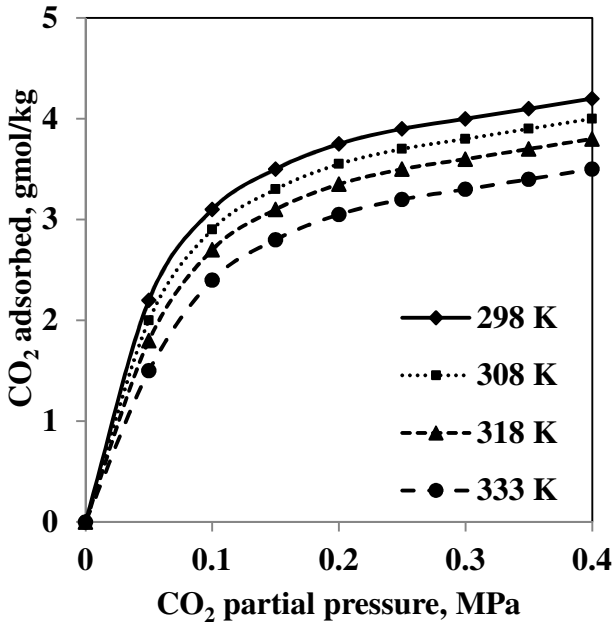

Fig 6.3 CO_2 adsorption isotherm on zeolite 4A

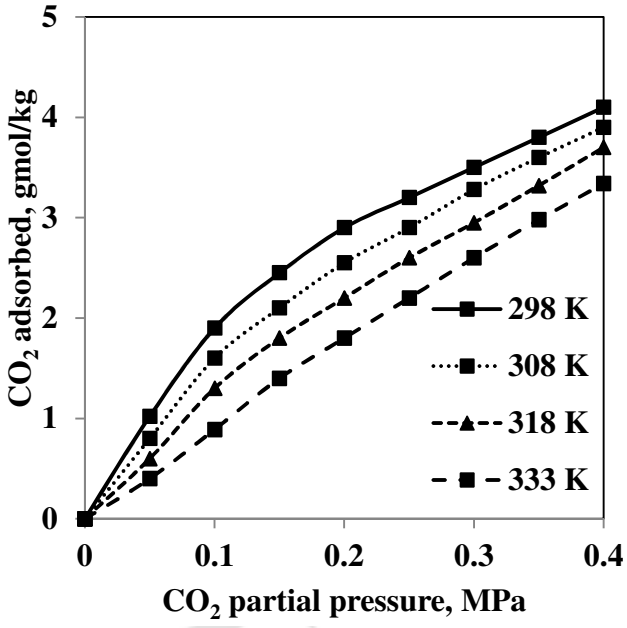

Fig 6.4 CO_2 adsorption isotherm on activated carbon

The rapid increase in the isotherm curve demonstrates the proper range of equilibrium pressure that promotes the majority of adsorption activity. This is important information that can be used to identify both adsorption pressure and regeneration pressure in the pressure swing adsorption process. The stabilized amount of CO_2 adsorbed in the curve shows that all adsorption sites are occupied by CO_2 gas, which represents the capacity limit of the adsorbent at the particular temperature. Similar result has been reported by Tlili et al., 2009, Pllerano et al., 2009 and Konduru et al., 2007.

6.3 ISOTHERM MODELS FOR CO_2 ADSORPTION

To allow the use of obtained adsorption isotherms for different purposes, the equilibrium data were correlated into different isotherm models. These models were the Langmuir, Freunlich, Toth and Sips equations presented previously in Chapter 4. Nonlinear regression analysis was performed to determine the model parameters for individual adsorbents. The obtained regression results for individual temperatures for Langmuir, Freunlich, Toth and Sips models are given in Tables 6.1 through 6.4 respectively.

From Tables 6.1 to Table 6.4, it can be seen that the percentage errors in the experiments were within 10.01 percent approximately which were calculated from Equation 4.17 at a temperature ranging from 298 K to 333 K. It can also be observed that Sip's model equation provides the best fit with the isotherm curves for zeolite 13X, zeolite 5A and zeolite 4A with an average R^2 value of 0.98 which indicates that an adsorbed molecule can occupy more than one adsorption site during the adsorption process [Morse et al., 2010]. On the other hand, Toth model equation provides the best fit for activated carbon with R^2 of 0.99 which indicates that the adsorbent surface is not ideal but, rather, it is energetically heterogeneous. It should be noted that both the Sips and Toth models correlated the obtained isotherm data well for temperatures ranging from 298 K to 333 K. This enabled us to develop a generic isotherm equation for each adsorbent that takes into account the effect of adsorption temperature.

Table 6.1 Langmuir constants and their regression coefficients

Material	Temperature (K)	Langmuir Constant		R^2	Δq%
		q_m	K		
Zeolite 13X	298	4.24	19.03	0.98	6.62
	308	3.97	16.87	0.97	9.73
	318	3.52	13.74	0.98	8.51
	333	3.17	11.20	0.97	10.85
Zeolite 5A	298	3.62	18.33	0.96	7.66
	308	3.37	15.57	0.97	5.77
	318	3.01	11.94	0.95	8.82
	333	2.87	10.34	0.96	9.81
Zeolite 4A	298	3.26	17.14	0.96	5.45
	308	3.07	14.35	0.97	12.56
	318	2.92	11.45	0.97	7.99
	333	2.61	9.97	0.96	9.57
Activated carbon	298	2.82	21.95	0.96	9.81
	308	2.71	19.11	0.97	8.53
	318	2.59	15.50	0.96	12.77
	333	2.49	11.75	0.97	10.54

Table 6.2 Freundlich constants and their regression coefficients

Material	Temperature (K)	Freundlich Constant		R^2	Δq%
		n	K		
Zeolite 13X	298	1.12	6.12	0.91	8.53
	308	1.03	5.48	0.93	6.75
	318	0.95	4.59	0.92	10.54
	333	0.83	3.81	0.97	9.57
Zeolite 5A	298	1.05	5.33	0.96	7.66
	308	0.92	4.57	0.97	5.78
	318	0.87	3.94	0.95	8.82
	333	0.81	3.34	0.96	9.81
Zeolite 4A	298	0.95	5.02	0.91	12.33
	308	0.76	4.38	0.92	9.56
	318	0.65	3.89	0.92	11.27
	333	0.58	3.31	0.93	10.49
Activated carbon	298	0.50	1.70	0.98	9.75
	308	0.44	1.55	0.98	5.46
	318	0.38	1.38	0.97	8.47
	333	0.34	1.31	0.98	9.13

Table 6.3 Toth constants and their regression coefficients

Material	Temperature (K)	Toth constant		R^2	Δq%
		b	*K*		
Zeolite 13X	298	3.94	12.03	0.95	6.93
	308	3.57	11.87	0.98	8.92
	318	3.12	9.74	0.96	8.93
	333	3.07	7.20	0.97	11.71
Zeolite 5A	298	3.65	10.93	0.96	7.86
	308	3.31	9.57	0.97	6.78
	318	3.02	7.94	0.95	7.55
	333	2.78	6.34	0.96	8.97
Zeolite 4A	298	3.15	10.03	0.98	7.42
	308	2.97	9.07	0.97	9.54
	318	2.76	7.54	0.98	7.96
	333	2.37	6.01	0.97	10.52
Activated carbon	298	2.72	16.55	0.99	6.62
	308	2.61	14.23	0.99	9.75
	318	2.49	11.30	0.98	8.57
	333	2.29	9.75	0.98	10.84

Table 6.4 Sips constants and their regression coefficients

Material	Temperature (K)	Sip's constant		R^2	Δq%
		b	*K*		
Zeolite 13X	298	4.84	12.03	0.99	7.97
	308	4.37	11.87	0.99	6.75
	318	3.92	9.74	0.98	5.23
	333	3.47	7.21	0.98	8.79
Zeolite 5A	298	4.03	18.33	0.96	8.94
	308	3.87	15.57	0.97	7.62
	318	3.11	11.94	0.95	10.17
	333	2.97	10.34	0.96	7.61
Zeolite 4A	298	3.35	10.03	0.99	5.46
	308	2.99	9.07	0.98	7.58
	318	2.67	7.54	0.99	6.94
	333	2.37	6.01	0.98	9.52
Activated carbon	298	2.62	16.55	0.96	9.63
	308	2.33	14.21	0.92	6.77
	318	2.19	11.33	0.97	7.52
	333	2.02	9.75	0.93	10.34

6.4 ADSORPTION BREAKTHROUGH CURVES

Adsorption is a transient process and the amount of material adsorbed within a bed depends both on position and time. Comparisons of experimental and simulation breakthrough curves for CO_2 adsorption on the four adsorbents are shown in Figures 6.5 - 6.8 and the experimental conditions are given in Table 5.3. Figure 6.5 shows ratio of the outlet concentration and the influent concentration against the contact time for zeolite 13X at an atmospheric pressure and temperatures of 298 K, 308 K, 318 K and 333 K respectively. The breakthrough simulation of CO_2 on zeolite 13X were performed using the Linear driving force (LDF) model described in Chapter 4. It can be found that the LDF model is suitable for describing the adsorption of CO_2 on zeolite 13X, and zeolite 5A, zeolite 4A and activated carbon as well. The overall mass transfer parameter used for the simulation and diffusivity factors are listed in Table 4.1. To estimate the pore diffusivity coefficient, a tortuosity factor of 4 is assumed for all the adsorbents.

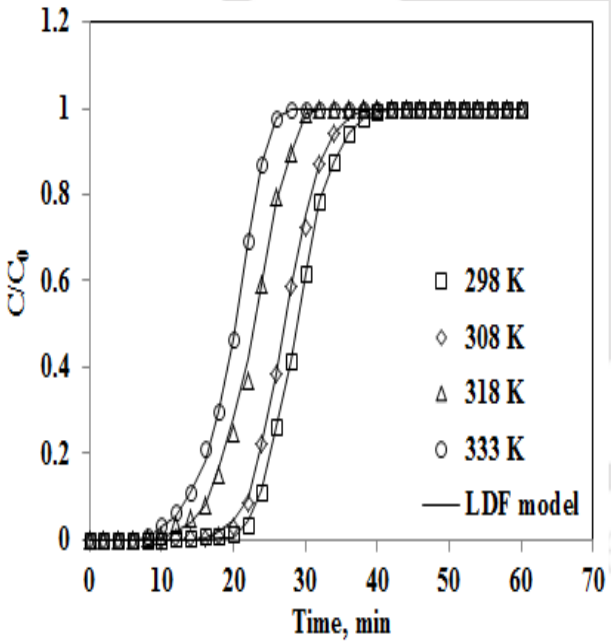

Fig 6.5 CO_2 breakthrough curve for zeolite 13X at 0.1 MPa

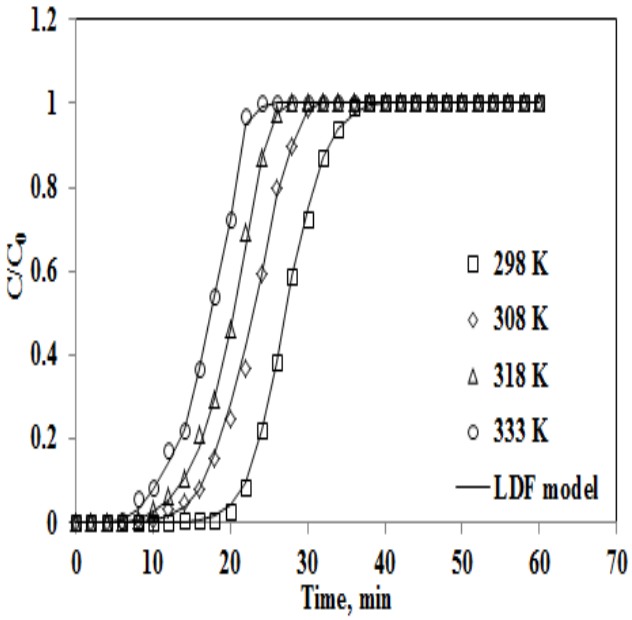

Fig 6.6 CO_2 breakthrough curve for zeolite 5A at 0.1 MPa

The general pattern of the breakthrough curves were achieved as expected for all adsorbents used for the present study. It can be observed that increased in the temperature leads to a shorter CO_2

breakthrough time due to the exothermic nature of adsorbent. This shows that the pore diameter of zeolite 13X is sufficient for the CO_2 to enter into the adsorbent materials channels. The major cations of zeolite based materials are Na and K and this major cation appears to play the main role in the adsorption of CO_2. Also, sodium appears to be the favorable cation for the adsorption of CO_2. The saturation time for zeolite 13X is occur at 40 min at 298 K. Three phases can be defined for all breakthrough curves. The breakthrough phase; where CO_2 quickly breakthrough the fixed-bed column. The competition phase; where CO_2 still diffuses in the upstream of the bed and still increases the trend in concentration. Lastly, the saturation phase; where the adsorbents are fully saturated with CO_2 and no longer adsorbed. The kinetics suggests that all adsorptions are controlled by the micropore diffusions.

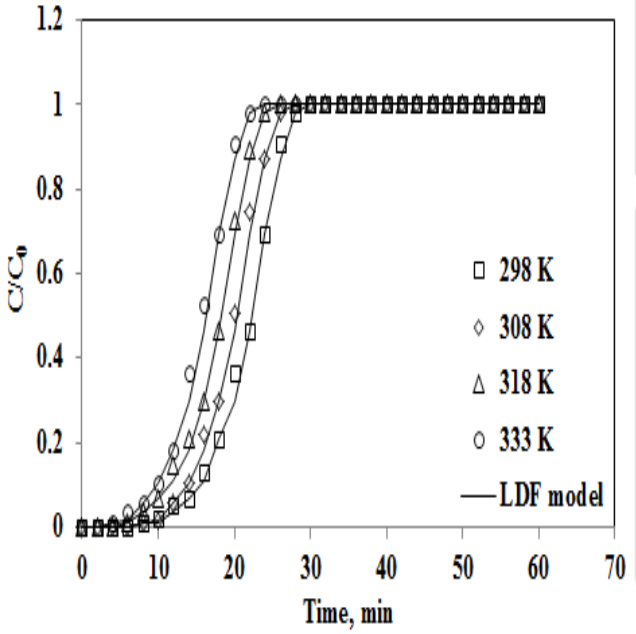

Fig 6.7 CO_2 breakthrough curve for zeolite 4A at 0.1 MPa

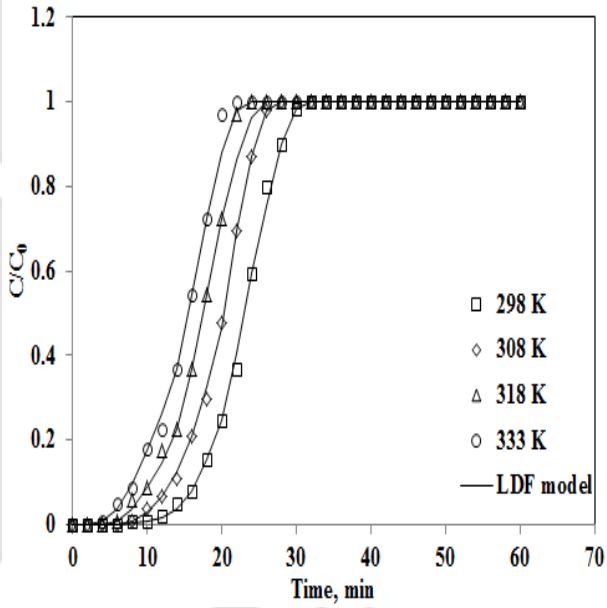

Fig 6.8 CO_2 breakthrough curve for activated carbon at 0.1 MPa

Figures 6.6 to 6.8 show a similar pattern of breakthrough curves for zeolite 5A, zeolite 4A and activated carbon respectively at a similar condition as zeolite 13X. The saturation time for zeolite 5A is 35 min, 29 min for zeolite 4A and 25 min for activated carbon at 298 K. Clearly, all the adsorbent materials have a large surface area and pores to trap CO_2 molecules. However, the breakthrough time with activated carbon was shorter as compared to zeolite based material, indicating that the CO_2 adsorption capacity of activated carbon is lower than that of zeolite based adsorbents. The differences in adsorption observed with zeolite based adsorbents and activated

carbon should be related to the differences in the surface structure and porosity. Zeolite based adsorbents have a higher surface area than activated carbon and that may have contributed to the higher adsorption capacity of zeolite 13X, zeolite 5A and zeolite 4A.

The specific capacity of CO_2 adsorption was calculated from Equation 5.1 and shows a similar data with the results of equilibrium adsorption isotherms. Also, the amount of adsorption decreases with increase in the bed temperature for all the adsorbents. To conclude, the adsorption performance of zeolite 13X is highest as compared to zeolite 5A, zeolite 4A and activated carbon in terms of breakthrough. According to the experimental results where the Bi number is far higher than that of 50, it suggests that film resistances show limited effect on the mass transfer resistances, thus the intra-particle diffusion in the pores is predominant and the external mass transfer resistance can be neglected for all the adsorbents. As it follows from Table 4.1, the mass transfer coefficient, k_g value of the different adsorbent increases in the following trend as zeolite 13X > zeolite 5A > zeolite 4A> activated carbon. Zeolite 13X has the most efficient mass transfer because of its widest pore distribution and highest pore volume.

6.5 MODEL SENSITIVITY ANALYSIS

A number of parameters have been varied such as bed height, flow rate, bed void fraction, zeolite pellet diameter, ambient temperature and adsorption isotherm data to better understand the LDF model. In order to study the model sensitivity the zeolite 13X was chosen as the adsorbent materials at pressure 0.1 MPa. Bed height was varied from 50 mm to 300 mm to show the increase in breakthrough time as shown in Figure 6.9. The plot shows that for increasing bed height, the breakthrough curve spreads out over a longer time.

Bulk flow rate was varied from 5 LPM to 10 LPM through our adsorption the adsorption column. Bed height was kept constant at 200 mm. Breakthrough times varied greatly and it can be concluded from Figure 6.10 by increasing the flow rate the breakthrough time decreases in the adsorption column. As flow rate increased, the breakthrough curves become steeper and reached the breakthrough quickly. This is because of the residence time of the adsorbate in the column, which is long enough for adsorption equilibrium to be reached at high flow rate. The residence

time was calculated as the fixed bed volume divided by the mass flow rates of the adsorbate. This means that the contact time between the adsorbate and the adsorbent is minimized, leading to early breakthrough (Sivakumar and Palanissamy, 2009). Increasing the flow rate gave rise to a shorter time for saturation.

Bed void fraction is a parameter which is hard to measure and can vary greatly between adsorption columns. Bed void fraction is the ratio of volume in a packed column to the volume of an unpacked column. This ratio can vary depending on how well the zeolite 13X is packed into the bed. For this analysis purpose the bed voidage was varied from 0.1 to 0.9 to investigate its effect on the LDF model, the results are shown in Figure 6.11. By increasing the bed voidage the adsorption breakthrough curve decreases.

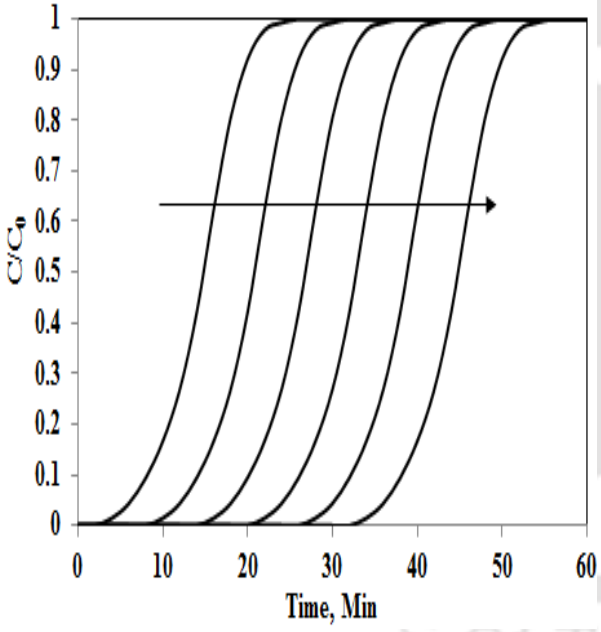

Fig 6.9 Breakthrough curves for various adsorption bed heights (50 mm to 300 mm)

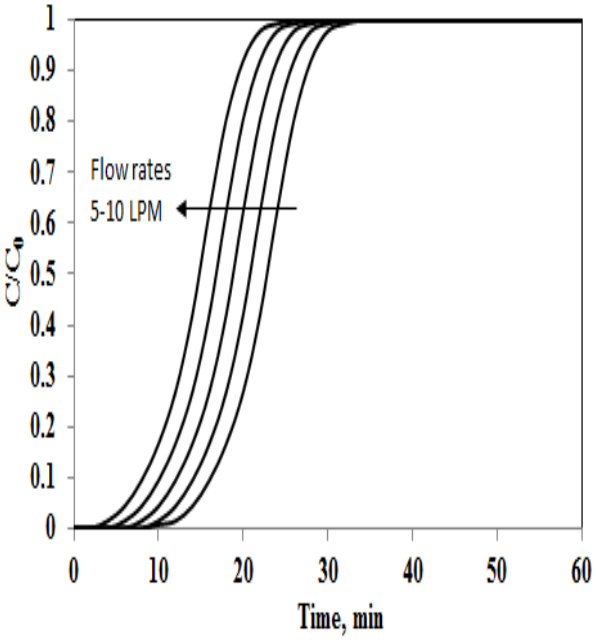

Fig 6.10 Breakthrough curves for various flow rates (5-10 LPM)

The diameter of a zeolite pellet is another parameter that is difficult to measure experimentally. The zeolite pellet diameter was varied from 0.1 mm to 2 mm to investigate its effect on the LDF model. A plot of varying pellet diameter shows that it affects the slope of the breakthrough curve as shown in Figure 6.12. Pellets with small diameters give breakthrough curves with steep

slopes, indicating that mass transfer and diffusion through the bed are negligible. Using a large zeolite pellet will result in early breakthrough, but a longer period until total breakthrough in the bed. This is because the adsorbed species will take longer to diffuse into the zeolite and become adsorbed on all available active sites.

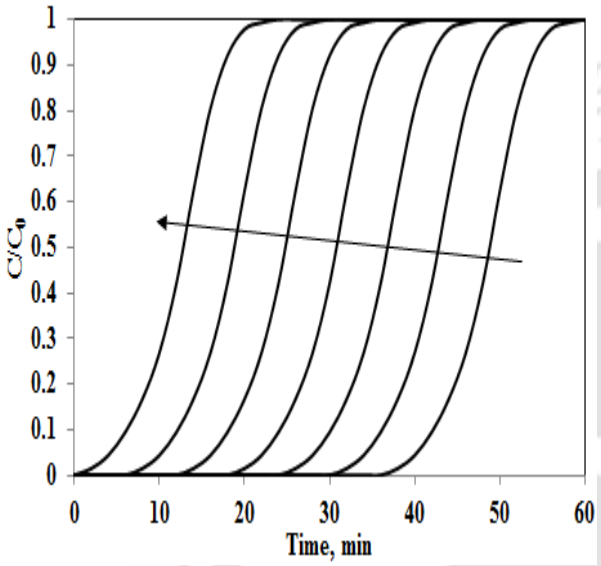

Fig 6.11 Breakthrough curves for various bed void fractions (0.1 to 0.9)

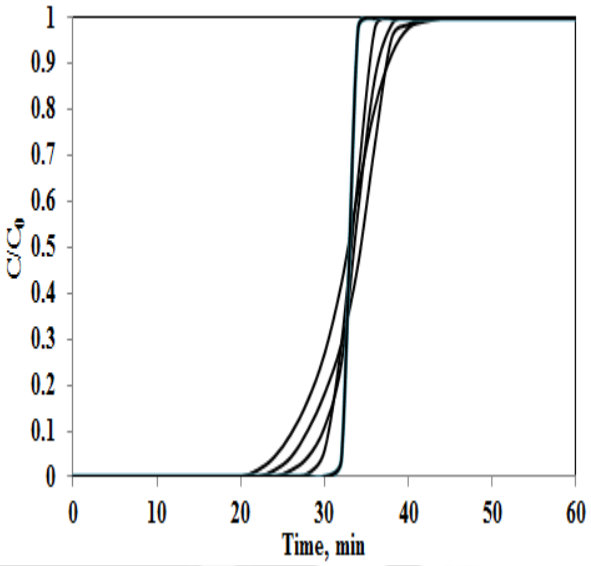

Fig 6.12 Breakthrough curves for varying pellet diameter (0.1 mm to 2 mm)

6.6 THERMODYNAMIC ANALYSIS ON CO_2 ADSORPTION

The van't Hoff's equation provides information about the temperature dependence of the equilibrium constant. The van't Hoff's equation may be derived from the Gibbs-Helmholtz equation, which gives the temperature dependence of the Gibbs free energy. The thermodynamic parameters can be calculated from Langmuir isotherms by using the Vant'Hoff's equation as follows through Equation 6.1 to Equation 6.3 [Alzaydien and Manasreh, 2009]:

$$\Delta G^{\circ} = -RT \ln K_l \tag{6.1}$$

$$\Delta H^{\circ} = R \frac{T_1 T_2}{T_2 - T_1} \ln \frac{K_2}{K_1} \tag{6.2}$$

$$\Delta S^{\circ} = \frac{\Delta H^{\circ} - \Delta G^{\circ}}{T} \tag{6.3}$$

where ΔG° is change in the Gibb's free energy, ΔH° is change in the enthalpy and ΔS° is change in the entropy. A plot of ln K_{eq} vs. 1/T should be a straight line with a slope = $-\Delta H^{o}/R$ and an intercept = $\Delta S^{o}/R$ which is called Van't Hoff's equation.

The thermodynamic parameters were calculated from the Langmuir isotherms by using the Van't Hoff's equation as given Equations 6.1 - 6.3. The detail parameters for CO_2 adsorption on the adsorbent like zeolite 13X, zeolite 5A, zeolite 4A and activated carbon are given in Table 6.5. The temperature effects on the adsorption of CO_2 were studied at 298 K, 308 K, 318 K and 333 K respectively. From adsorption isotherm curve, it can be seen that by increasing the bed temperature there is a decrease in CO_2 adsorption capacity which is due to the exothermic nature of the adsorption process. The optimum temperature for CO_2 adsorption on the four adsorbents was found to be 298 K within the temperature range studied.

Table 6.5 Thermodynamic parameters for the adsorption of CO_2

Material	Temperatures (K)	ΔG° (kJ/mol)	ΔH° (kJ/mol)	ΔS° (J/mol.K)
Zeolite 13X	298	-7. 93	-11.27	17.57
	308	-7. 68		
	318	-6.29		
	333	-6.24		
Zeolite 5A	298	-7.54	-12.16	17.07
	308	-7.15		
	318	-6.95		
	333	-6.76		
Zeolite 4A	298	-7.29	-12.85	18.49
	308	-7.24		
	318	-6.93		
	333	-6.64		
Activated carbon	298	-7.65	-14.98	24.37
	308	-7.55		
	318	-7.25		
	333	-6.83		

The thermodynamic parameter of Gibbs free energy change, ΔG°, was calculated using Langmuir constants and the results are listed in Table 6.5. The enthalpy change, ΔH° and the entropy change, ΔS°, for the CO_2 adsorption process on zeolite 13X were -11.27 kJ/mol and

17.57 J/mol.K respectively while the enthalpy change and entropy change for zeolite 5A were calculated to give -12.16 and 17.07 respectively. For zeolite 4A the enthalpy change, ΔH° and the entropy change, ΔS° are -12.85 kJ/mol and -18.49 J/mol.K and for activated carbon -14.98 kJ/mol and -24.37 J/mol.K respectively. The negatives values of ΔG° confirm the feasibility of the process and the spontaneous nature of the adsorption process. The negative values in ΔH° indicated that the adsorption reaction is exothermic for all the adsorbent used. The positive value of ΔS° reflects the affinity of both the adsorbents with CO_2 and suggests some structural change in CO_2 and the adsorbents.

6.7 REGENERATION STUDY

The four adsorbents (zeolite 13X, zeolite 5A, zeolite 4A and activated carbon) were tested for material aging by using the same adsorbent over 5 adsorption-desorption cycles at 298 K and at 0.1 MPa. The desorption process is achieved by increasing the bed temperature up to 373 K which increases the internal energy of the gas and allowed to escaped from the reactor. Figures 6.13 and 6.16 shows adsorption isotherm of zeolite 13X and zeolite 5A respectively at 298 K for five cycles. Up to 0.02 MPa the CO_2 adsorption increased rapidly when the pressure was increased. The increase in CO_2 adsorption after 0.02 MPa appeared to be gradual. The adsorption isotherms for repeated cycles showed a reduction in the amount of adsorption for the next cycles. This indicated that the adsorption is not reversible and complete regeneration cannot be obtained by adsorption of the material after adsorption. The amount of adsorption is almost similar for cycles 4 and 5 which indicate that the adsorbent is almost saturated with CO_2.

The adsorption isotherms for zeolite 4A for 5 cycles is shown in Figure 6.15 and shows that the adsorption isotherm for zeolite 4A is not highly reproducible, indicating that the adsorption is not completely reversible. The adsorption at the first cycle was the highest and the uptake of CO_2 for zeolite 4A was lower than that of zeolite 13X and zeolite 5A at CO_2 partial pressures up to 0.4 MPa. The adsorption isotherm for activated carbon for 5 cycles of adsorption desorption are shown in Figure 6.16. It is interesting to note that all the isotherms were extremely reproducible, which indicates the excellent reversibility of adsorption. This is due to the fact that activated

carbon (coconut fiber based) have a weaker bond which can easily be penetrated by CO_2 molecules using pressure modulation while zeolite based adsorbents have stronger bond structure which cannot be easily broken by CO_2 molecules.

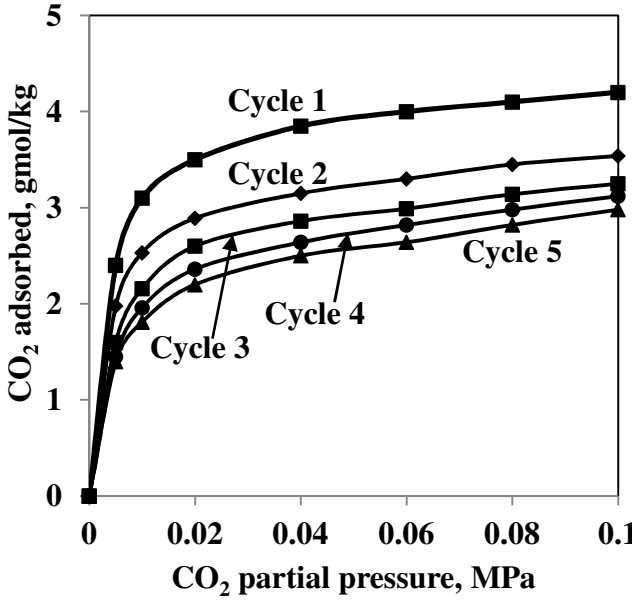

Fig 6.13 Adsorption isotherms of zeolite 13 X

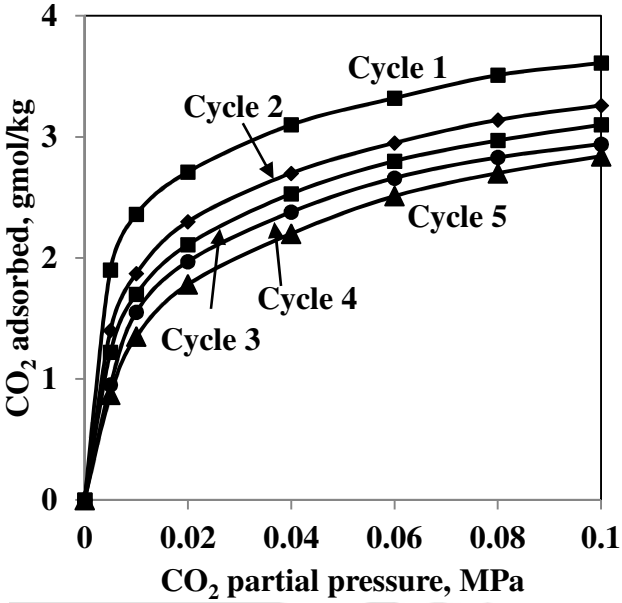

Fig 6.14 Adsorption isotherms of zeolite 5A

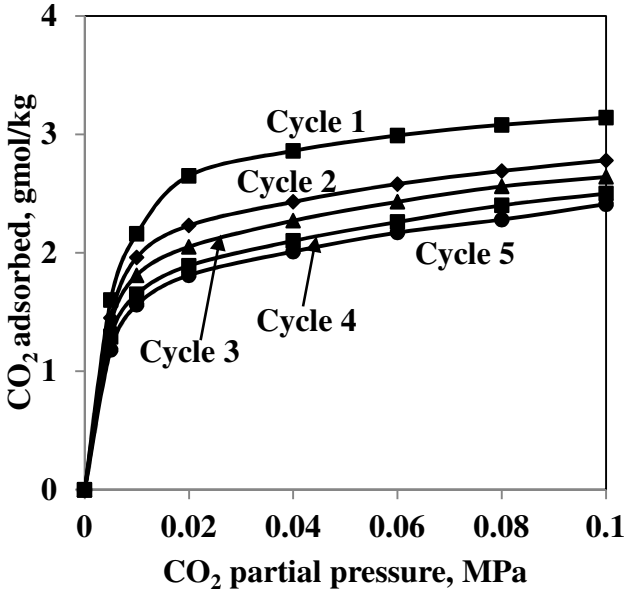

Fig 6.15 Adsorption isotherms of zeolite 4A

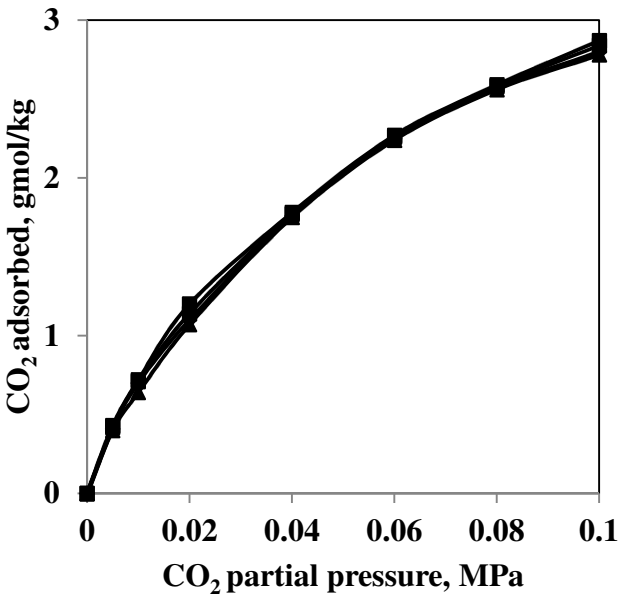

Fig 6.16 Adsorption isotherms of activated carbon

Therefore, there will always be a residual after each cycles of adsorption desorption for zeolite based adsorbents. For activated carbon there was no residual after the adsorption desorption cycles hence the complete reversibility. The CO_2 uptake for activated carbon was lower than that of the two zeolite based adsorbents at lower pressure, but at higher pressure up to 3.5 MPa, the CO_2 uptake for activated carbon was higher than that of the zeolites [Pellerano et al., 2009].

6.8 VALIDATION OF EXPERIMENTAL WORK

The experimental method was validated by comparing the CO_2 adsorption isotherms obtained in this study with those reported in the open literature. Based on the availability of the published data, the comparison was made at 298 K and pressure up to 0.4 MPa two adsorbents (i.e. zeolite 13X and activated carbon). Comparisons of surface area, pore volume and adsorbent diameter are presented in Table 6.6 for the two adsorbents.

Table 6.6 Comparison of materials with published data

Author	Particle diameter (mm)	Surface area (m^2/g)	Pore volume (cm^3/g)	Material
Present work	2.0	720	0.254	
Cavani et al., 2004	2.7	454.35	0.267	
Siriwardane et al., 2005	2.5	614	0.257	Zeolite 13X
Wang et al., 2012	2.4	507.9	0.201	
Present work	0.92	214	0.068	
Guo et al., 2006	1.5	667	0.241	
Pellerano et al., 2009	1.9	589	0.197	Activated carbon
Goetz et al., 2006	1.2	612	0.213	

It is clear from Figure 6.17 that the CO_2 adsorption isotherms in this study remained within the range of the published data, thereby validating the experimental method and analysis carried out in this study. For the activated carbon, Figure 6.18 also indicates significant deviations in the isotherm data among the published works as the difference in adsorbent physical property (such as pore volume, pore diameter and available surface area) results in the variation of CO_2

adsorption capacity on the adsorbent surface. The current experimental results deviated from the published data within 10 percent deviation as shown by error bars in Figure 6.17 and 6.18.

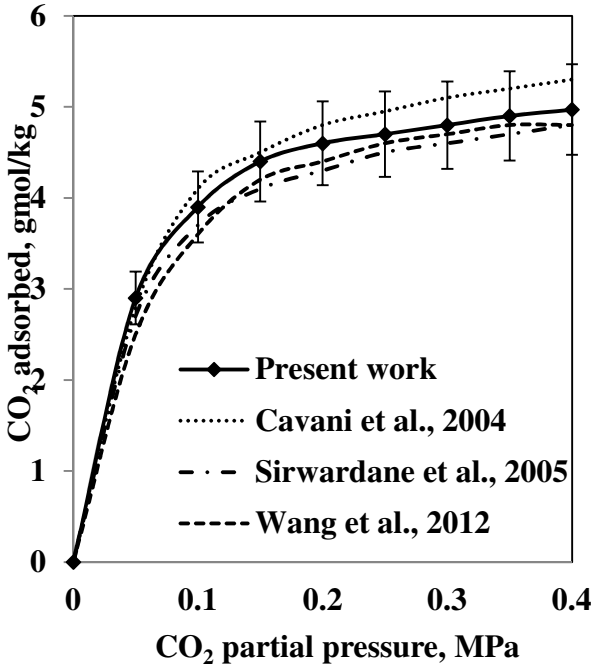

Fig 6.17 Comparison of adsorption isotherm with published data for zeolite 13X

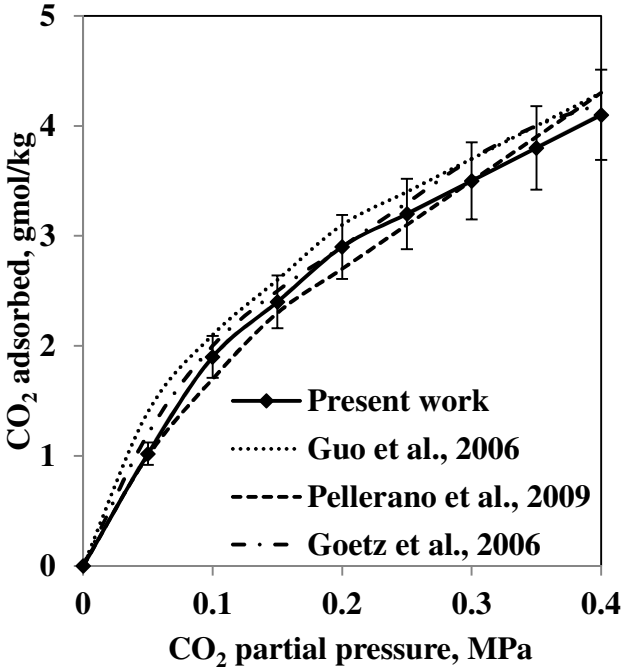

Fig 6.18 Comparison of adsorption isotherm with published data for activated carbon

6.9 SUMMARY

In the present work, a single bed pressure swing adsorption process was employed to determine the adsorption capacity of zeolite 13 X, zeolite 5A, zeolite 4A and activated carbon. The adsorption breakthrough curve, adsorption isotherm, thermodynamics parameters, material aging and the experimental validations were presented. The simulated breakthrough curves by using LDF showed a good agreement with the experimental curves. Also, the experimental data were fitted with adsorption isotherm models like Langmuir, Freunlich, Toth and Sips isotherm models. The following chapter (Chapter 7) discussed CO_2 adsorption in a fluidized bed and its comparison with fixed bed studies.

CHAPTER 7

CO_2 ADSORPTION IN A FLUIDIZED BED – RESULTS AND DICUSSION

7.1 INTRODUCTION

This chapter presents the experimental results of CO_2 adsorption on the selected adsorbent materials like zeolite 13X, zeolite 5A, zeolite 4A and activated carbons in a fluidized bed. The CO_2 adsorption experiments were conducted under test conditions provided earlier in Chapter 5 (Table 5.4). The results reported here can be categorized into four main aspects: i) Hydrodynamic characteristics of the bubbling bed like suspension density, pressure drop, bed voidage profile, ii) CO_2 breakthrough curve presenting the transient behavior, iii) CO_2 adsorption isotherm in a fluidized bed and comparison with fixed bed, iv) CO_2 concentration effect on the heat transfer in the fluidized bed were investigated.

7.2 HYDRODYNAMIC CHARACTERISTICS

The experiment for hydrodynamics study were carried out on zeolite 13X, zeolite 5A, zeolite 4A and activated carbons in a fluidized bed with an inventory of 200 g, 250 g and 300 g respectively. The superficial velocities were varied at the range of 0.8 m/s to 2.1 m/s for the entire inventory. Details of the results are discussed below.

7.2.1 FLUIDIZATION BEHAVIOUR

The experiments carried using the mentioned inventory revealed agglomerate fluidization behavior. During the initial stages of increasing the gas velocity, the total bed lifts up and then settles down. On gradually increasing the velocity further, channel formation was observed

inside the bed though fluidization was also evident at localized regions. Further increased in the gas velocity results in total fluidization of the bed with simultaneous formation of large agglomerates of particles in the fluidized bed; indicating agglomerate fluidization behavior. These agglomerates were the results of surface interaction forces on the individual particle surfaces. The bed expended very little with increase in the gas velocity and bubbles were seen through the bed and the smaller agglomerate appeared to be fluidized in the upper part of the bed whereas the larger agglomerate were found moving slowly at the bottom as the properties of the agglomerate bubbling fluidized bed. During fluidization it was also observed that the agglomerate size decreased with the increased in gas velocity shown in Figure 7.1.

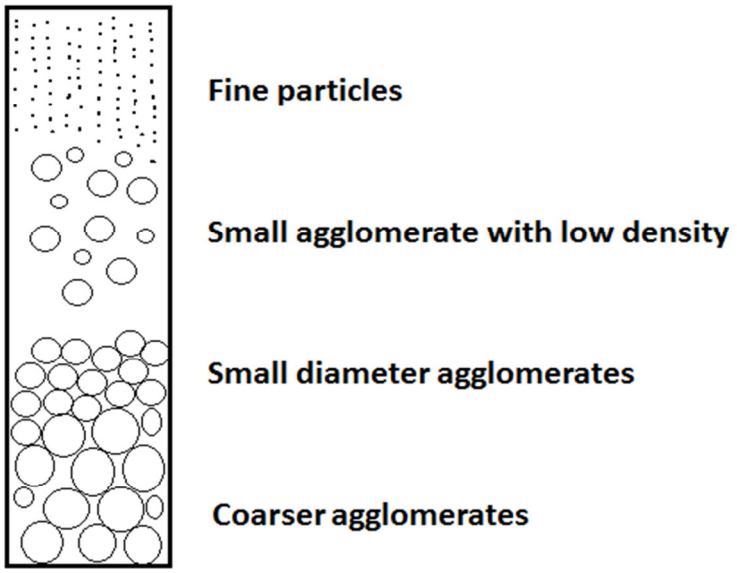

Fig 7.1 Fluidization behavior

7.2.2 MINIMUM FLUIDIZATION VELOCITY

Typical fluidization curves, pressure drop versus superficial velocities for different inventory are shown in Figures 7.2 - 7.4. The pressure drop increases with increase in superficial velocities and then reaches a plateau where it is independent of the gas velocity and become constant. Figure 7.2 through Figure 7.4 showed that the minimum fluidization velocity for zeolite 13X is 2.345 m/s, zeolite 5A is 2.367 m/s, zeolite 4A is 2.415 m/s and activated carbon is 2.18 m/s.

The minimum fluidization can also be calculated from the following as given in Equation 7.1 [Kunii and Levenspiel, 1991]. The Archimedes number, A_r, was calculated by Equation 7.2 and found to be 6.485 x 10^{10} for zeolite 13X, 7.295 x 10^{10} for zeolite 5A, 10.013x 10^{10} for zeolite 4A, 7.896 x 10^{10} for activated carbon. The minimum fluidization, U_{mf}, calculated from Equation 7.1 matched well with the experimental results given in Figures 7.2 - 7.4.

$$U_{mf} = 0.202\sqrt{\frac{(\rho_s - \rho_g)\times g \times d_p}{\rho_g}} \quad Ar < 10^7 \tag{7.1}$$

$$A_r = \frac{\rho_g \times (\rho_s - \rho_g)\times g \times d_p^{-3}}{\mu_g^{-2}} \tag{7.2}$$

The difference in the minimum fluidization was due the difference in the sizes of the particles used and difference in the densities. These results also indicate that U_{mf} is independent of the amount of inventory used to fluidize. The fluidization started in some localized region of the bed before U_{mf} and with the increase in superficial velocity; the fluidization started in more regions. Therefore, there is fluctuation in the pressure drop which becomes stable after the minimum fluidization velocities as all particles are embedded in the fluidized bed, bed pressure drop become stable and at this point it is full fluidization.

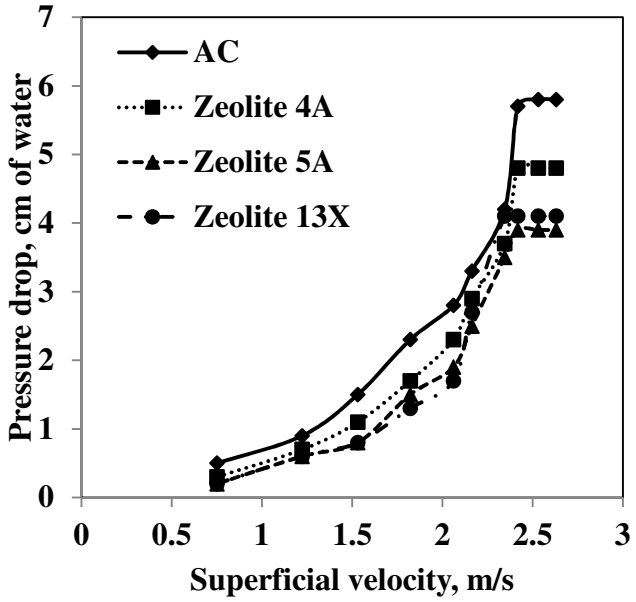

Fig 7.2 Minimum fluidization curve for inventory of 200 g

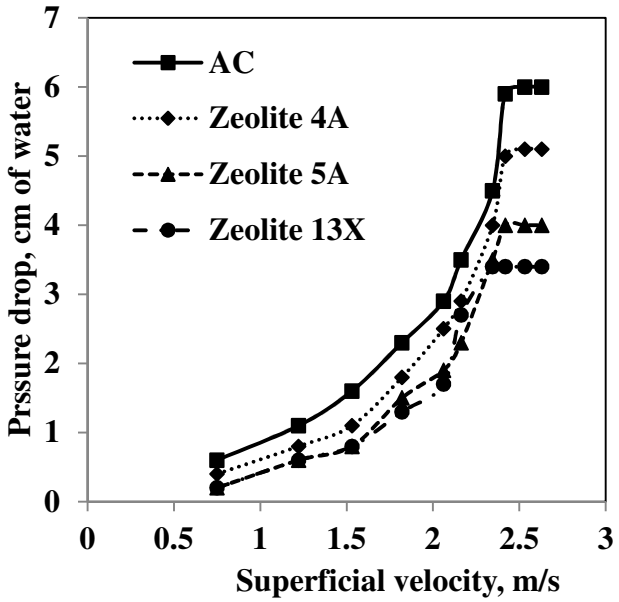

Fig 7.3 Minimum fluidization curve for inventory of 250 g

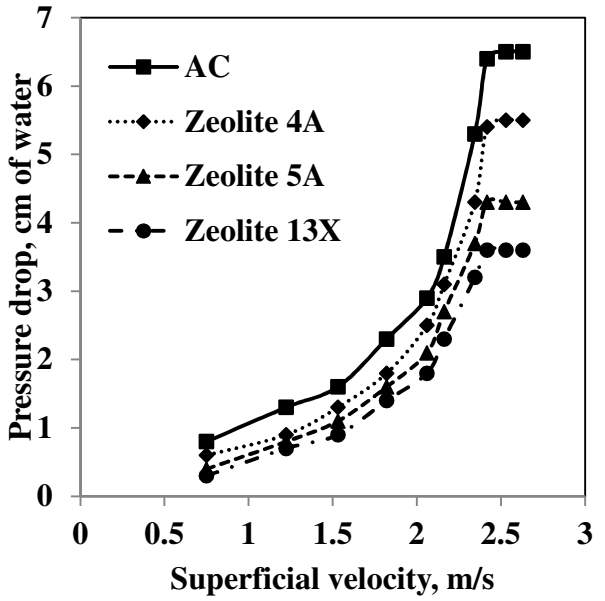

Fig 7.4 Minimum fluidization curve for inventory of 300 g

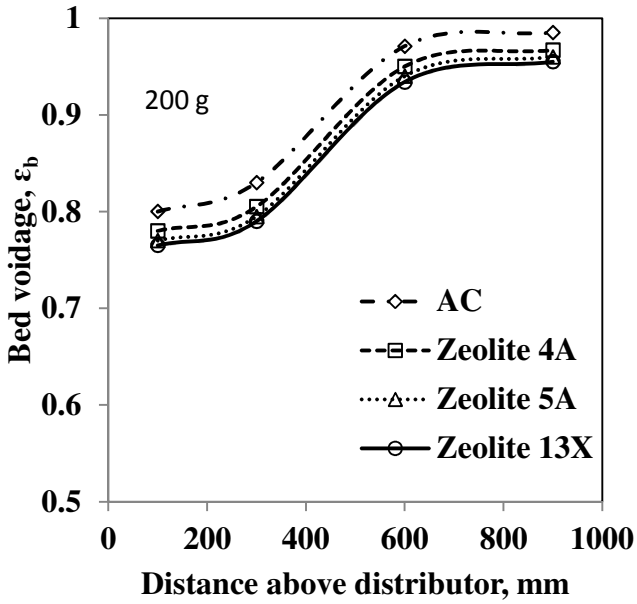

Fig 7.5 Bed voidage profile with inventory of 200 g

7.2.3 BED VOIDAGE PROFILE

Typical flattened S - Shaped bed voidage profile appeared for all the adsorbents used. With an increase in bed weight and larger particles size, the bed voidage decreases while increase in the superficial velocity lead to increase in bed voidage. Figures 7.5 - 7.7 shows the effect of change in inventory bed weight on the voidage profile with varying superficial velocities. The bed voidage, ε, was calculated using Equation 7.3.

$$\varepsilon = 1 - \frac{10\Delta h}{\rho_s L_m} \tag{7.3}$$

It shows that the increase in velocity from 0.8 m/s to 2.1 m/s leads to increase in voidage with a little variation along the height of the column. This effect was observed due to the fact that by increasing the air velocities, there will be a large carryover of particles and hence voidage increases. It can also be seen that there is a change in bed voidages for the different inventory viz. zeolite 13X, zeolite 5A, zeolite 4A and activated carbon along the column. This difference in voidage profile can be related to difference in their particles size as well as difference in density. For a larger particle size there was a lower voidage at the bottom of the column as it was denser

compared to the smaller size particles. This was because both the large and fine particles were present at bottom of the column and fine particles were embedded on larger diameter particles and hence the voidage decreases [Zhou et al. 1994].

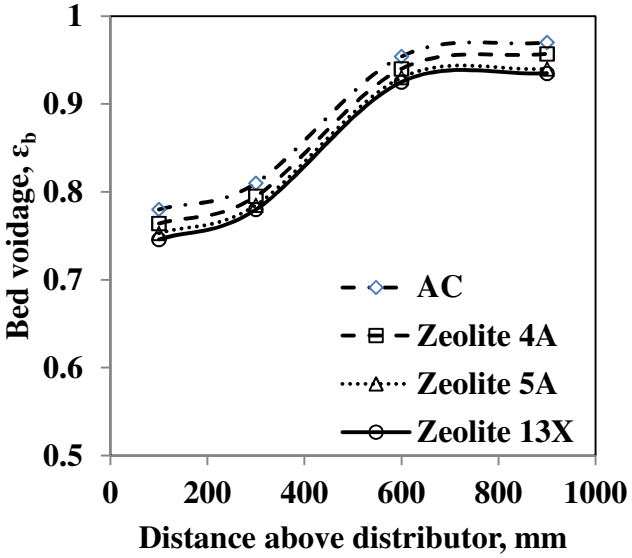

Fig 7.6 Bed voidage profile with inventory of 250 g

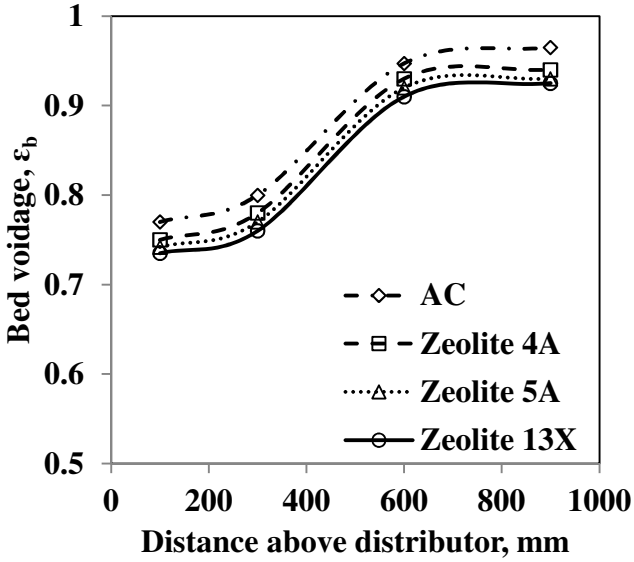

Fig 7.7 Bed voidage profile with inventory of 300 g

7.2.4 BED SUSPENSION DENSITY

Suspension density, ρ_{sus}, was evaluated using Equation 7.4 along the height of the column and variations of suspension density are shown in Figures 7.8 - 7.10. It was observed that average suspension density was more at the bottom portion of column and was comparatively very less at the upper portion of the column. The three figures represent the effect of change in bed weight of inventory on suspension density variation along the column. It was observed that suspension density increases with increase in the bed weight of inventory. It was also observed that suspension density decreases along the height of the column with increase in superficial velocity. This was due to the fact that the hold-up of particle decreases across the column and near to the wall with increase in superficial velocities.

$$\rho_{sus} = \rho_s (1-\varepsilon) + \varepsilon \rho_g \tag{7.4}$$

It was also observed that suspension density increases with increase in particle sizes for similar operating conditions. Comparing the four types of inventory viz. zeolite 13X, zeolite 5A, zeolite 4A and activated carbon, it was seen that the solid concentration at the column bottom for the larger size particles (zeolite 13X, zeolite 5A and zeolite 4A) were higher than that for the smaller particles, activated carbon. In other words, the solids concentration for the smaller particles is more uniform along the column height, while the larger particles tend to distribute denser at the column bottom [Grulovic et al., 2008].

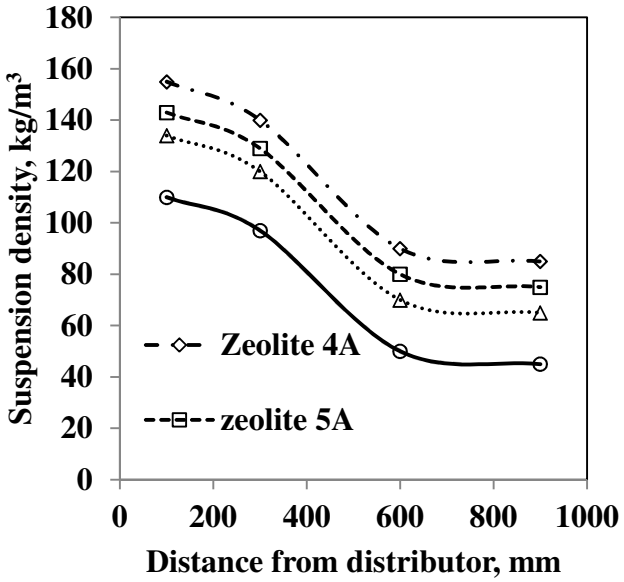

Fig 7.8 Suspension density with inventory of 200 g

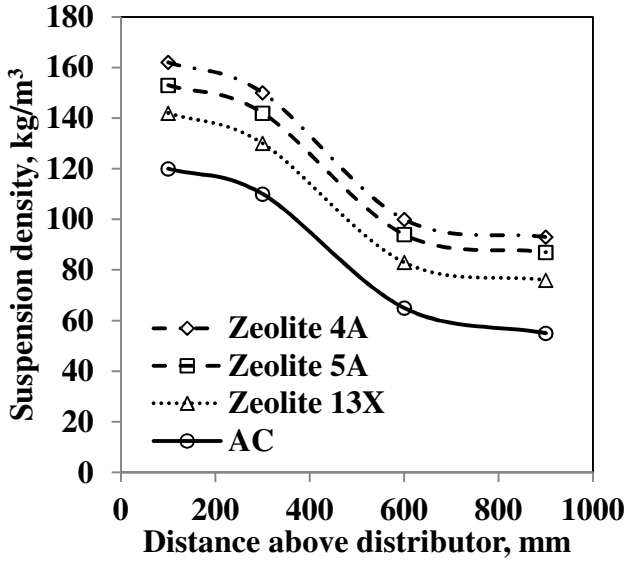

Fig 7.9 Suspension density with inventory of 250 g

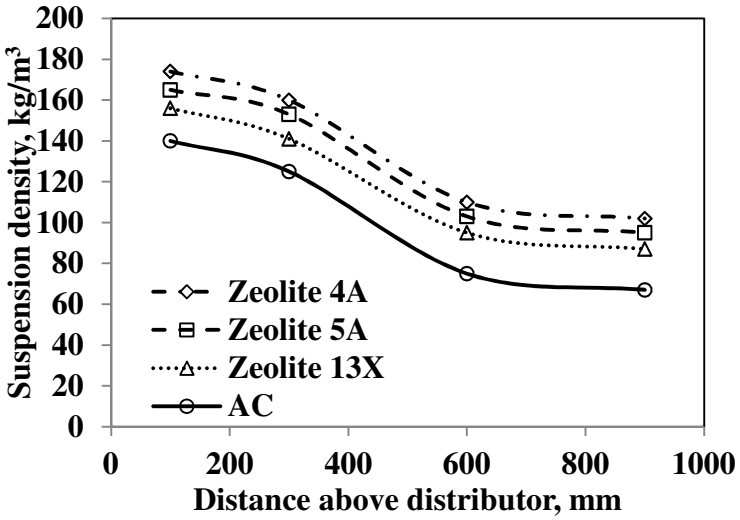

Fig 7.10 Suspension density with inventory of 300 g

7.3 ADSORPTION BREAKTHROUGH CURVES

The CO_2 breakthrough curves for the four adsorbents viz. zeolite 13X, zeolite 5A, zeolite 4A and activated carbon in the fluidized bed are shown in Figures 7.11 - 7.14 and the experimental conditions are given in Table 4.4. Figures 7.11 show the ratio of outlet concentration and the influent concentration against the contact time for zeolite 13X at an atmospheric pressure for different bed weight of 200 g, 250 g and 300 g at a temperature of 298 K and 0.1 MPa. The general pattern of the breakthrough curves similar to fixed bed study were achieved as expected though different breakthrough time for all adsorbents used. The breakthrough started at 22 min and saturation time occur at 45 min for zeolite 13X at a temperature of 298 K for 300g bed weight.

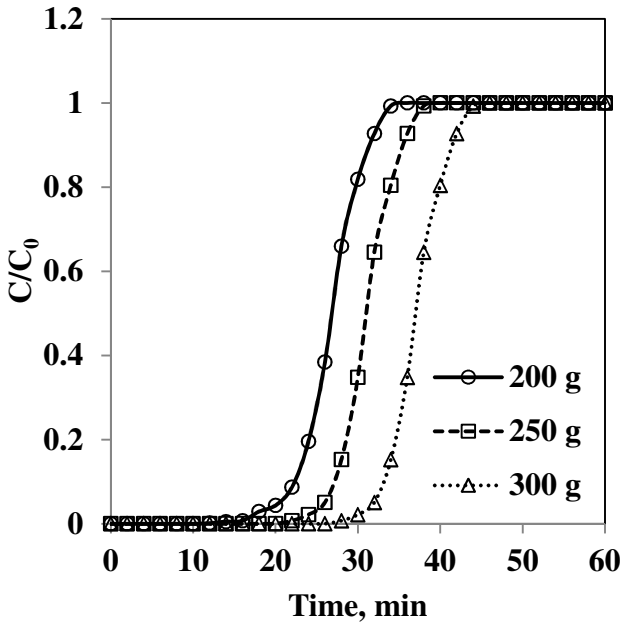

Fig 7.11 Breakthrough curve for zeolite 13X at U =1.5 m/s, 0.1 MPa and 298 K

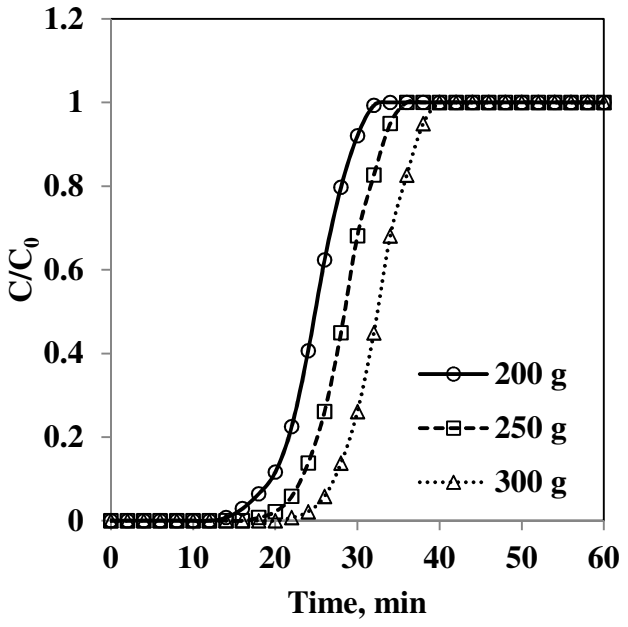

Fig 7.12 Breakthrough curve for zeolite 5A at U =1.5 m/s, 0.1 MPa and 298 K

Similar pattern can be observed for zeolite 5A, zeolite 4A and activated carbon from Figures 7.12 – 7.14 and shows that there was practically an improvement in the breakthrough time with an increase in bed weight for the adsorbents. At 300 g of bed weight, the breakthrough for zeolite 5A occurs at 18 min, 15 min for zeolite 4A and 12 min for activated carbon. The adsorption saturation time was approximately 40 min for zeolite 5A, 35 min for zeolite 4A and 29 min for

activated carbon. However, the breakthrough and adsorption times were found to considerably decrease as the amount of bed weight was decreased to 250 g and 200 g. More, the quantity of adsorbents means more surface area to trap the CO_2 molecules. Hence, increase in bed weight leads to increase in amount of CO_2 adsorption. This shows that the pore diameters are sufficient for the CO_2 to enter into the zeolite channels and activated carbon.

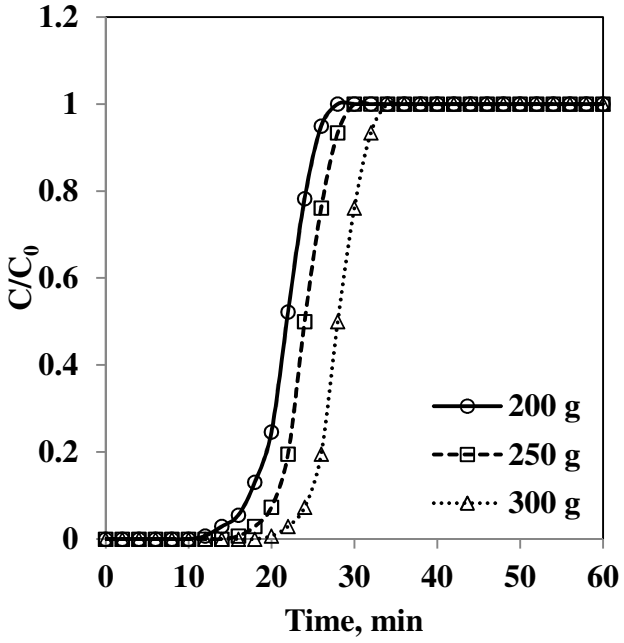

Fig 7.13 Breakthrough curve for zeolite 4A at U =1.5 m/s, 0.1 MPa and 298 K

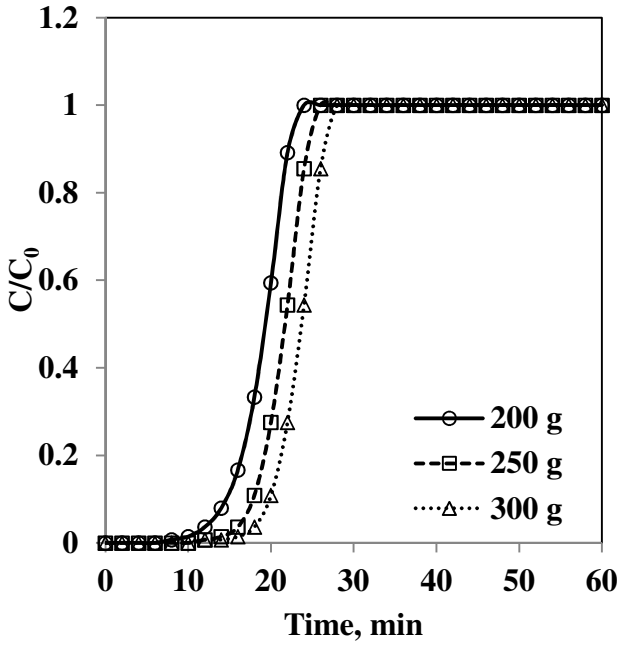

Fig 7.14 Breakthrough curve for activated carbon at U =1.5 m/s, 0.1 MPa and 298 K

It can be concluded that zeolite 13X gives the best breakthrough curve as compared to the other two zeolites while activated carbon gives the least breakthrough time. Clearly, all the adsorbent materials have a large surface area and pores to trap CO_2 molecules. However, the breakthrough time with activated carbon was shorter as compared to zeolite based adsorbent, indicating that the CO_2 adsorption capacity of activated carbon is lower than that of zeolites. The differences in adsorption observed with zeolites and activated carbon should be related to the differences in the surface structure and porosity. Zeolite based adsorbents have a higher surface area than activated carbon and that may have contributed to the higher adsorption capacity of zeolite 13X, zeolite 5A and zeolite 4A.

7.4 RADIAL HEAT TRANSFER COEFFICIENT

It can be seen from Figures 7.15 - 7.18 that the heat transfer coefficient changes with change in superficial velocity, bed weight and inventory along the column height. The heat transfer coefficient can be calculated from Equation 7.5.

$$h = \frac{q}{A_s (T_s - T_b)} \tag{7.5}$$

It was observed that the heat transfer coefficient was becoming almost constant after 15 minutes though there was still a small fluctuation at some location of the bed. It can be considered that the system took just 15 minutes to become stable, independent of the fluxes and velocities. It was observed that the heat transfer coefficient decreases along the height of the column and maximum at the bottom. This was due to the fact that the coarser agglomerates were contained at the bottom of the column and small agglomerates were at the top with greater density of very small voidage, flowing with lower density of fine particles. Also, by comparing Figure 7.15 to Figure 7.18, it can be seen that increase in particle size (different sizes of the adsorbents/ inventory) greatly reduced the local heat transfer coefficient due the increase in porosity of the bed.

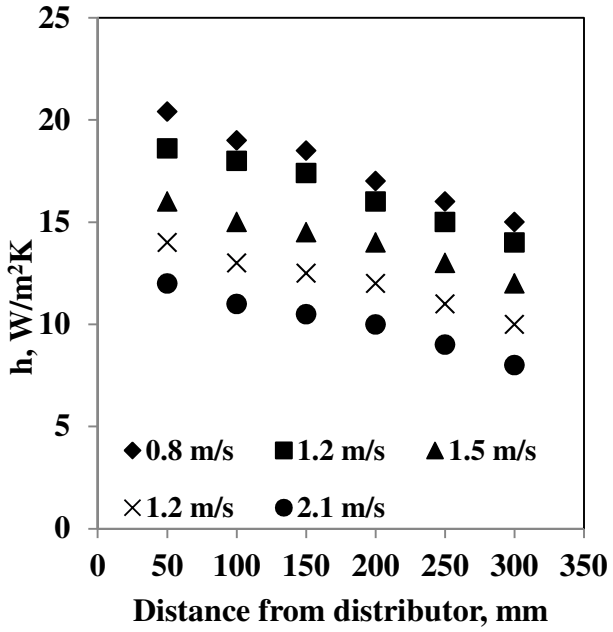

Fig 7.15 Radial heat transfer for zeolite 13X

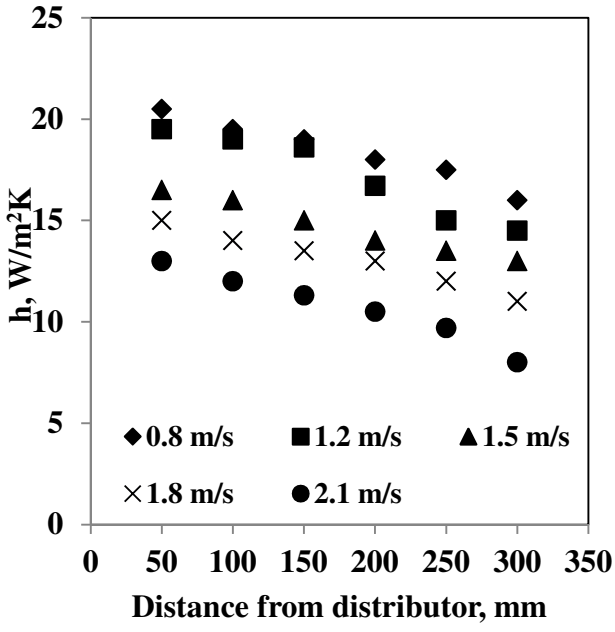

Fig 7.16 Radial heat transfer for zeolite 5A

Higher heat transfer coefficient for smaller particles was also observed by several investigators like [Mickley et al., 1949; Basu and Nag, 1987]. The effect of superficial velocity of air on heat transfer coefficient can be observed. It can be seen that the heat transfer coefficient decreases with increase in superficial air velocity. The reason behind this fact is that bed temperature decreases with increase in superficial air velocity which results in increase in the driving temperature difference ($T_s - T_b$). A similar result had been reported for radial variation of heat transfer coefficient [Fox et al., 1999].

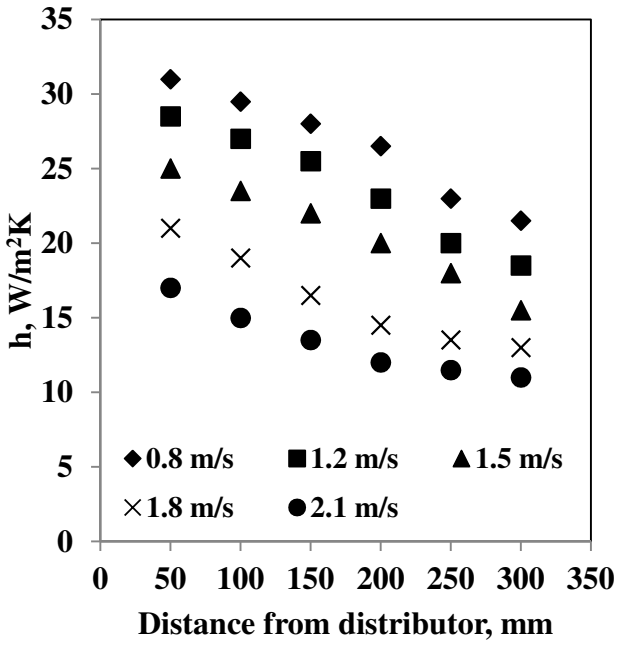

Fig 7.17 Radial heat transfer for zeolite 4A

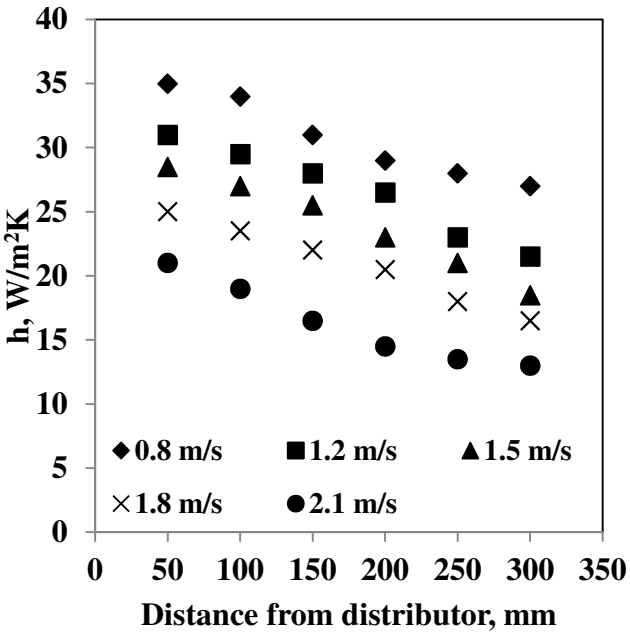

Fig 7.18 Radial heat transfer for activated carbon

7.5 EFFECT OF CO_2 CONCENTRATION ON HEAT TRANSFER

For this study, experiments were conducted to study the effects of CO_2 concentration and system pressure on avg. heat transfer coefficient. Average heat transfer coefficient (h_{avg}) along the heater section at any particular location above the distributor plate is calculated by Equation 7.6;

$$h_{avg} = \frac{1}{H}\int_0^H h_y .dy \tag{7.6}$$

where H is the height of the heater (0.6 m), h_y is the local heat transfer coefficient.

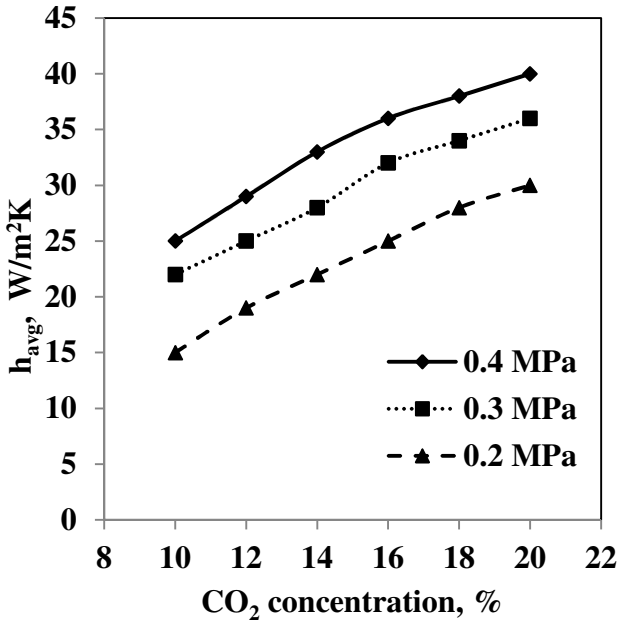

Fig 7.19 Avg. heat transfer coefficient for zeolite 13X, at 1.5 m/s

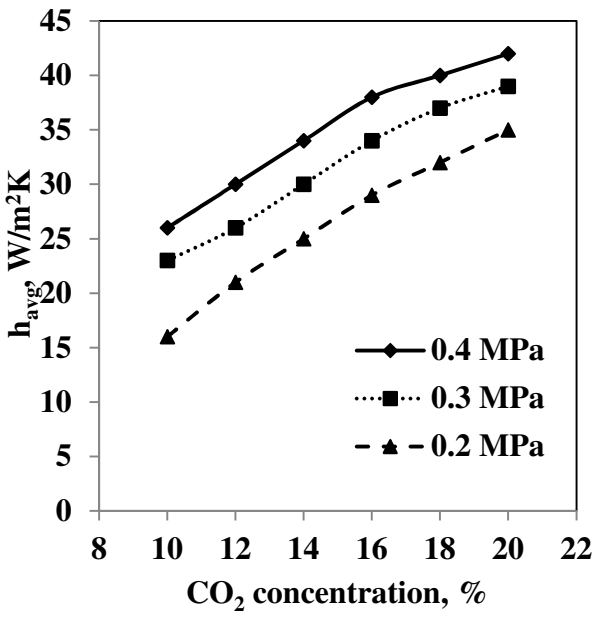

Fig 7.20 Avg. heat transfer coefficient for zeolite 5A, at 1.5 m/s

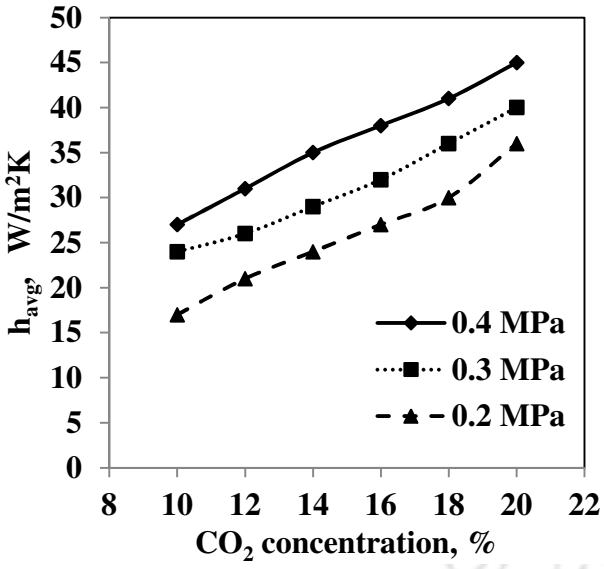

Fig 7.21 Avg. heat transfer coefficient for zeolite 4A, at 1.5 m/s

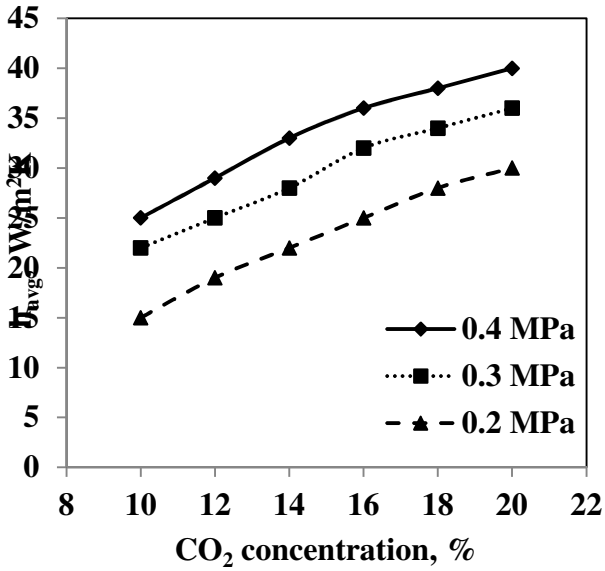

Fig 7.22 Avg. heat transfer coefficient for activated carbon, at 1.5 m/s

The effect of volumetric concentration of CO_2 in fluidized bed on heat transfer coefficient in fluidized bed is shown through Figure 7.19 to Figure 7.22. The experiment was set at three different pressures which are 0.2 MPa, 0.3 MPa and 0.4 MPa respectively. Obviously, it was seen that the average heat transfer coefficient increases with the increase in CO_2 concentration

for the different adsorbents used viz. zeolite 13X, zeolite 5A, zeolite 4A and activated carbon. At a given system pressure and bed temperature, the gas emissivity rises when the volumetric concentration of CO_2 increases. This results in higher radiative flux, and consequently higher heat transfer coefficients. The increase in gas emissivity is due to the increase in partial pressure of CO_2, which could happen either due to the increase in the total system pressure or due to the increase in volumetric concentration. The heat transfer coefficient may also increase due to increase in thermal conductivity of gas-particle clusters at higher pressures. The net effect is that in a fluidized bed, the increase in CO_2 concentration at a given operating condition results in higher heat transfer coefficients. However, the mean beam length in the present set-up is much shorter than that expected in commercial boilers. Therefore, the effect of pressure on heat transfer coefficient will be much more prominent in commercial boilers [Winaya and Basu, 2001].

7.6 COMPARISON OF FIXED AND FLUIDIZED BED

This particular study had been conducted in order to compare the adsorption capacity of fixed bed and fluidized bed onto adsorbents like zeolite 13X, zeolite 5A, zeolite 4A and activated carbon. In this study, the CO_2 adsorption for each adsorbent was measured under an isothermal condition of a temperature of 298 K and up to a CO_2 partial pressure of 0.4 MPa. For a given temperature, the amount of adsorption was obtained as a series of data pairs that shows the maximum amount CO_2 adsorbed at the corresponding pressure of CO_2 gas. Details of the experimental procedures and experimental conditions are given in Chapter 3. The relationships between the adsorbed amount of CO_2 and the adsorption pressure is commonly known as isotherm curves which are given in Figure 7.23 through Figure 7.26.

The adsorption capacity of zeolite 13X is 6.13 $gmol_{CO_2} kg^{-1}_{sorbent}$, zeolite 5A is 5.54 $gmol_{CO_2} kg^{-1}_{sorbent}$, zeolite 4A is 5.02 $gmol_{CO_2} kg^{-1}_{sorbent}$ and activated carbon is 5.31 $gmol_{CO_2} kg^{-1}_{sorbent}$ at 298 K and 0.4 MPa. Compared with the fixed bed system, there is an increase in CO_2 adsorption capacity of 1.16 $gmol_{CO_2} kg^{-1}_{sorbent}$ for zeolite 13X, 1.02 $gmol_{CO_2} kg^{-1}_{sorbent}$ for zeolite 5A, 0.8 $gmol_{CO_2} kg^{-1}_{sorbent}$ for zeolite 4A and 1.17 $gmol_{CO_2} kg^{-1}_{sorbent}$ for activated carbon. It can be seen that the fluidized bed

was very effective for increasing the adsorption capacities of the adsorbents used and allowed approx. 15-20 % increase in the adsorption capacity at 298 K and 0.4 MPa.

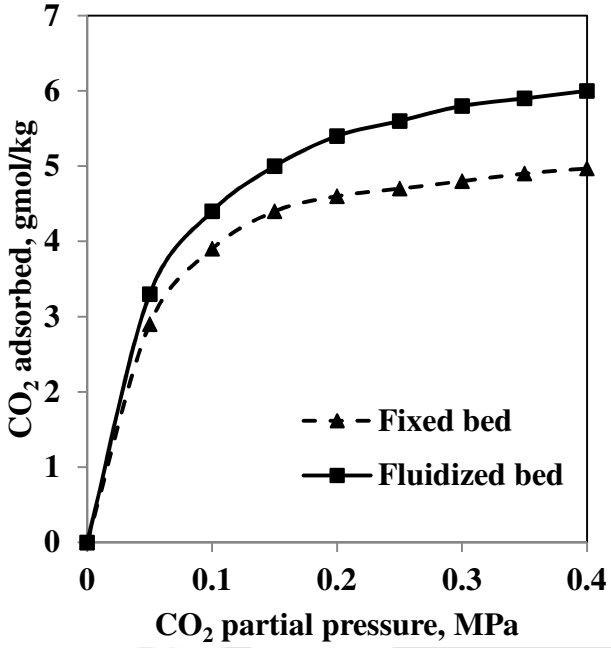

Fig 7.23 Adsorption isotherm for zeolite 13X at U =1.5 m/s and 298 K

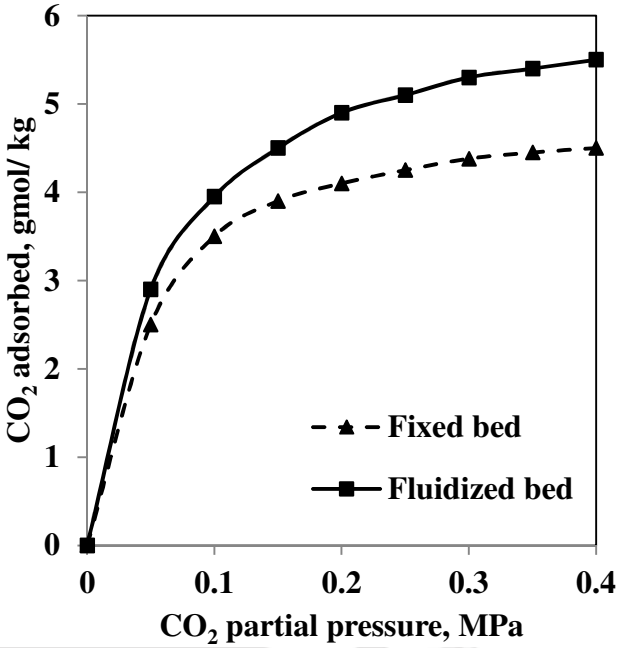

Fig 7.24 Adsorption isotherm for zeolite 5A at U =1.5 m/s and 298 K

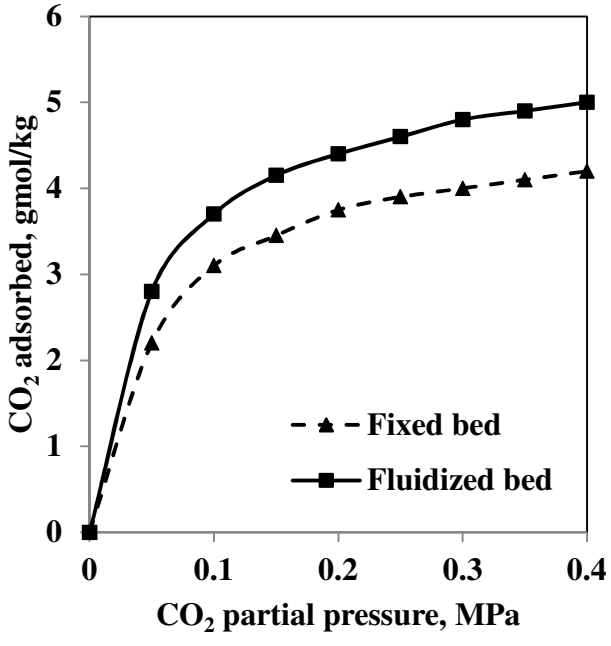

Fig 7.25 Adsorption isotherm for zeolite 4A at U =1.5 m/s and 298 K

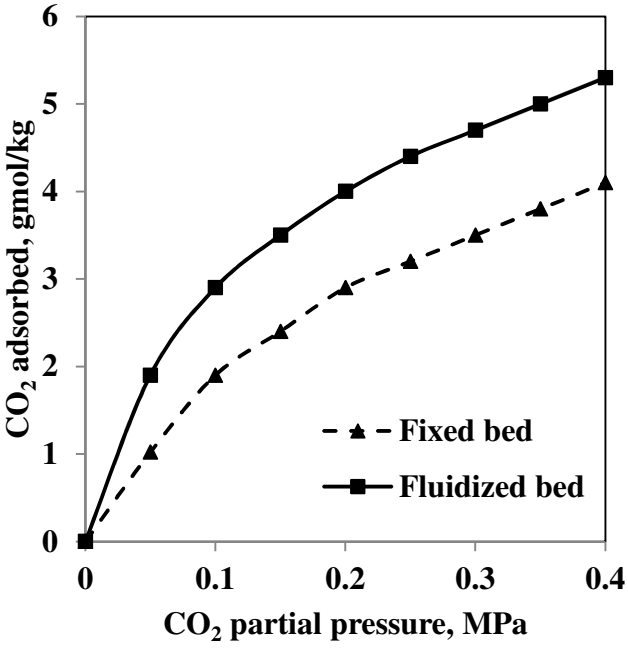

Fig 7.26 Adsorption isotherm for activated carbon at U =1.5 m/s and 298 K

At the lower pressure, the adsorption capacities are almost similar but at higher pressure, the adsorption capacity in the fluidized bed rises as compared to the fixed bed. This is due to the fact that the employment of fluidized bed for adsorption process presents an advantage of better gas-solid contact, which propitiates a better coefficient of mass transfer. Hence, fluidization allows enhancement of maintaining relatively higher capture capacities at large values of the gas flow rate. The rapid increase in the isotherm curve demonstrates the proper range of equilibrium pressure that promotes the majority of adsorption activity. This is important information that can be used to identify both adsorption pressure and regeneration pressure in the pressure swing adsorption process. The stabilized amount of CO_2 adsorbed in the curve shows that all adsorption sites are occupied by CO_2 gas, which represents the capacity limit of the adsorbent at the particular temperature. In addition, the slope of adsorption isotherm curves reveals the strength of interaction between CO_2 molecules and adsorption sites for individual adsorbents. It appears that zeolite based adsorbents exhibit strong adsorption as compared to activated carbon.

The flow rates were related to gas residence time as this is a key factor in rationalizing the differences in CO_2 uptake between the fixed and fluidized beds. Residence time is the average time that a particle spends in a particular bed. This measurement varies directly with the amount of substance that is present in the bed. Figure 7.27 shows the comparison of the residence time against the mass flow rate for fixed bed and fluidized bed.

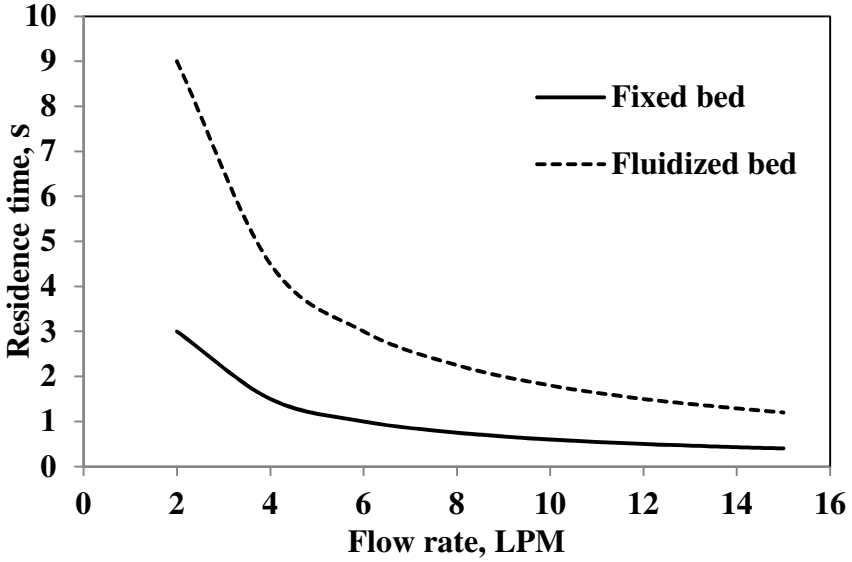

Fig. 7.27 Comparison of the residence time for fixed and fluidized beds

From the Figure it can be observed that there is a decrease in the residence time with increase in the flow rate for a fixed as well as fluidized beds. However, there is a higher residence time for fluidized bed as compared to the fixed bed simply due to the longer bed length in the fluidized bed. The higher adsorption of CO_2 in fluidized bed can be attributed to the higher residence as compared to fixed bed system. When the residence time exceeds 10 s, the dimensions of the bed become useless for practical application. Hence, the bed dimensions for the present work can be used for practical application as the residence time is less than 10 s for both the fixed as well as fluidized beds.

7.7 SUMMARY

In this chapter, the experimental results of CO_2 adsorption in a fluidized bed on zeolite 13 X, zeolite 5A, zeolite 4A and activated carbon were presented. The hydrodynamics characteristics like bed voidage profiles, pressure drop in the bed, bed suspension density, effect of superficial velocity and pressure were present. The heat transfer coefficient characteristics and effect of CO_2 concentration on heat transfer coefficient were also described. Lastly, the adsorption breakthrough curves, adsorption isotherm and comparison of adsorption capacity in fixed and fluidized bed were reported. The following chapter (Chapter 8) discussed the conclusion of this thesis and the future scope for more research work related to this topic.

CHAPTER 8
CONCLUSION AND SCOPE FOR FUTURE WORK

8.1 CONCLUSION

In the present work an extensive investigation was conducted for adsorption of CO_2 from flue gas. Both simulations as well as experimental works were conducted to observe the behavior of bed material, pressure and temperature on CO_2 adsorption. Comparative experimental studies were conducted both on fixed bed as well as fluidized beds. A large set of experimental data on CO_2 adsorption and kinetics were produced for three commercial adsorbents such as zeolite 13X, zeolite 5A, zeolite 4A. Coconut shell, which is cheap and abundantly available locally, was converted to activated carbon and used as an adsorbent material and compared the adsorption capacity with commercial zeolite based adsorbents. Major conclusions drawn from the present study are presented in the following sub sections.

8.1.1 CONCLUSION FROM FIXED BED STUDY

The CO_2 adsorption experiments were conducted using adsorption method at different temperatures and pressures in a fixed bed. From this study, the following conclusions can be drawn:

- The CO_2 adsorption isotherm obtained in this study followed general gas adsorption behaviour, demonstrating that the CO_2 adsorption capacity increases with increasing pressure and decreases with increasing temperature. At higher temperature, CO_2 adsorption capacity for all adsorbents is decrease by 20 to 30 percent.
- Adsorption isotherm follows a type-I isotherm classification according to IUPAC, representing a monolayer adsorption mechanism. Among the four adsorbents tested,

zeolite 13X offers the highest adsorption capacity of 4.97 $gmol_{CO_2} kg^{-1}_{sorbent}$, and activated carbon provides the lowest capacity of 4.14 $gmol_{CO_2} kg^{-1}_{sorbent}$ at temperatures ranging from 298 K to 333 K and pressures up to 0.4 MPa. Hence, the low cost and easily available coconut based activated carbon can be used effectively for CO_2 capture though the adsorption capacity is lower than zeolite based adsorbents at the present experimental condition.

- The experimental data of CO_2 adsorption were correlated to fit with different model equations (i.e., the Langmuir, Freunlich, Toth and Sips equations). It was found that the Sips model showed the best fit with the zeolite 13X, zeolite 5A and zeolite 4A while the Toth model provided excellent fit with the data for the activated carbons.
- The thermodynamics parameters were calculated from Van't Hoff's equation and concluded that the adsorption experiment were exothermic in nature for all adsorbents used in this study.
- The adsorption isotherms for zeolites (zeolite 13X, zeolite 5A and zeolite 4A) for repeated cycles showed a reduction in the amount of adsorption for the next cycles. This indicated that the adsorption was not reversible and complete regeneration cannot be obtained by adsorption of the material after the first adsorption. For AC, it was interesting to note that all the isotherms were extremely reproducible, which indicates the excellent reversibility of adsorption.
- The breakthrough curves were simulated using the linear driving force (LDF) model and found to be matching with the experimental work. The adsorption model showed that the use of LDF model was very sensitive to a few parameters. The bed length, bed void fraction, gas flow rate and pellet diameter are four of the more sensitive parameters.

8.1.2 CONCLUSION FROM FLUIDIZED BED STUDY

In this investigation, the effect of superficial velocity, operating pressures and solid inventory on hydrodynamics and heat transfer characteristics in a bubbling fluidized bed has been studied. The experiments were carried out at five different superficial velocities such as 0.8, 1.2, 1.5, 1.8 and 2.1m/s. At each superficial velocity, the experiments were performed at three different weight of

inventory 200g, 250 g and 300 g. The hydrodynamics and heat transfer characteristics has been investigated by using four different adsorbents like zeolite 13X, zeolite 5A, zeolite 4A and activated carbon.

From this study, it has been found that;

- Flattened S Shaped bed voidage profile appeared for all the adsorbents used. With an increase in bed weight and larger particles size, the bed voidage decreases while increase in the superficial velocity lead to increase in bed voidage.
- The suspension density increases with the decrease in particle size and increases with an increase in operating pressure. The suspension density was also found to increase towards the riser exit with an increase in pressure. With increase in superficial velocity, the suspension density along the height of the column is found to be higher at higher pressure except at the column exit. The increase in suspension density results in an increase of heat transfer coefficient, which indicated a lower consumption of blower power.
- The heat transfer coefficient decreases with the increase in particle size (adsorbents). It was also seen that with the increase in both superficial velocity and system pressure, the heat transfer coefficient increases along the height of the heat transfer probe. With the increase in CO_2 concentration, the heat transfer coefficient increases.
- In comparison to fixed bed, the employment of fluidized bed for CO_2 adsorption process resulted in a better gas-solid contact, which gives a better coefficient of mass transfer. Fluidization allows enhancement of maintaining relatively higher capture capacities upto15 - 20 % at 298 K and 0.4 MPa.

8.2 SCOPE FOR FUTURE WORK

In the present work, CO_2 capture onto zeolite 13X, zeolite 5A, zeolite 4A and activated carbon by using pressure swing adsorption in a fixed as well as fluidized bed were studied. The important research findings have already been highlighted. However, there are still large scopes for further research which can be carried out by using the developed units. Some of the scopes and suggestions for further studies are given below. To improve selection of the best adsorbent for the removal of CO_2 from flue gas, the following future research activities are recommended:

- The kinetic and equilibrium selectivity for CO_2 adsorption compared to other gases should be investigated in the future for the four adsorbents as selectivity is an important criterion to choose an adsorbent for the separation of a gas from the mixture of gases.
- Adsorption capacity of the adsorbents used in the present work can be improved by changing the sizes of the particle and by impregnating with other chemicals like KOH, NaOH, etc. Finding new type and better adsorbent materials are always a promising research work.
- In the present work, experiments were limited up to 0.4 MPa. Therefore, the effect of higher pressure on the adsorption capacity can be carried out to establish the effect of pressure on gas adsorption.
- Simulations of the adsorption process were done in a fixed bed by considering isothermal system in the process. In reality, most of the adsorption systems behave non-isothermally thus work may be extended to non-isothermal condition.

REFERENCES

Abanades J. C., Anthony E. J., Lu D. Y., Salvador C., Alvarez D., 2004. Capture of CO_2 from combustion gases in a fluidized bed of CaO, AICHE Journal. 50, 1614–1622.

Abele A. R., Kindt G. S., Clark W. D., Payne R., Chen S. L., 1988. An experimental program to test the feasibility of obtaining normal performance from combustors using oxygen and recycled gas instead of air. Argonne National Lab Report ANL/CNSV-TM-204.

Abramov A. Elizarov I., D. P., Remezov A. N., 2003. Enhancing the Environmental Safety of Thermal Power Stations. MEI Moscow.

Adeyemo A., Kumar R., Linga P., Ripmeester J., Englezos P., 2010. Capture of carbon dioxide from flue or fuel gas mixtures by clathrate crystallization in a silica gel column, International Journal of Greenhouse Gas Control. 4, 478–485.

Ahn H., Moon J., Hyun S., Lee C., 2004. Diffusion Mechanism of Carbon Dioxide in Zeolite 4A and CaX Pellets. Adsorption 10, 111–128.

Ahn H., Brandani S., 2005. Dynamics of carbon dioxide breakthrough in a carbon monolith over a wide concentration range. Adsorption 11, 473–477.

Agarwal, A., Biegler, L. T., Zitney, S. E., 2010b. A super structure-based optimal synthesis of PSA cycles for post-combustion CO_2 capture. AIChE J. 56, 1813–1828.

Aguilar-Vega M., Paul D.R., 1993. J. Polym. Sci. 31 (11), 1577–1589.

Alvis R. S., et al, 2012. CO_2 removal from syngas using piperazine-activated MDEA and Potassium Dimethyl Glicinate, Proceedings of Nitrogen + Syngas, 2012, 20-23.

Amoros D. C., Alcaniz-Monge J. and Linares-Solano A., 1996. Characterization of activated carbon fibers by CO_2 adsorption. Langmuir 12, 2820-2824.

Avtonomov A. B., 2003. World Power Industry: State, Scales, Prospects, Sustainability of Development, Environmental Problems, and Dynamics of Prices for Fuel and Energy Resources. Elektr. Stn., 5, 55–64.

AxeL M., Xiaoshan S., 1997. Research and development issues in CO_2 capture. Energy Conversion and Management, 38, 37e42.

Babcock and Wilcox, 1992. Steam: Its Generation and Use, 40th ed., The Babcock and Wilcox Company, Barberton, Ohio.

Babu P., Ho C. Y., Kumar R., Linga P., 2014. Enhanced kinetics for the clathrate process in a fixed bed reactor in the presence of liquid promoters for pre-combustion carbon dioxide capture, Energy, 70, 664-673.

Bae Y. S. and Lee C. H., 2005. Sorption kinetics of eight gases on a carbon molecular sieve at elevated pressure. Carbon 43, 95–107.

Bai H., Yeh A.C., 1997. Ind. Eng. Chem. Res. 36, 2490–2493.

Basu P., Nag P. K., 1987. An investigation into heat transfer in circulating fluidized beds, Int. J. Heat Mass Transfer. 30 (11), 2399–2409.

Besong M. T., Maroto-Valer M. M., Finn A. J., 2013. Study of design parameters affecting the performance of CO_2 purification units in oxy-fuel combustion, International Journal of Greenhouse Gas Control, 12, 441–449.

Blomen E., Hendriksa C., Neele F., 2009. Capture technologies: improvements and promising developments. Energy Procedia, 1, 1505-12.

Bouillon P.A., Hennes S., Céline Mahieux C., 2009. Post-combustion or Oxyfuel - A comparison between coal power plants with integrated CO_2 capture. Energy Procedia 1, pp. 4015–4022.

Bousquet P., Peylin P., Ciais P., Corinne L. Q., Friedlingstein P., Tans P. P., 2000. Regional Changes in Carbon Dioxide Fluxes of Land and Oceans Since 1980, Science 290, 1342–1346.

Butler J. W., JimLim C., Grace J. R., 2010. CO_2 capture capacity of CaO in long series of pressure swing sorption cycles.Chem Eng Res Des., doi:10. 1016/j. cherd. 2010. 10. 004.

Calleja G., Jimenez A., Pau J., Dominguez L., Perez, P., 1994. Multicomponent adsorption equilibrium of ethylene, propane, propylene and CO_2 on 13X zeolite. Gas Separation and Purification 8, 4.

Car A., Stropnik C., Yave W., Peinemann K. V., 2008. Pebax/polyethylene glycol blend thin film composite membranes for CO2 separation: performance with mixed gases. Separation and Purification Technology, 62,110-7.

Carta G., 2003. Adsorption calculations using the film model approximation for intraparticle mass transfer. Adsorption 9, 55–65.

Cavenati S., Grande C.A., Rodrigues, A.E., 2004. Adsorption Equilibrium of Methane, Carbon Dioxide, and Nitrogen on Zeolite 13X at High Pressures. J. Chem. Eng. Data 49, 1095-1101.

Cen P. and Yang R.T., 1985. Separation of a five-component gas mixture by pressure swing adsorption. Sep. Sci. Technol. 20, 725–747.

Chihara K., Suzuki M. and Kawazoe K., 1978. Adsorption rate on Molecular Sieving Carbon by Chromatography. AIChE 24, 242.

Cheung O., Bacsik Z., Liu Q., Mace A., Hedin N., 2013. Adsorption kinetics for CO_2 on highly selective zeolites NaKA and nano-NaKA, Applied Energy. 112, 1326–1336.

Chen C., Park D. W., Ahn W. S., 2014. CO_2 capture using zeolite 13X prepared from bentonite, Applied Surface Science. 292, 63– 67.

Choi W. J., Seo J. B., Jang S. Y., Jung J. H., Oh K. J., 2009. Removal characteristics of CO_2 using aqueous MEA/AMP solutions in the absorption and regeneration process. Journal of Environmental Sciences, 21, 907e13.

Chue K. T., Kim J. N., Yoo Y. J., Cho S., H., 1995. Comparison of Activated Carbon and Zeolite 13X for CO_2 Recovery from Flue Gas by Pressure Swing Adsorption. Ind. Eng. Chem. Res. 34, 591-598.

Clodic D., Younes M., 2002. Sixth International Conference on Greenhouse Gas Control Technologies, GHGT6, Kyoto, 155–160.

Clodic D., Hitti R.E., Younes M., Bill A., Casier F., 2005. Fourth Annual Conference on Carbon Capture and Sequestration, Alexandria, USA.

Comstock C.S., Dodge B.F., 1937. Ind. Eng. Chem. 29 (5), 520–529.

Czakiert T., Sztekler K., Karski S., Markiewicz D., Nowak W., 2010. Oxy-fuel circulating fluidized bed combustion in a small pilot-scale test rig. Fuel Processing Technology, 91, 1617–1623.

Cobden P. D., Beurden P. V., Reijers H. T. J., Elzinga G. D., Kluiters S. C. A., Dijkstra J. W., Jansen D., Brink R. W., 2007. Sorption-enhanced hydrogen production for pre-combustion CO_2 capture: Thermodynamic analysis and experimental results. International journal of greenhouse gas control 1, 170 – 179.

Costa E., Calleja G., Jlmenez A., Pau J., 1991. Adsorption Equilibrium of Ethylene, Propane, Propylene, Carbon Dioxide, and Their Mixtures on 13X Zeolite. J. Chem. Eng. Data, 36, 218-224.

de Montgareuil P. G. and Domine D., 1964. Process for Separating a Binary Gaseous Mixture by Adsorption, US Patent 3155468.

De Wilde J., Das A. K., Heynderickx G. H., Marin G. B., 2001. Development of a Transient Kinetic Model for the Simulteneous Adsorption of SO_2-NOx over Na/γ-AL_2O_3 Sorbent, Ind. Eng. Che. Res. 40, 119-130.

Dekker F. M. H., Bliek A., Kapteijn F., Moulijn J. A., 1995. Analysis of Mass and Heat Transfer in Transient Experiments over Heterogeneous Catalysts. Chem. Eng. Sci. 50, 3573.

Do D.D., 1998. Adsorption Analysis: Equilibria and Kinetics. Imperial College Press, London.

Drage T. C., Arenillas A., 2007. Smith K. M., Pevida C., Piippo S., Snape C. E., Preparation of carbon dioxide adsorbents from the chemical activation of urea–formaldehyde and melamine–formaldehyde resins, Fuel. 86, 22–31.

Drage T. C., Blackman J. M., Pevida C. and Snape C. E., 2009. Evaluation of activated carbon adsorbents for CO_2 capture in gasification. Energy & Fuels *23,* 2790–2796.

Dreisbach F., Staudt R., Keller, J.U., 1999. High pressure adsorption data of methane, nitrogen, carbon dioxide and their binary and ternary mixtures on activated carbon. Adsorption, 5, 215–227.

Eagan J. D. and Anderson R. B., 1975. Kinetics and Equilibrium of Adsorption on 4A Zeolite. Journal of Colloid and Interface Science 50, 3, 419-433.

Favre E., Svendsen H. F., 2012. J. Membr. Sci. 407–408, 1–7.

Feng B., Du M., Dennis T. J., Anthony K., Perumal M.J., 2010. Reduction of energy requirement of CO_2 desorption by adding acid into CO2-loaded solvent. Energy and Fuels, 24, 213-9.

Feron P. H. M., Hendriks C. A., 2005. CO_2 capture process principles and costs. Oil and Gas Science and Technology-Rev, IFP 60(3), 451–459.

Figueroa J. D., Fout T., Plasynski S., McIlvried H., Srivastava R. D., 2008. Review of advances in CO_2 capture technology of the U.S. department of energy's carbon sequestration program. International Journal of Greenhouse Gas Control, 2, 9-20.

Fridleifsson I. B., 2003. Status of geothermal energy amongst the world's energy sources. Geothermics. 32, 379–388.

Gibbins J., Chalmers H., 2008. Carbon capture and storage. Energy Policy, 36, 4317-22.

Glebov V. P., Medik E. N., Chugaeva A. N., 2002. The United Nation's Convention on the Change of Climate and Power Engineering. Elektr. Stn., 7, 27.

Goetz V., Pupier O., Guillot, A., 2006. Carbon dioxide-methane mixture adsorption on activated carbon. Adsorption, 12, 55-63.

Golub A. A., Rogankov M. P., and Safonov G. V., 2005. Experience Gained around the World with Solving the Problem of Reducing Emissions of Greenhouse Gases. Proceedings of the 2nd

International Scientific–Practical Conference Environmental Issues in Power Engineering, Moscow. MEI Moscow, 75-78.

Grande C.A. and Rodrigues A.E., 2008. Electric swing adsorption forCO2removal from flue gases. Int. J. Greenh. Gas Con. 2,194–202.

Grulovic G. R., Vragolovic N.B., Grbavcic Z., Arsenijevic Z., 2008. Wall-to-bed heat transfer in vertical hydraulic transport and in particulate fluidized beds, Int. J. Heat Mass Transfer. 51, 5942–5948.

Guo B., Chang L., Xie K., 2006. Adsorption of carbon dioxide on activated carbon. Journal of Natural Gas Chemistry, 15, 223-229.

Heldebranta D. J., Yonkera C. R., Jessopb P. G., Phan L., 2009. CO_2 binding organic liquids (CO_2 BOLs) for post-combustion CO_2 capture, Energy Procedia, 1, 1187–1195.

Herzog H., Golomb D., 2004. Encyclopedia Energy 1, 1–11.

Hoffman, J. S., Pennline, H. W., 2001. Study of regenerable sorbents for CO_2 capture, J. Energy and Environ. Res. 1(1), 90-100.

Hjärtstam S., Andersson K., Johnsson F., Leckner B., 2009. Combustion characteristics of lignite-fired oxy-fuel flames". Fuel 88, 2216–2224.

Howe H.E., 1928. Ind. Eng. Chem. 20 (10), 1091–1094.

Huang H. P., Shi Y., Li W., Chang S.G., 2001. Energy Fuels 15, 263–268.

Illing G., Hellgardt K., Wakemana R. J., Jungbauer A., Membr J., 2001. Science. 184 (1), 69–78.

IPCC, 2007. Summary for policymakers. In: climate change 2007: the physical science basis, contribution of working group i to the fourth assessment report of the intergovernmental panel on climate change. Geneva: World Meteorological Organization/United Nations Environment Program.

IPCC, 1990. Policymaker's summary of the scientific assessment of climate change; report to IPCC from working group. Meteorological Office: Branknell, United Kingdom. www.ipcc.ch/activity/srccs

IPCC (Intergovernmental Panel on Climate Change), 2000a. Emissions Scenarios. A Special Report of Working Group III. Summary for Policymakers, UNEP, WMO, 20.

Kaguei S., Yu Q., Wakao N., 1985. Thermal waves in an adsorption column: parameter estimation. Chem. Eng. Sci. 40, 1069–1076.

Kaguei S., Shemilt L.W., Wakao, N., 1989. Models andexperiments on adsorption columns with constant walltemperature-radially varying and radially lumped models.Chem. Eng. Sci. 44, 483–491.

Keller J. U. and Staudt, R., 2005. Gas Adsorption Equilibria: Experimental Methods and Adsorptive Isotherms. Boston, Springer Science and Business Media, Inc.

Kidnay A. J. and Parrish W. R., 2006. Fundamentals of Natural Gas Processing. New York , Taylor and Francis Group, LLC.

Kiga T, Takano S, Kimura N, Omata K, Okawa M, Mori T., 1997. Characteristics of pulverised-coal combustion in the system of oxygen/recycled flue gas combustion. Energy Convers Manage 38,129–S34.

Kim W. G., Yang J., Han S., Cho C., Leer C. H., Lee H., 1995. Experimental and theoretical study on H_2/CO_2 separation by a five-step one column psa process. Korean J. of Chem. Eng., 12, 5, 503-511.

Khalili S., et al, 2012. CO_2 separation from syngas by Multiwall Carbon Nanotubes, Iranica Journal of Energy and Environment, 3(1), 52-58.

Khoo H.H., Tan R.B.H., 2006. Environ. Sci. Technol. 40, 4016–4024.

Ko D., Siriwardane R., Biegler L. T., 2003. Optimization of a Pressure- Swing Adsorption Process Using Zeolite 13X for CO_2 Sequestration. Ind. Eng. Chem. Res., 42, 339-348.

Ko D., Siriwardane R., Biegler L. T., 2005. Optimization of pressure swing adsorption and fractionated vacuum pressure swing adsorption processes for CO_2 capture. Ind. Eng. Chem. Res. 44, 8084–8094.

Knuutila H., Svendsen H.F., Anttila M., 2009. Int. J. Greenhouse Gas Contr. 3, 143–151.

Knuutila H., Juliussen O., Svendsen H.F., 2010. Chem. Eng. Sci. 65, 6077–6088.

Krishnamoorthy G, Veranth JM., 2003. Computational modeling of CO/CO_2 ratio inside single char particles during pulverized coal combustion". Energy Fuels 17, 1367–71.

Kunii D., Levenspiel O., 1991. Fluidization Engineering, second ed., Butterworth- Hememann, USA. 313.

Leci C. L., 1996. Financial implications on power generation costs resulting from the parasitic effect of CO_2 capture using liquid scrubbing technology from power station flue gases. Energ. Convers. Manag. 37, 915–921.

Lee J. S., Kim J. H., Kim J. T., Suh J. K., Lee J. M., Lee C. H., 2002. Adsorption equilibria of CO_2 on zeolite 13X and zeolite X/ Activated carbon composite, J. Chem. Eng. Data, 47, 1237-1242.

Lee S. S., Yoo J. S., Moon G. H., Park S. W., Park D. W., Oh K. J., 2004. CO_2 adsorption with attrition of dry sorbents in a fluidized bed, Prepr. Pap.-Am. Chem. Soc., Div. Fuel Chem., 49 (1), 314.

Li G., Xiao P., Webley P., Zhang J., Singh R., Marshall M., 2008. Capture of CO_2 from high humidity flue gas by vacuum swing adsorption with zeolite 13X. Adsorption, 14, 415–422.

Lin H., Freeman B. D., 2004. J. Membr. Sci. 239 (1), 105–117.

Linga P., Kumar R., Englezos P., 2007. The clathrate hydrate process for post and pre-combustion capture of carbon dioxide, Journal of Hazardous Materials, 149, 625–629.

Liu H., Zailani R., Gibbs B. M., 2005. Comparisons of pulverized coal combustion in air and in mixtures of O_2/CO_2. Fuel, 84, 833-40.

Liu J., Wang S., Zhao B., Tong H., Chen C., 2009. Energy Procedia 1, 933–940.

Liu Z., Grande C. A., Li P., Yu J., Rodrigues A.E., 2011. Adsorption and Desorption of Carbon Dioxide and Nitrogen on Zeolite 5A. Separation Science and Technology, 46, 434–451.

Lu J. G., Cheng M., Ji Y., Hui Z., 2009. Membrane-based CO_2 absorption into blended amine solutions. Journal of Fuel Chemistry and Technology, 37, 740e6.

Lyngfelt A., Leckner B., Mattisson T., 2001. A fluidized-bed combustion process with inherent CO_2 separation; application of chemical-looping combustion, Chemical Engineering Science, 3101-3113.

Mamun S., Dindore V. Y., Svendsen H. F., 2007. Kinetics of the reaction of carbon dioxide with aqueous solutions of 2-((2-aminoethyl) amino) ethanol. Industrial & Engineering Chemistry Research, 46, 385e94.

Metz B., Davidson O., Coninck H. de, Loos M., Meyer L., 2005. Carbon dioxide capture and storage, International Panel on Climate Control (IPCC), Cambridge University Press.

Millward A. R. and Yaghi O. M., 2005. Metal-organic frameworks with exceptionally high capacity for storage of carbon dioxide at room temperature. J. AM. Chem. Soc., 127, 17998-17999.

Mickley H. S., Trilling C. A., 1949. Heat transfer characteristics of fluidized beds, Ind. Eng. Chem. 41, 1135.

Mokhatab S., Poe W.A., Speight J. G., 2006. Handbook of Natural Gas Transmission and Processing. USA: Elsevier Inc., ISBN-10: 0-7506-7776-7.

Mori Y., Masutani S. M., Nihous G. C., Vega L.A., Kinoshitat C. M., 1993. Pre-combustion removal of carbon dioxide from hydrocarbon-fuelled power plants". Fuel 72, 1293-1299.

Morse G., Jones R., Thibault J., Tezel F. H., 2010. Neural network modeling of adsorption isotherms. Adsorption, 17(2), 303-309.

Mulgundmath V. P., Jones R. A., Tezel, F.H., Thibault, J., 2012. Fixed bed adsorption for the removal of carbon dioxide from nitrogen: breakthrough behaviour and modelling for heat and mass transfer. Sep. Purif. Technol. 85, 17–27.

Nathalie C., Johanna S., Richard B., Marco M., 2013. MOF and UiO-67/MCM-41 adsorbents for pre-combustion CO2 capture by PSA: Breakthrough experiments and process design, separation and Purification Technology, 112, 34–48.

Nord L. O., Anantharaman R., Bolland O., 2009. Design and off-design analyses of a pre-combustion CO_2 capture process in a natural gas combined cycle power plant". International Journal of Greenhouse Gas Control 3, 385–392.

Nozaki T., S-i Takano., Kiga T., Omata K., Kimura N., 1997. Analysis of the flame formed during oxidation of pulverized coal by an O_2/CO_2 mixture. Energy, 22,199-205.

Olajire A. A., 2010. Energy 35, 2610–2628.

Park J. H., Beum H. T., Kim J. N., Cho S. H., 2002. Numerical analysis on the power consumption of the PSA process for recovering CO_2 from flue gas. Ind. Eng. Chem. Res. 41, 4122–4131.

Pakseresht S., Kazemeini M., Akbarnejad M. M., 2002. Equilibrium isotherms for CO, CO_2, CH_4 and C_2H_4 on the 5A molecular sieve by a simple volumetric apparatus. Separation and Purification Technology, 28, 53–60.

Patil R.S., Pandey M., Mahanta P., 2011. Parametric studies and effect of scale-up on wall-to-bed heat transfer characteristics of circulating fluidized bed risers, Experimental Thermal and Fluid Science. 35, 485–494.

Pellerano M., Pre P., Kacem M., Delebarre A., 2009. CO_2 capture by adsorption on activated carbon by pressure modulation. Energy Procedia 1, 647-653.

Perez A. R. and Armenta G. A., 2010. Adsorption Kinetics and Equilibria of Carbon Dioxide, Ethylene, and Ethane on 4A (CECA) Zeolite. J. Chem. Eng. Data, *55,* 3625–3630.

Pires J. C. M., Martins F. G., Alvim-Ferraz M. C. M., Simoes M., 2011. Chem. Eng. Res. Des. 89, 1446–1460.

Pixton M. R., Paul D. R., 1995. J. Polym. Sci. 33 (7), 1135–1149.

Powell C.E., Qiao G.G., 2006. J. Membr. Sci. 279 (1–2), 1–49.

Pugsley T. S., Berruti F., Chakma A., 1994. Computer simulation of a novel circulating fluidized bed pressure- temperature swing adsorber for recovering carbon dioxide from flue gasses, Chemical Engineering Science. 49 (24A), 4465-4481.

Quadrelli R. and Peterson S., 2007. The energy–climate challenge: Recent trends in CO_2 emissions from fuel combustion. Energy Policy. 35, 5938–5952.

Raghavan N. S., Hassan M. M., Ruthven D. M., 1985. Numerical simulation of a PSA system. Part I: Isothermal trace component system with linear equilibrium and finite masstransfer resistance. AIChE J. 31, 385–392.

Raghavan N. S., Hassan M. M., Ruthven D. M., 1986. Numerical simulation of a PSA system using a pore diffusion model.Chem. Eng. Sci. 41, 2787–2793.

Rao A. B. and Rubin E. S., 2002. A technical, economic, and environmental assessment of amine-based CO_2 capture technology for power plant greenhouse gas control. Environ. Technol. 36, 4467–4475.

Rehfeldt S., Kuhr C., Ehmann M., Bergins C., Scheffknecht G., Maier J., 2009. Basic experiments and CFD calculations of air and oxyfuel firing of lignite and bituminous coals in 0.5 and 1 MW scale combustion test facilities. In: The 34th international technical conference on clean coal and fuel systems. Clearwater, FL.

Resnik K. P., Yeh J. T., Pennline H. W., 2004. Int. J. Environ. Technol. Manage. 4 (1/2).

Ribeiro R. P. P. L., Grande C. A., Rodrigues A. E., 2013. Activated carbon honeycomb monolith–Zeolite13X hybrid system to capture CO_2 from flue gases employing Electric Swing Adsorption, Chemical Engineering Science. 104, 304–318.

Romano M. C., Chiesa P., Lozza G., 2010. Pre-combustion CO_2 capture from natural gas power plants, with ATR and MDEA processes. International Journal of Greenhouse Gas Control 4, 785–797.

Roy B., Bhattacharya S., 2014. Oxy-fuel fluidized bed combustion using Victorian brown coal: An experimental investigation Fuel Processing Technology, 117, 23–29.

Rutherford S. W. and Do D. D., 2000. Adsorption dynamics of carbon dioxide on a carbon molecular sieve 5A. Carbon, 38, 1339–1350.

Ruthven D., Farooq S., Knaebel K. S., 1994. Pressure Swing Adsorption. VCH, New York. 352.

Saha D. E., Bao Z., Jia F., Deng S., 2010. Adsorption of CO_2, CH_4, N_2O, and N_2 on MOF-5, MOF-177, and Zeolite 5A. Environ. Sci. Technol., 44, 1820– 1826.

Scholes C.A., Kentish S.E., Stevens G.W., 2008. Recent Patents Chem. Eng. (1), 52–66.

Scholes C. A., Smith K. H., Kentish S. E., Stevens G.W., 2010. CO_2 capture from pre-combustion processes—Strategies for membrane gas separation. International Journal of Greenhouse Gas Control, 4, 739–755.

Self et al., 2012. Review of underground coal gasification technologies and carbon capture. International Journal of Energy and Environmental Engineering 3, 16.

SeoY., Kang S. P., 2010. Enhancing CO_2 separation for pre-combustion capture with hydrate formation in silica gel pore structure". Chemical Engineering Journal 161, 308–312.

Shendalman L. H. and Mitchell J. E., 1972. A study of heatless adsorption in the model system CO_2 in He, I. Chem. Eng. Sci.27, 1449–1458.

Sircar S., Kratz W.C., 1988. Simultaneous production of hydrogen and carbon dioxide from steam reformer off-gas by pressure swing adsorption. Sep. Sci. Technol. 23, 2397–2415.

Siriwardane R. V., Shen M. S., Fisher E. P., Poston J. A., 2001. Adsorption of CO_2 on Molecular Sieves and Activated Carbon. Energy and Fuels, 15, 279-284.

Siriwardane R. V., Shen M. S., Fisher E. P., 2005. Adsorption of CO_2 on Zeolites at Moderate Temperatures. Energy and Fuels, 19, 1153-1159.

Shaddix CR, Murphy JJ., 2003. Coal char combustion reactivity in oxy-fuel applications. Twentieth Pittsburgh coal conference.

Shaddix C. R., Molina R., 2010. Fundamental investigation of NOx formation during oxy-fuel combustion of pulverized coal". Proc. Combust. Inst., doi: 10. 1016/ j. proci. 2010. 07. 072.

Shafeeyan M.S., Wan Daud W.M.A., Houshmand A., Shamiri A., 2010. A review on surface modification of activated carbon for carbon dioxide adsorption. J. Anal. Appl. Pyrolysis. 89, 143–151.

Shafeeyan M. S., Wan Daud W. M. A., Houshmand A., Arami-Niya A., 2012. The application of response surface methodology to optimize the amination of activated carbon for the preparation of carbon dioxide adsorbents. Fuel. 94, 465–472.

Skarstrom C. W., 1960. Method and Apparatus for Fractionating Gaseous Mixtures by Adsorption, US Patent 2944627, 1960.

Sivakumar P., Palanisamy P. N., (2009). Adsorption studies of basic Red 29 by a non-conventional activated carbon prepared from Euphorbia antiquorum L. International Journal of Chem. Tec. Research, 1 (3), 502- 510.

Smart J. P., O'Nions P., Riley G. S., 2010. Radiation and convective heat transfer, and burn out in oxy-coal combustion. Fuel, 89, 2468-76.

Spigarelli B. P., **Kawatra S. K., 2013.** Opportunities and challenges in carbon dioxide capture, Journal of CO_2 Utilization, 1, 69–87.

Stephan B., Marie H.M., Jean N.F., 2001. Mass transfer in VOC adsorption on zeolite: experimental and theoretical breakthrough curves. Environ. Sci. Technol. 35, 3571- 3575.

Sudibandriyo M., Pan Z., Fitzgerald J. E., Jr. R. L. R., Gasem K. A. M., 2003. Adsorption of methane, nitrogen, carbon dioxide, and their binary mixtures on dry activated carbon at 318.2 K and pressures up to 13.6 MPa. Langmuir, *19,* 5323-5331.

Soundararajan R., Gundersen T., 2013. Coal based power plants using oxy-combustion for CO_2 capture: Pressurized coal combustion to reduce capture penalty, Applied Thermal Engineering 61, 115-122.

Steeneveldt R., Berger B., Torp T. A., 2006. CO_2 capture and storage closing the knowing of doing gap. Chemical Engineering Research and Design, 84 (A9), 739-63.

Stern S.A., Mi Y., Yamamoto H., Clair A.K.S., 1989. J. Polym. Sci. 27 (9), 1887–1909.

Stern S.A., 1994. J. Membr. Sci. 94 (1), 1–65.

Tan Y., Croiset E., Douglas M. A., Thambimuthu K. V., 2006. Combustion characteristics of coal in a mixture of oxygen and recycled flue gas. Fuel, 85, 507-12.

Taniguchi M., Shibata T., Kobayashi H., 2010. Prediction of lean flammability limit and flame propagation velocity for oxy-fuel fired pulverized coal combustion" Proc. Combust. Inst., doi:10. 1016/ j. proci. 2010. 07. 020.

Takamura Y., Narita S., Aoki J., Hironaka S., Uchida S., 2001. Evaluation of dual-bed pressure swing adsorption for CO_2 recovery from boiler exhaust gas. Sep. Purif. Technol. 24, 519–528.

Thang H. V., Grajciar L., Nachtigall P., Bludsk´y O., Areán C. O., Fr´ydová E., Bulánek R., 2014. Adsorption of CO_2 in FAU zeolites: Effect of zeolite composition, Catalysis Today. 227, 50–56.

Tlili N., Grevillot G., Vallieres C., 2009. Carbon dioxide capture and recovery by means of TSA and/or VSA. International Journal of Greenhouse Gas Control 3, 519–527.

Treybal R.E., 1955. Mass-Transfer Operations Chemical Engineering Series, McGraw-Hill Book Company, Inc., New York.

Triebe R.W. and Tezel F. H., 1995. Adsorption of nitrogen, carbon monoxide, carbon dioxide and nitric oxide on molecular sieves. Gas. Sep. Purif. 9, 4, 223-230.

Tuiniera M. J., Annalanda M. v. S., Kramer G. J., Kuipers J. A. M., 2010. Chem. Eng. Sci. 65, 114–119.

Tuiniera M. J., Annaland v. S. M., Kuipers J. A. M., 2011. Int. J. Greenhouse Gas Contr. 5, 694–701.

Vaart R. V., Huiskes C., Bosch H., Reith T., 2000. Single and mixed gas adsorption equilibria of carbon dioxide/methane on activated carbon. Adsorption, 6, 311–323.

Valverde J. M., Duran F.J., Pontiga F., Moreno H., 2012. CO_2 capture enhancement in a fluidized bed of a modified Geldart C powder, Powder Technology. 224, 247–252.

Va´rheyi G., Till F., 1999. Comparison of temperature-programmed char combustion in CO_2–O_2 and Ar–O_2 mixtures at elevated pressure. Energy Fuels, 13, 539–40.

Veneman R., Li Z. S., Hogendoorn J. A., Kersten S. R. A., Brilman B. W. F., 2012. Continuous CO_2 capture in a circulating fluidized bed using supported amine sorbents, Chemical Engg. Jounal, 207-208.

Wall T., Liu Y., Spero C., Elliott L., Khare S., Rathnam R., 2009. An overview on oxyfuel coal combustion e State of the art research and technology development. Chemical Engineering Research and Design, 87, 1003-16.

Wang Y. and Le Van M. D., 2009. Adsorption Equilibrium of Carbon Dioxide and Water Vapor on Zeolites 5A and 13X and Silica Gel Pure Components. J. Chem. Eng. Data, 54, 2839–2844.

Wang L., Liu Z., Li P., Yu J., Rodrigues A. E., 2012. Experimental and modeling investigation on post-combustion carbon dioxide capture using zeolite 13X-APG by hybrid VTSA process. Chemical Engineering Journal, 197, 151–161.

Wappela D., Khana A., Shallcrossa D., Joswiga S., Kentisha v, Stevensa G., 2009. Energy Procedia 1, 125–131.

Willis R. R., Benin A. I., Low J. J., Bedard R., Lesch D., 2006. Annual Report, Project DE-FG26-04NT42121, National Energy Technology Laboratory.

Winaya N. S., Basu P., 2000. Effect of pressure and carbon dioxide concentration on heat transfer at high temperature in a pressurized circulating fluidized bed (PCFB) combustor. International journal of heat and mass transfer, 44, 2965-2971.

World Resources, 1996–97. A Guide to the Global Environment: The Urban Environment, World Resource Institute, A Report by the United Nations Environment Programme, United Nations Development Programme and The World Bank, 400.

Woycenko D., van de Kamp W., Roberts P., 1995. Combustion of pulverized coal in a mixture of oxygen and recycled flue gas. Technical Report Doc F98/y/2. International Flame Research Foundation.

Xu Z. K., Dannenberg C., Springer J., Banerjee S., Maier G., 2002. Journal of Membrane. Sci. 205 (1–2), 23–31.

Xu X., Song C., Miller B. G., Scaroni A. W., 2005. Adsorption separation of carbon dioxide from flue gas of natural gas-fired boiler by a novel nanoporous "molecular basket" adsorbent. Fuel Process. Technol. 86, 1457–1472.

Xuezhong H., Jon Lie J. A., Sheridan E., Hägg M. B., 2009. CO_2 Capture by Hollow Fibre Carbon Membranes: Experiments and ProcessSimulations. Energy Procedia 1, 261–268.

Yang H., Xu Z., Fan M., Gupta R., Slimane R. B., Bland A. E., Wright I., 2008. Progress in carbon dioxide separation and capture: A review, Journal of Environmental Sciences, 20, 14–27.

Yang R., 1987. Gas separation by adsorption processes. Stoneham**,** MA: Butterworth Publishers.

Yeh A. C., Bai H., 1999. Sci. Total Environ. 228 (2–3), 121–133.

Yi C. K., Jo S. H., Lee J. B., Ryu C. K., 2007. Continuous operation of potassium based dry sorbent CO_2 capture process with two fluidized bed reactors, International journal of greenhouse gas control, I, 31-36.

Younger A.H., 2004. Natural Gas Processing Principles and. Technology – Part I. Canada: University of Calgary.

Yucel H. and Ruthven D. M., 1980. Diffusion of CO_2 in 4A and 5A Zeolite Crystals. Journal of Colloid and Interface Science, 74, No. 1.

Yun Z., Zhen-Zhong L., Xin L., Jiang-Xun D., Yang W., 2003. Preliminary Study to Capture CO_2 in Flue Gas by Spraying Aqueous Ammonia to Produce NH_4HCO_3, National Power Plant Combustion Engineering Technology Research Center, Shenyang, PR China.

Zhang J., Xiao P., Li G., Webley P. A., 2009. Effect of Flue Gas Impurities on CO_2 Capture Performance from Flue Gas at Coal-fired Power Stations by Vacuum Swing Adsorption. Energy Procedia, 1, 1115–1122.

Zhou J., Grace J. R., Qin S., Brereton C. M. H., Lim C.J., Zhu J., 1994. Voidage profiles in a circulating fluidized bed of square cross-section, Chem. Eng. Sci. 49 (19), 3217–3226.

APPENDIX I

SPECIFICATION OF VARIOUS EQUIPMENTS

1. Motor

15 HP, Primo 3 phase induction motor

Voltage 445 volts 50 Hz

Amperes 27.6

Manufacture: Kirloskar

2. Blower

It is a high pressure, centrifugal type blower. It was installed to supply air to the main column to fluidize the solid particles.

Air quantity	: 3000-4000 m^3/hr
Temperature	: 60 ˚C
Serial No.	: 0503468
Total pressure	: 1600-1900 mm w. g
Speed	: 2880 RPM
Flow rate	: 1275 m^3/hr
Manufacturer	: Everest transmission

3. Variac

Input	: 240 volts
Output	: 0-270 Volts
Type	: 6P-1
Capacity	: 6 Amps
Manufacturer	: Varivolt

4. Heating Element - Nichrome Wire

Capacity	: 1000 W

Resistance of the wire : 29 Ohms

Diameter of the wire : 0.6 mm

5. The Data Acquisition System (DAS)

It consists of two RS-232 converter modules, six analog input modules, each module has eight channels to connect thermocouples and the software named as VPL-EASYLAB 1.0. DAS is used to receive the data from various transducers or sensors and then transfer the data to computer, where output can be measured in the form of digital or analog or in the graphical form of signal. The software VPL-EASYLAB 1.0 is used to convert the data of DAS into required output.

6. Flue Gas Analyzer

The Testo Model 350 XL is the most innovative portable combustion analyzer to date. Keystone features of the Testo 350 XL include interchangeable, pre-calibrated sensors with temperature control; a CO sample dilution system for test range expansion; complete, onboard sample conditioning; and an abundance of opportunities to interface with the entire system. The cells of the Testo 350 XL can be easily replaced or exchanged for greater testing flexibility.

Constituents Measured : Temperature, Draft Pressure, O_2, CO_2, CO, NO, NO_2, SO_2, Velocity, Differential Pressure with optional cells for hydrocarbons

Power Requirement **:** 110-230V, 90-260V or rechargeable battery

Accuracy **:** ±5 %

7. Scanning Electron Microscope

Model : 1430 vp Carl Zeiss

Beam current : 100 µA

Probe current	: 200-500 pA
EHT	: 20 KeV-vacuum < 8×10^{-6} torr
Low working distance	: 7-8 mm
VP pressure	: 100 pa
Optimum working pressure	: 20-30 pa

8. Surface area analyser

Make	: Quantachrome
Model	: Autosorb-IQ MP
Wetted Surfaces	: Inconel
Temperature stability ratio	: 35
Internally thermostatted	: 45 ˚C
Temperature coefficient (span)	: 0.005% FS/ ˚C
Overpressure limit	: 45 psia(>23,000 × full scale)
Resolution	: 1×10^{-7} torr
P/P_0	: 10^{-8}, 10^{-7}, 10^{-6}, 10^{-5}
Accuracy	: ± 0.15 % reading

APPENDIX II

MEASUREMENT OF MEAN PARTICLE SIZE OF ACTIVATED CARBON

The actual particles are of varieties of shape and size. To measure the mean size of the particles following procedure has been followed (Kunii and Levenspiel, 1991).

Following assumptions have been made,

1. Volume remains same.
2. Surface area remains same.

Now, let there be:

n_1: Particles of diameter d1.

n_2: Particles of diameter d2.

n_3: Particles of diameter d3.

And so on.

From assumption no.1:

$$\text{N x } \frac{\pi \bar{d}_p^3}{6} = n_1 \frac{\pi d_1^3}{6} + n_2 \frac{\pi d_2^3}{6} + n_3 \frac{\pi d_3^3}{6} + \ldots\ldots\ldots\ldots\ldots\ldots$$

Where N is the number of replaced, uniformly sized particles of diameter $\bar{d}_p$.

$$N \times \bar{d}_p^3 = n_1 \times d_1^3 + n_2 \times d_2^3 + n_3 \times d_3^3 + \ldots\ldots\ldots\ldots$$

From assumption no.2:

$$\text{N x } \pi \bar{d}_p^2 = n_1 \pi d_1^2 + n_2 \pi d_2^2 + n_3 \pi d_3^2 + \ldots\ldots\ldots\ldots\ldots\ldots$$

or,

$$N\times \bar{d}_p^{\,2} = n_1\times d_1^2 + n_2\times d_2^2 + n_3\times d_3^2 + \ldots\ldots\ldots\ldots$$

Let X_1 be the weight fraction of solids of diameter d_1.

Therefore

$$X_1 = \frac{\frac{n_1\times \bar{d}_1^{\,3}}{6}\times\rho_s}{\frac{N\times \bar{d}_p^{\,3}}{6}\times\rho_s} = \frac{n_1\times d_1^3}{N\times \bar{d}_p^{\,3}}$$

where ρ_s represents the density of sand.

Similarly, $X_2 = \dfrac{n_2\times d_2^3}{N\times \bar{d}_p^{\,3}}$

Hence, $n_1\times d_1^2 = X_1\times N\times \bar{d}_p^{\,3}/d_1$

$$n_2\times d_2^2 = X_2\times \bar{d}_p^{\,3}/d_2$$

$$N\times \bar{d}_p^{\,2} = n_1\times d_1^2 + n_2\times d_2^2 + n_3\times d_3^2 + \ldots\ldots\ldots\ldots$$

$$= X_1\times N\times\frac{\bar{d}_p^{\,3}}{\bar{d}_1} + X_2\times N\times\frac{\bar{d}_p^{\,3}}{\bar{d}_2} + X_3\times N\times\frac{\bar{d}_p^{\,3}}{\bar{d}_3}$$

or, $$\frac{1}{\bar{d}_p} = \frac{X_1}{d_1} + \frac{X_2}{d_2} + \frac{X_3}{d_3} + \ldots\ldots\ldots\ldots\ldots$$

or, $$\frac{1}{\bar{d}_p} = \sum\frac{X_i}{d_i}$$

or, $$\bar{d}_p = \frac{1}{\sum \frac{X_i}{d_i}}$$

Table II.1 Mean particles size data for activated carbon

Mesh (BSS)	Mean particle size (d_i), µm	Weight in grams	Weight fraction (Xi)	X_i / d_i
18-22	950.3	121	0.249	0.263×10^{-3}
22-25	749.4	146	0.936	0.125×10^{-3}
25-30	549.5	126	0.125	0.229×10^{-3}
30-36	461	192	0.053	0.116×10^{-3}
36-44	388	192	0.075	0.194×10^{-3}
44-52	325.5	4	0.036	0.0113×10^{-3}
52-pan	274	96	0.042	0.147×10^{-3}

Hence for Mean particle size calculation, following formula has been used

$$\bar{d}_p = \frac{1}{\sum \frac{Xi}{d_i}}$$

Thus, mean particle size = 920 µm.

APPENDIX III

CALIBRATION OF THERMOCOUPLE (K-TYPE)

The calibration of thermocouple is done by keeping one junction of the two dissimilar metals (Copper-Constantan) at constant temperature (at 0 °C) and other junction is maintained at variable temperatures. In order to maintain variable temperature, a water circulating bath is used. A high precision multi-meter is connected in the circuit to see the emf generation. In every 5 °C, the increase of water temperature the emf (millivolt) generation is recorded. The calibration curve so obtained is presented in Figure III.1. Chormel-alumel thermocouple calibration chart was used for high temperature measurement.

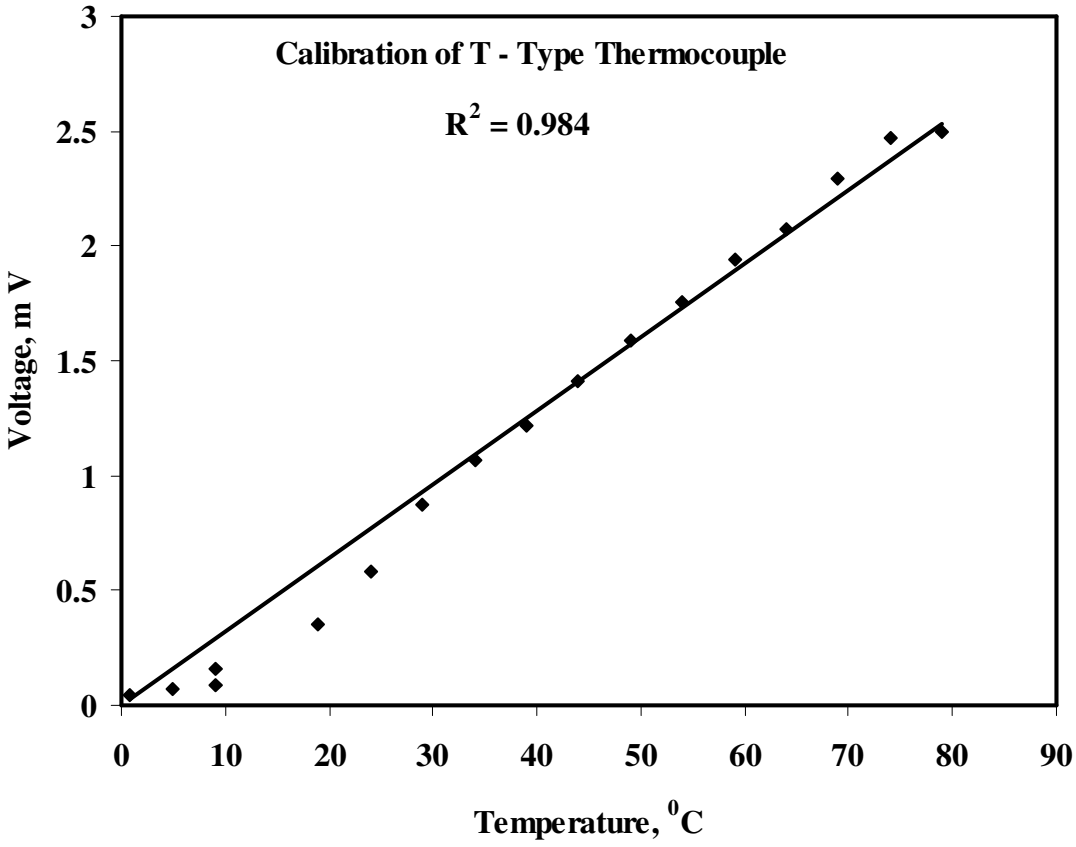

Fig III.1 Calibration of Thermocouple

APPENDIX IV

EXPERIMENTAL DATA

1. Langmuir isotherm model regression analysis

Table IV.1 Experimental data for zeolite 13X

Pressure (Bar)	Adsorption (mol/kg)				P/q			
	298 K	308 K	318 K	333 K	298 K	308 K	318 K	333 K
0	0	0	0	0	0	0	0	0
0.05	2.5	2.25	1.98	1.45	0.02	0.02222	0.02525	0.03448
0.1	3.1	2.82	2.532	1.96	0.0322	0.03546	0.03949	0.05102
0.2	3.5	3.21	2.89	2.36	0.0571	0.06230	0.06920	0.08474
0.4	3.75	3.46	3.15	2.64	0.1066	0.11560	0.12698	0.15151
0.6	3.98	3.68	3.3	2.82	0.1507	0.16304	0.18181	0.21276
0.8	4.1	3.81	3.45	2.98	0.1951	0.20997	0.23188	0.26845
1	4.2	3.92	3.54	3.12	0.2380	0.25510	0.282486	0.320513

Table IV.2 Experimental data for zeolite 5A

Pressure (Bar)	Adsorption (mol/kg)				p/q			
	298 K	308 K	318 K	333 K	298 K	308 K	318 K	333 K
0	0	0	0	0	0	0	0	0
0.05	1.9	1.4	1.22	0.95	0.026316	0.035714	0.040984	0.052632
0.1	2.36	1.95	1.73	1.39	0.042373	0.051282	0.057803	0.071942
0.2	2.71	2.39	2.11	1.78	0.073801	0.083682	0.094787	0.11236
0.4	3.1	2.8	2.53	2.23	0.129032	0.142857	0.158103	0.179372
0.6	3.32	3.06	2.81	2.51	0.180723	0.196078	0.213523	0.239044
0.8	3.51	3.24	3.02	2.74	0.22792	0.246914	0.264901	0.291971
1	3.61	3.36	3.15	2.89	0.277008	0.297619	0.31746	0.346021

Table IV.3 Experimental data for zeolite 4A

Pressure (Bar)	Adsorption (mol/kg)				P/q			
	298 K	308 K	318 K	333 K	298 K	308 K	318 K	333 K
0	0	0	0	0	0	0	0	0
0.05	1.6	1.4	1.22	0.95	0.03125	0.035714	0.040984	0.052632
0.1	2.16	1.92	1.73	1.39	0.046296	0.052083	0.057803	0.071942
0.2	2.65	2.36	2.11	1.78	0.075472	0.084746	0.094787	0.11236
0.4	2.86	2.7	2.46	2.16	0.13986	0.148148	0.162602	0.185185
0.6	2.97	2.77	2.58	2.25	0.20202	0.216606	0.232558	0.266667
0.8	3.02	2.88	2.7	2.39	0.264901	0.277778	0.296296	0.334728
1	3.14	2.89	2.723	2.39	0.318471	0.346021	0.367242	0.41841

Table IV.3 Experimental data for activated carbon

Pressure (Bar)	Adsorption (mol/kg)				P/q			
	298 K	308 K	318 K	333 K	298 K	308 K	318 K	333 K
0	0	0	0	0	0	0	0	0
0.05	0.41	0.32	0.27	0.18	0.121951	0.15625	0.185185	0.277778
0.1	0.7	0.6	0.5	0.36	0.142857	0.166667	0.2	0.277778
0.2	1.1	0.96	0.83	0.7	0.181818	0.208333	0.240964	0.285714
0.4	1.76	1.61	1.5	1.34	0.227273	0.248447	0.266667	0.298507
0.6	2.25	2.1	2	1.82	0.266667	0.285714	0.3	0.32967
0.8	2.57	2.4	2.3	2.14	0.311284	0.333333	0.347826	0.373832
1	2.8	2.67	2.56	2.4	0.357143	0.374532	0.390625	0.416667

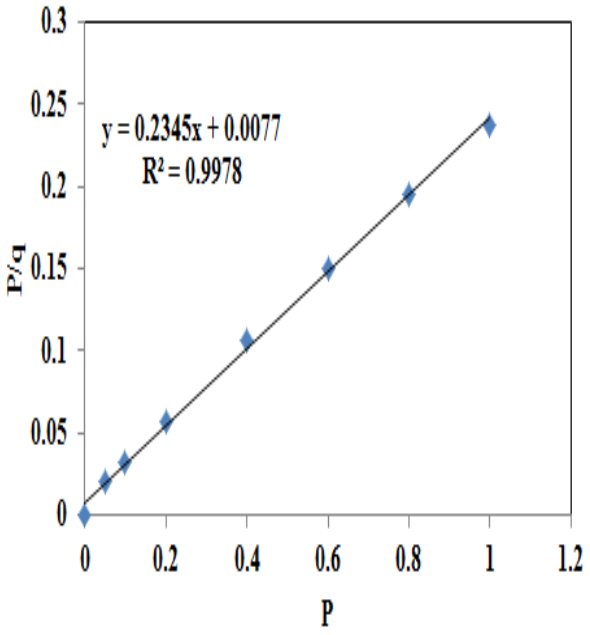

Fig IV.1 Regression analysis for zeolite 13X at 298 K

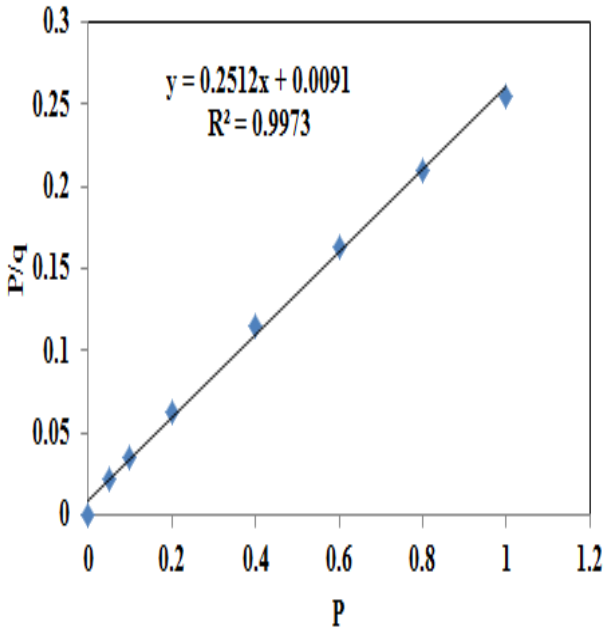

Fig IV.2 Regression analysis for zeolite 13X at 308 K

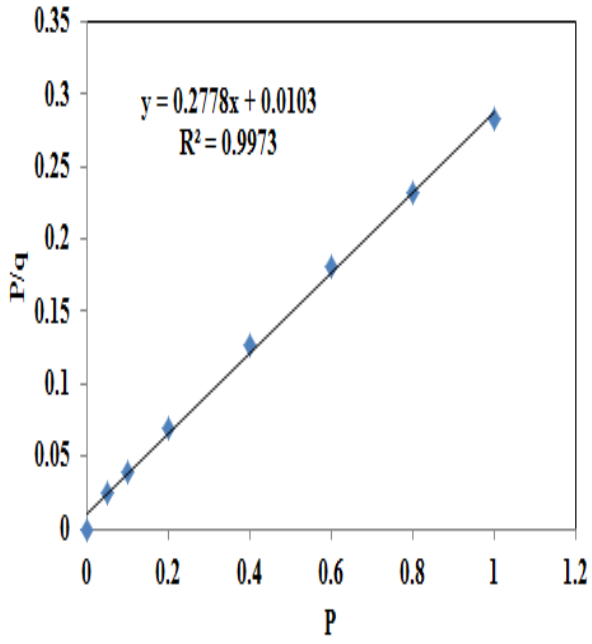

Fig IV.3 Regression analysis for zeolite 13X at 318 K

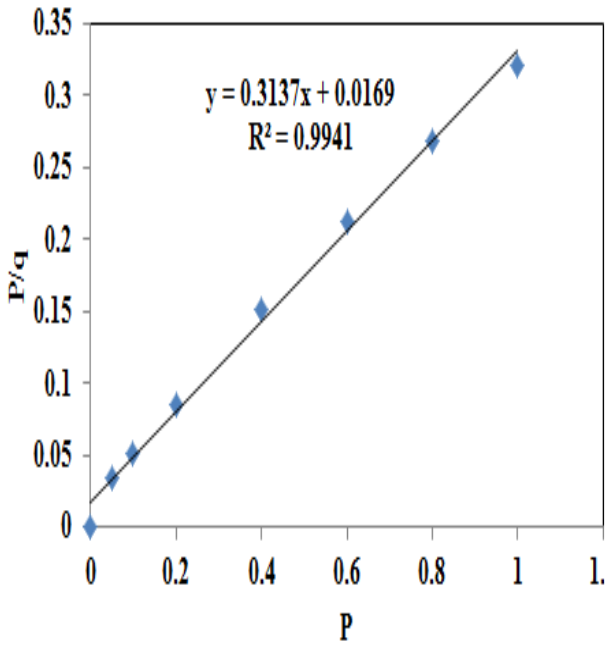

Fig IV.4 Regression analysis for zeolite 13X at 333 K

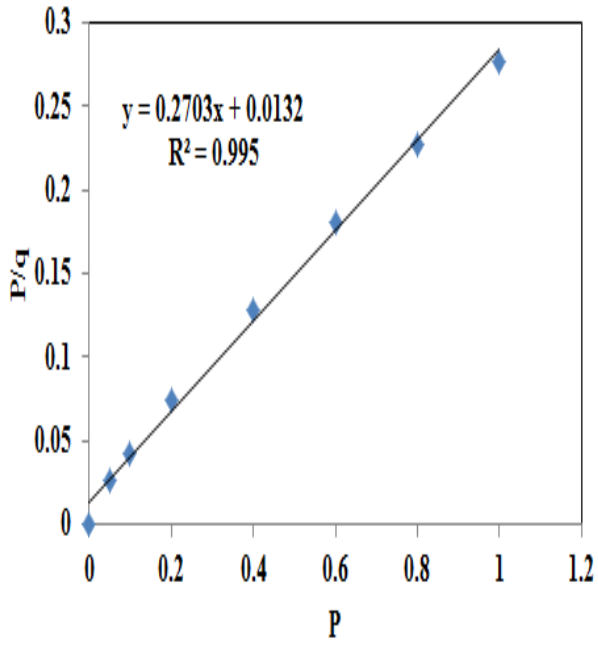

Fig IV.5 Regression analysis for zeolite 5A at 318 K

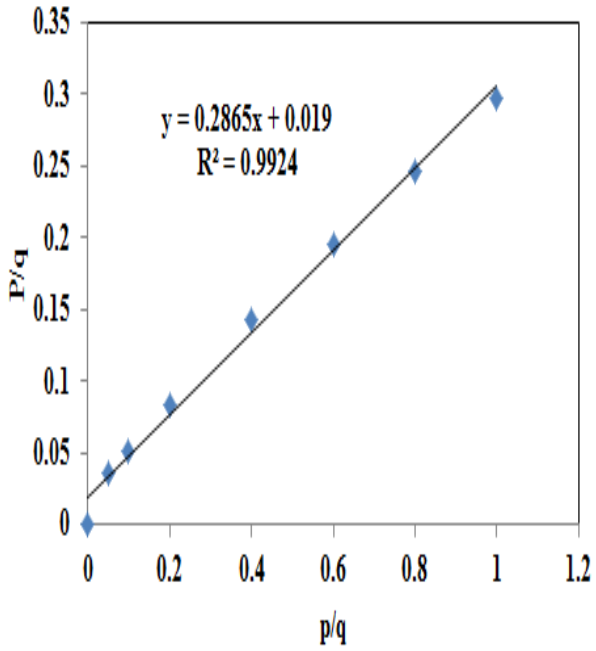

Fig IV.6 Regression analysis for zeolite 5A at 318 K

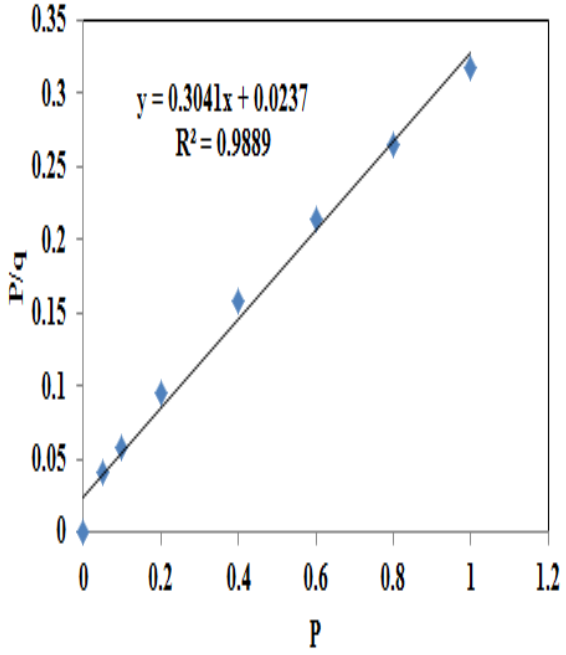

Fig IV.7 Regression analysis for zeolite 5A at 318 K

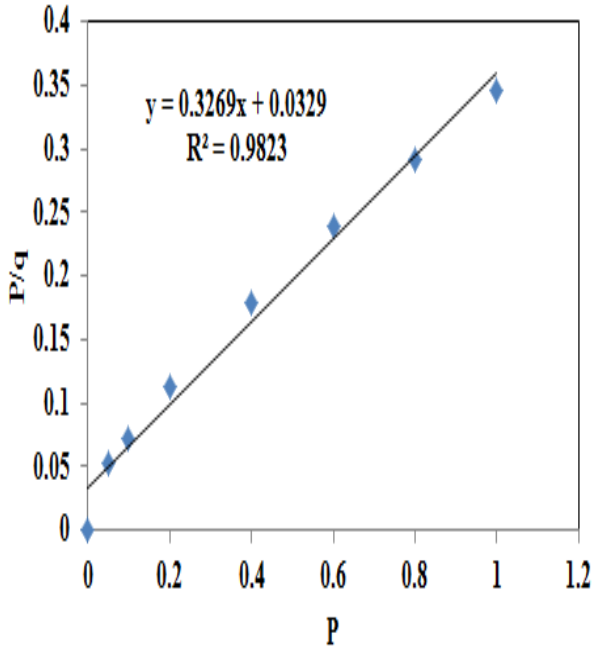

Fig IV.8 Regression analysis for zeolite 5A at 318 K

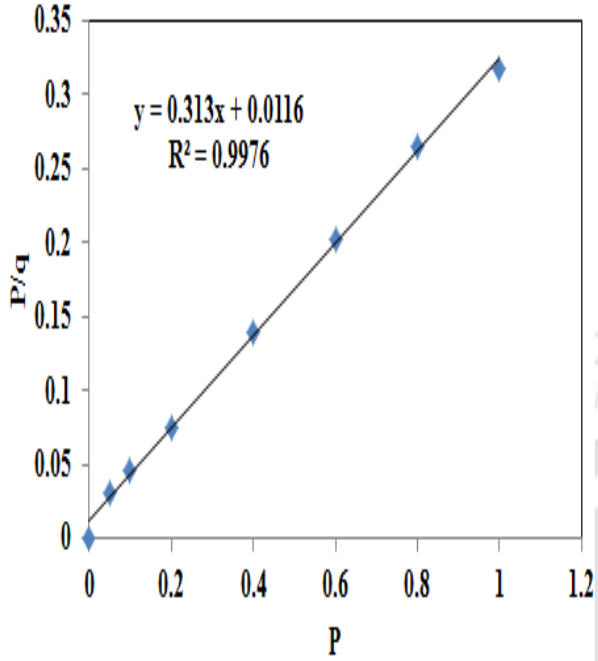

Fig IV.9 Regression analysis for zeolite 4A at 298 K

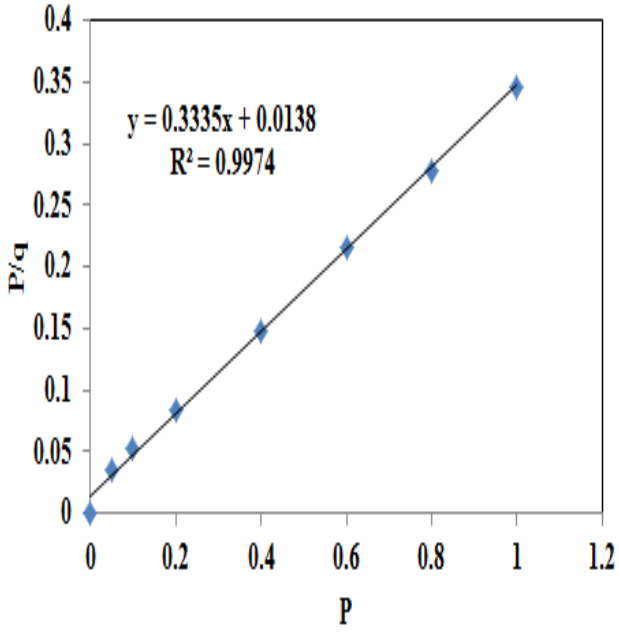

Fig IV.10 Regression analysis for zeolite 4A at 308 K

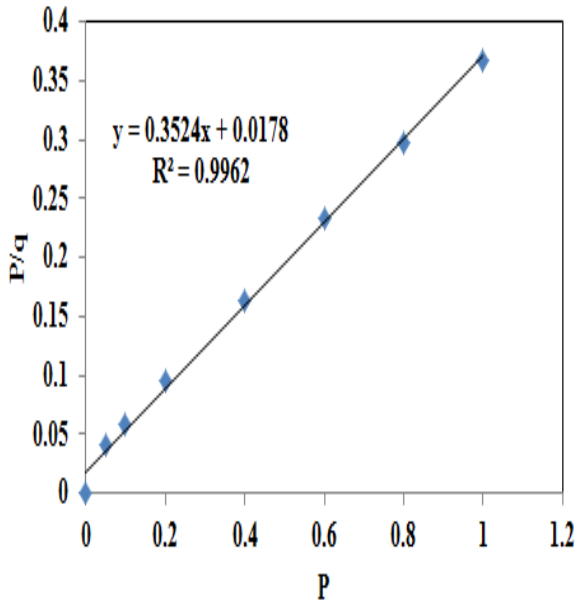

Fig IV.11 Regression analysis for zeolite 4A at 318 K

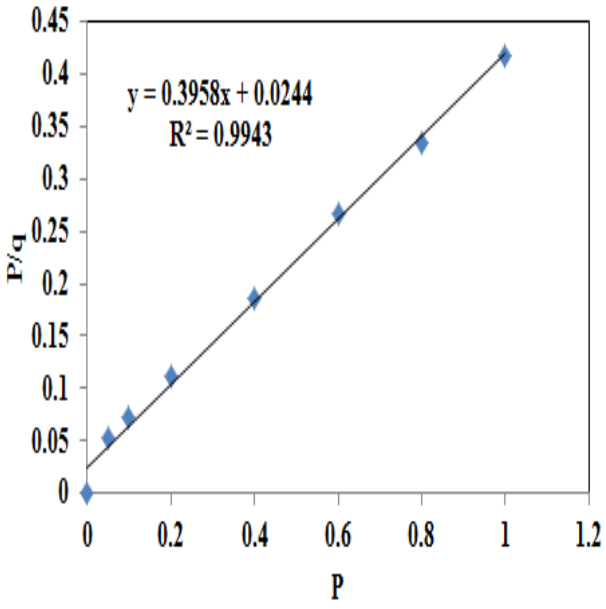

Fig IV.12 Regression analysis for zeolite 4A at 333 K

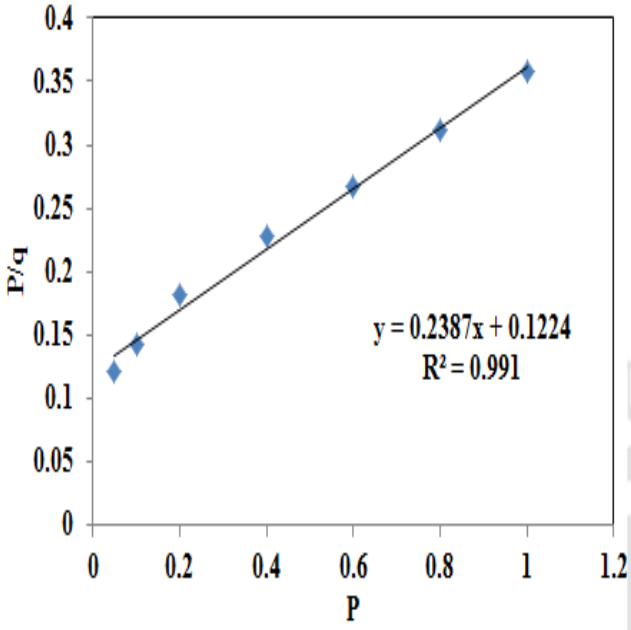

Fig IV.13 Regression analysis for activated carbon at 298 K

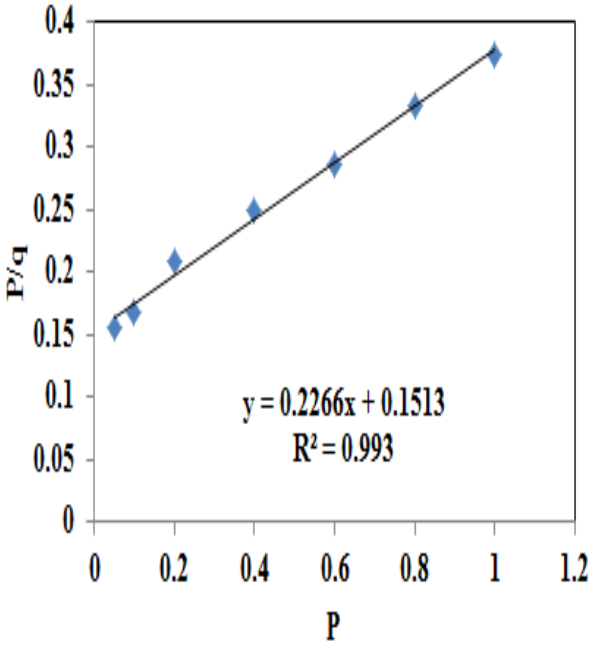

Fig IV.14 Regression analysis for activated carbon at 308 K

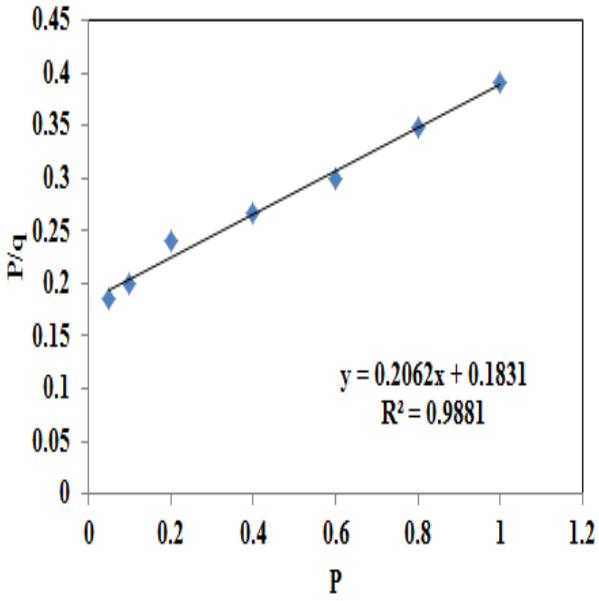

Fig IV.15 Regression analysis for activated carbon at 318 K

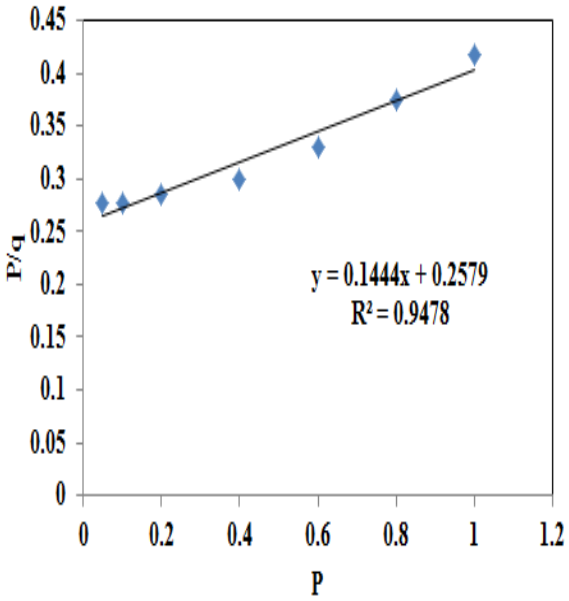

Fig IV.16 Regression analysis for activated carbon at 333 K

2. Freundlich isotherm model regression analysis

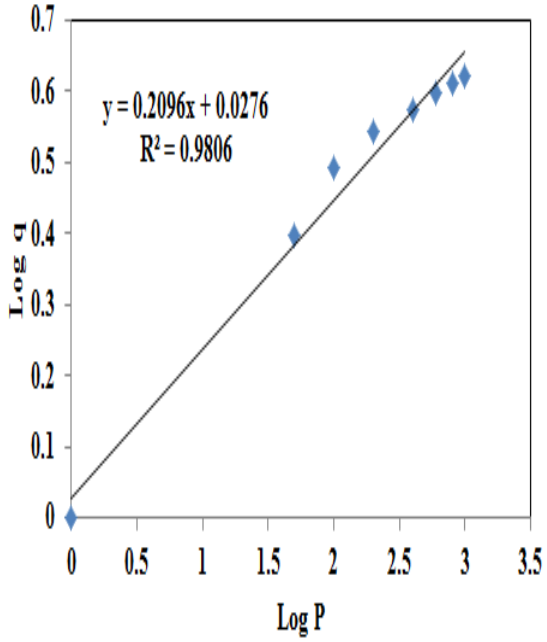

Fig IV.17 Regression analysis for zeolite 13X at 298 K

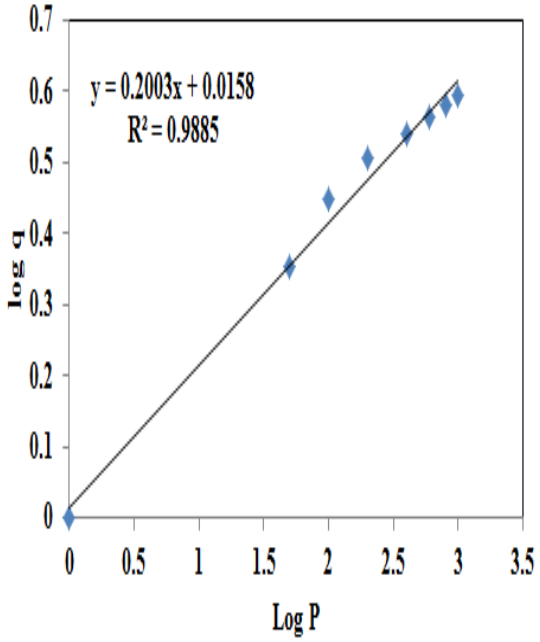

Fig IV.18 Regression analysis for zeolite 13X at 308 K

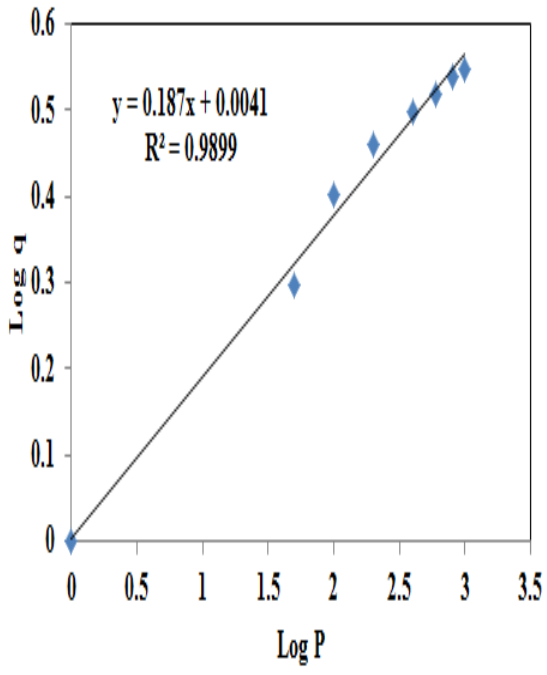

Fig IV.19 Regression analysis for zeolite 13X at 318 K

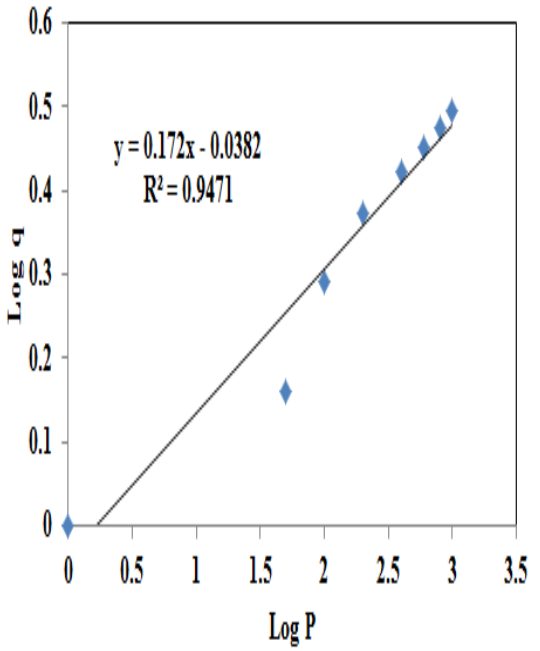

Fig IV.20 Regression analysis for zeolite 13X at 333 K

3. Thermodynamic parameters determination

Thermodynamic parameters were determined through Langmuir isotherm model by Van't Hoff's equation given in Chapter 6.

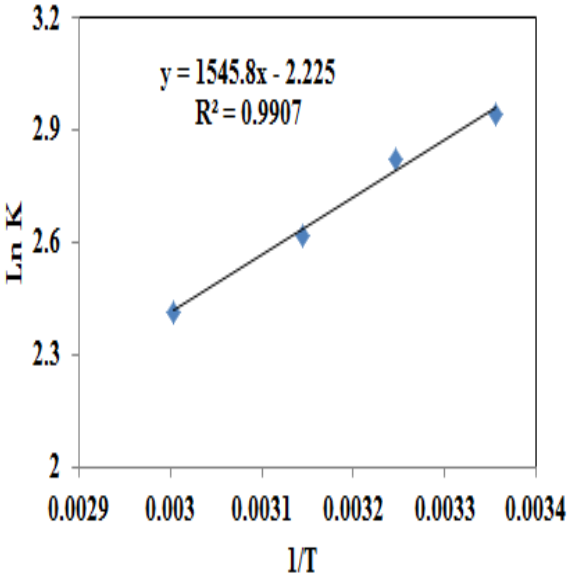

Fig IV. 21 Curve for zeolite 13X

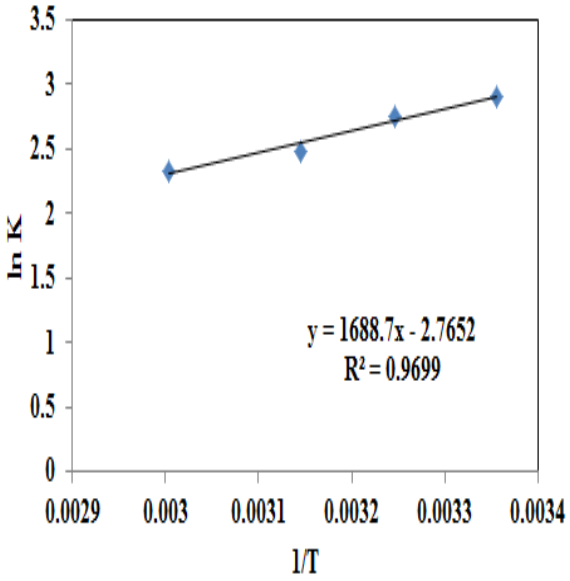

Fig IV. 22 Curve for zeolite 5A

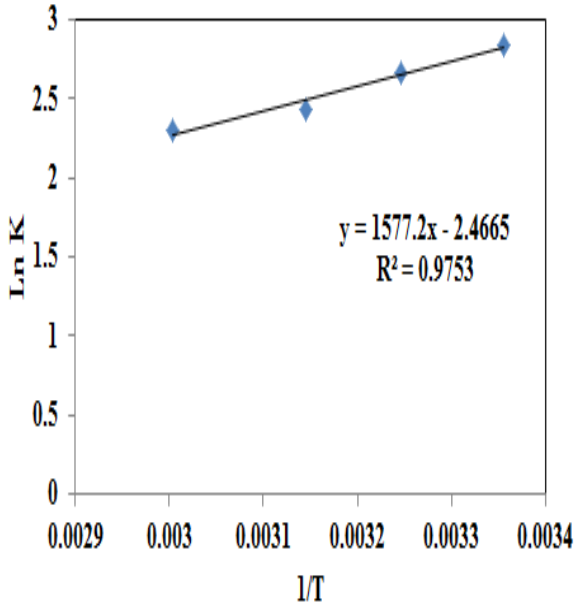

Fig IV. 23 Curve for zeolite 4A

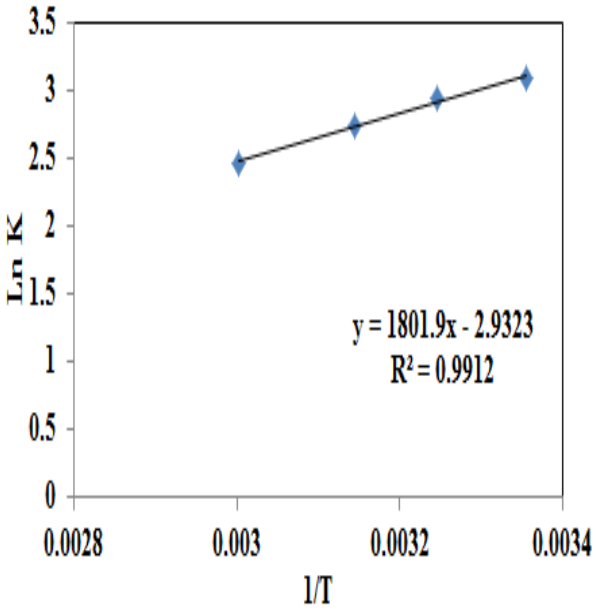

Fig IV. 24 Curve for activated carbon

APPENDIX V

UNCERTAINTY ANALYSIS

For overall uncertainty measurement the following quantities have been considered:

- Orifice : ± 0.5 mm
- Manometer : ± 0.2 mm
- Temperature : ± 0.5 °C
- Distributor plate : ± 0.6 % opening area
- Center to center pressure tapings: 1 mm (error)
- Pressure gauge error: ± 0.5
- Loss of inventory: ± 1 g
- Visual Error : ± 0.5
- Bulk temperature calculation: ± 5 °C
- Thermocouple temperature measurement error: ± 0.5 °C

Percent uncertainty in the heat transfer coefficient can be determined by using Kline and McClintok method (Kline and McClintok, 1953).

The local heat transfer coefficient along the fluidized bed column may be evaluated using Equation V.1

$$h = \frac{q}{A_s (T_s - T_b)} \quad \text{W.m}^{-2}\text{.K}^{-1} \qquad \text{(V.1)}$$

where

q: Heat supplied, W

H: Height of heated section, m

B: Width of heated section, m

T_b: Bed temperature, °C

T_S: Surface temperature, °C

Now,

$$h = f(q, H, B, T_S, T_b)$$

Therfore, Percentage uncertainty = $\frac{Error}{h} \times 100$

$$= 100 \times \sqrt{\left(\frac{w_1}{q}\right)^2 + \left(\frac{-w_2}{B}\right)^2 + \left(\frac{w_3}{H}\right)^2 + \left(\frac{-w_4}{T_s - T_b}\right)^2 + \left(\frac{w_5}{T_s - T_b}\right)^2} \quad \text{(V.2)}$$

Here, w_1, w_2, w_3, w_4, w_5 are uncertainties associated with independent variables q, B, H, T_S, T_B, respectively.

Uncertainty in heat transfer coefficient

A) The sample calculation for, Inventory, I= 200 g, q''= 230.63 w/m^2, U_s= 0.75 m/s, A_s = 0.21425 m^2, T_s= 45.4 ˚C, T_b= 30.6 ˚C, h= 15.724 w/m^{2}K is given below in Table V.1. Now, through Equation V.1, it can be calculated that;

$$\frac{\partial h}{\partial q} = \frac{1}{A_s (T_s - T_b)}$$

$$\frac{\partial h}{\partial q} = 0.315$$

$$\Delta q = 0.02 \ W$$

Then,

$$\frac{\partial h}{\partial A_s} = \frac{-q}{A_s^2 (T_s - T_b)}$$

$$\frac{\partial h}{\partial A_s} = -74.54$$

$$\Delta A_s = 3.245 \times 10^{-4} \ mm^2$$

$$\frac{\partial h}{\partial T_s} = \frac{-q}{A_s (T_s - T_b)^2}$$

Now,

$$\frac{\partial h}{\partial T_s} = -1.127$$

$$\Delta T_s = 0.83\ ^\circ C$$

And

$$\frac{\partial h}{\partial T_b} = \frac{-q}{A_s (T_s - T_b)^2}$$

$$\frac{\partial h}{\partial T_b} = 1.122$$

$$\Delta T_b = 0.53^\circ C$$

Therefore, through Equation V.2, the uncertainty can be calculated as;

$$U_h = \sqrt{\left(\frac{\partial h}{\partial q} \times \Delta q\right)^2 + \left(\frac{\partial h}{\partial A_s} \times \Delta A_s\right)^2 + \left(\frac{\partial h}{\partial T_s} \times \Delta T_s\right)^2 + \left(\frac{\partial h}{\partial T_b} \times \Delta T_b\right)^2}$$

U_h=0.985

Therefore,

Percentage uncertainty, $\%U_h$= 6.264 %

Table V.1 Calculation of different weight of inventory and velocities

U_s (m/s)	I (g)	Δq (W)	ΔA_s (m^2)	ΔT_s (°C)	ΔT_b (°C)	% U_h
0.75	200	0.02	3.245×10^{-4}	0.83	0.53	6.264
	250	0.03	3.384×10^{-4}	0.87	0.61	6.752
	300	0.01	3.121×10^{-4}	0.75	0.52	5.851
1.5	200	0.04	3.841×10^{-4}	0.91	0.65	6.893
	250	0.03	3.525×10^{-4}	0.78	0.61	6.457
	300	0.02	3.265×10^{-4}	0.67	0.54	5.923
2.1	200	0.04	3.642×10^{-4}	0.86	0.58	6.565
	250	0.02	3.354×10^{-4}	0.78	0.52	6.132
	300	0.03	3.287×10^{-4}	0.82	0.57	6.368

Root mean square value of percentage uncertainty for heat transfer coefficient is 6.356 %.

For discharge of air through orifice

$\Delta H = 1.2$ cm, $d_0 = 2.5$ cm, $d_1 = 5$ cm, $m_a = 1.66375 \times 10^{-7}$ m^3/s

$$m_a = 2.3958 \; d_0^2 \times \rho_a \left[\frac{1}{\sqrt{1 - \left(\frac{d_0}{d_1} \right)^2}} \right] \sqrt{\frac{\Delta H}{10}} \qquad \text{(V.3)}$$

i)

$$\frac{\partial m_a}{\partial d_0} = \frac{2.3958}{3600} \times \sqrt{\frac{\Delta H}{10}} \left[2 d_0 \left(1 - \left(\frac{d_0}{d_1} \right)^2 \right)^{-1/2} + \left(1 - \left(\frac{d_0}{d_1} \right)^2 \right)^{-3/2} + \left(\frac{d_0}{d_1} \right) \right]$$

$$\frac{\partial m_a}{\partial d_0} = 1.8742 \times 10^{-4}$$

$$\Delta d_0 = 0.02 \; mm$$

ii)

$$\frac{\partial m_a}{\partial (\Delta H)} = \frac{1.3955}{3600} d_0^2 \times \left[\frac{1}{\sqrt{1 - \left(\frac{d_0}{d_1} \right)^2}} \right] \times \left(\frac{\Delta H}{10} \right)^{3/2}$$

$$\frac{\partial m_a}{\partial (\Delta H)} = 9.933 \times 10^{-9}$$

$$\Delta (\Delta H) = 1 mm$$

$$U_{m_a} = \sqrt{\left(\frac{\partial m_a}{\partial d_0} \times \Delta d_0 \right)^2 \times \left(\frac{\partial m_a}{\partial (\Delta H)} \times \Delta (\Delta H) \right)^2}$$

$$U_{m_a} = .748 \times 10^{-9}$$

Therefore, % uncertainty of $U_{ma} = (3.748 \times 10^{-9}) / (1.663 \times 10^{-7}) \times 100 = 2.253$ %.

Uncertainty in calculating bed voidage

The expression of bed voidage calculation is:

$$\varepsilon = 1 - \frac{10\Delta h}{\rho_s L} \quad \text{(V.4)}$$

$$\frac{\partial \varepsilon}{\partial(\Delta h)} = -\frac{10}{\rho_s \times L} \quad \text{(V.5)}$$

$$\frac{\partial \varepsilon}{\partial L} = \frac{10\Delta h}{\rho_s \times L^2} \quad \text{(V.6)}$$

$$\frac{\partial \varepsilon}{\partial \rho_s} = \frac{10\Delta h}{\rho_s^2 \times L} \quad \text{(V.7)}$$

Overall uncertainty may be calculated as;

$$U = \sqrt{\left(\frac{\partial \varepsilon}{\partial(\Delta h)} \times \Delta h\right)^2 + \left(\frac{\partial \varepsilon}{\partial L} \times \Delta L\right)^2 + \left(\frac{\partial \varepsilon}{\partial \rho_s} \times \Delta \rho_s\right)^2}$$

U= ±0.005-0.647 %

Uncertainty associated with solid density is considered to be ±0.5 kg/m^3.

By using the above mathematical expression the uncertainties at different inventories and at different operating pressures are calculated and presented in the following tables:

Table V.2 Variation of uncertainty at inventory of I = 200 g

ΔL (m)	Δh (m)			Δ(Δh) (m)	Percentage Uncertainty %		
	0.75 m/s^2	**1.5 m/s^2**	**2.1 m/s^2**		**0.75 m/s^2**	**1.5 m/s^2**	**2.1 m/s^2**
0.006	0.004	0.005	0.005	0.005	0.025	0.031	0.002
0.005	0.003	0.041	0.002	0.003	0.041	0.004	0.052
0.006	0.010	0.003	0.003	0.002	0.234	0.003	0.321
0.004	0.004	0.013	0.002	0.003	0.035	0.015	0.046

Table V.3 Variation of uncertainty at inventory of I = 250 g

ΔL (m)	Δh (m)			Δ(Δh) (m)	Percentage Uncertainty %		
	0.75 m/s^2	1.5 m/s^2	2.1 m/s^2		0.75 m/s^2	1.5 m/s^2	2.1 m/s^2
0.005	0.004	0.004	0.005	0.004	0.023	0.021	0.005
0.005	0.003	0.003	0.003	0.003	0.031	0.004	0.042
0.006	0.020	0.004	0.004	0.002	0.334	0.003	0.421
0.005	0.004	0.023	0.012	0.003	0.045	0.025	0.045

Table V.4 Variation of uncertainty at inventory of I = 300 g

ΔL (m)	Δh (m)			Δ(Δh) (m)	Percentage Uncertainty %		
	0.75 m/s^2	1.5 m/s^2	2.1 m/s^2		0.75 m/s^2	1.5 m/s^2	2.1 m/s^2
0.004	0.005	0.005	0.004	0.005	0.025	0.041	0.031
0.005	0.013	0.041	0.032	0.023	0.041	0.002	0.002
0.005	0.034	0.003	0.003	0.003	0.234	0.003	0.121
0.004	0.005	0.013	0.003	0.004	0.005	0.045	0.006

Journal Publications from the present work

- Hauchhum L. and Mahanta P., 2014. Kinetic, Thermodynamic and Regeneration Studies for CO_2 Adsorption onto Activated Carbon, International Journal of Advanced Mechanical Engineering. 4(1), 27-32.
- Hauchhum L. and Mahanta P., 2014. Adsorption of CO_2 on Activated carbon and zeolites, International Journal of Energy and Environmental Engineering, 5, 131. (DOI: 10.1007/s40095-014-0131-3)
- Hauchhum L. and Mahanta P., 2014. CO_2 Capture onto Zeolite 13X and Zeolite 4A by Pressure Swing Adsorption in a Fixed Bed, Applied Mechanics and Materials, 592-594, 1456-1460. (doi:10.4028/www.scientific.net/AMM.592-594.1456)
- Hauchhum L., Mahanta P. and De Wilde J., 2014. Capture of CO_2 from Flue Gas onto Coconut Fibre Based Activated Carbon and Zeolites in a Fixed Bed, Transport in Porous Media. (under review)
- Hauchhum L. and Mahanta P., 2014. Performance Enhancement of CO_2 Capture from Flue Gas by Using a Bubbling Fluidized Bed, Fuel and Energy. (communicated)

International and National conferences

- Hauchhum L. and Mahanta P., 2012. CO_2 Capture by Adsorption Process in a Fixed Bed using Activated Carbon. International conference on Energy, UCL, Belgium.
- Hauchhum L. and Mahanta P., 2013. Adsorption of CO_2 and N_2 on molecular sieves by using pressure swing adsorption. All India seminars on green fuels and clean energy technologies, The Institute of Engineers, Guwahati.
- Hauchhum L. and Mahanta P., 2014. Kinetic, thermodynamic and regeneration studies for CO_2 adsorption onto activated carbon, International conference on "Innovative Trends in Mechanical, Material, Manufacturing, Automotive, Automobile and Aeronautical Engineering" (ITMMMAAAE-2014), New Delhi.
- Hauchhum L. and Mahanta P., 2014. Bubbling fluidized bed for post combustion CO_2 capture from flue gas by using adsorption process, AMETI, NERIST, Arunachal Pradesh.